Harpur Hill, Buxton
Derbyshire, SK17 9JN
T: +44 (0)1298 218000
F: +44 (0)1298 218590
W: www.hsl.gov.uk

HEALTH & SAFETY LABORATORY

Quality and Reliability Issues with Large-Eddy Simulation

MSU/2008/10

Project Leader: **S. E. Gant**

Author(s): **S. E. Gant**

Science Group: **Health Improvement**

DISTRIBUTION

C. Elliot-Minty	Customer Project Officer, HSE
H. Harte	Customer Authorising Officer, HSE
K. O'Donnell	Chemical Industries Division, HSE
S. Connolly	OD3.2, HSE
M. Bilio	OD3.2, HSE
A. Curran	Health Improvement Group Director, HSL
D. Morgan	Mathematical Sciences Unit Head, HSL
M. J. Ivings	Fluid Dynamics Team Leader, HSL

PRIVACY MARKING:

Available to the public

HSL report approval:	**A. Curran**
Date of issue:	**March 2009**
Job number:	**JH72106**
Registry file:	**24975**
Electronic file name:	**MSU200810.doc**

ACKNOWLEDGEMENTS

The author would like to thank the following people for assistance in preparing this report: Professor Lars Davidson (Chalmers University) for providing the DNS data used to illustrate the statistical techniques, Raf Theunissen and Professor Riethmuller (Von Kármán Institute), Dr. Andrew Patton (Oxford University) and Dr. Adrian Kelsey (HSL) for assistance with the bootstrapping approach, and also Dr. Richard Howard and Professor Dominique Laurence (Electricité de France/Manchester University) for providing useful comments on an earlier draft.

CONTENTS

EXECUTIVE SUMMARY

There has been a steady increase in the use of Large-Eddy Simulation (LES) for safety-related studies over the last few years. This has particularly been the case in the fire-safety industry, largely due to the increasing popularity of the free LES-based code Fire Dynamics Simulator (*FDS*). A recent publication by the Organisation for Economic Co-operation and Development (OECD) has also suggested that LES should be used in assessing nuclear reactor safety, although it acknowledged that there was relatively little experience within the nuclear community on LES.

LES has not yet reached a sufficient level of maturity for quality issues to be well documented. The approach has a number of key underlying differences compared to the more traditional Reynolds-Averaged Navier-Stokes (RANS) turbulence modelling techniques which makes the issue of quality control more challenging.

The present work identifies the possible sources of errors in LES and the key areas where these differ from RANS. For industrial applications, issues related to the unsteady, time-varying nature of the simulations and the computational grid resolution are highlighted as being of primary importance in affecting the quality of the results from the simulations.

To assess the statistical uncertainty in time-averaged values, a relatively novel technique for calculating confidence intervals from correlated time-varying data is presented. The approach, based on bootstrapping, has a number of advantages over previous methods used to assess confidence intervals in LES.

From a survey of the literature, a total of ten separate measures to assess the quality of the computational grid resolution used in LES are identified. These involve approaches based on rules-of-thumb or prior RANS simulations, single-grid estimators involving just one LES calculation, and other approaches involving multiple LES calculations. The advantages and disadvantages of each approach is documented and references are provided for examples of their use in the literature.

Simulations of a low-pressure choked gas release in a ventilated room using Detached-Eddy Simulation (DES) are then presented. The DES model is a hybrid approach that uses LES in most of the flow domain and RANS near walls or where the grid is relatively coarse. The particular flow studied is typical of a practical scenario investigated as part of an industrial safety study. The DES results are compared to those obtained using steady and unsteady RANS models and another recently developed approach known as Scale-Adaptive Simulation (SAS). A number of the grid quality indices identified in the literature survey are used to assess the grid resolution. Overall, these measures indicate that even the finest grid used in the present simulations is relatively coarse for LES. The practical limitations of various indices are also documented.

The results from the simulations are compared to experimental measurements where it is found that the DES model performs relatively poorly in comparison to the RANS-based models. Contrary to the anticipated behaviour, the DES and SAS predictions also deteriorate slightly as the grid is refined. The size of the gas clouds predicted using the various models are calculated together with their confidence intervals, using the bootstrapping technique. Of the four models tested, the SAS model is found to exhibit greatest sensitivity to the grid resolution. Computing times for the different modelling approaches are also compared.

The literature review and case study suggest that there is no single criterion that provides wholly reliable estimates of the quality of the grid used in LES of complex industrial flows. Some of the quality indices can provide useful indications of the required grid resolution before performing an LES, based on prior RANS results, but have difficulties when the flow is transitional or laminar. Quality measures based on the size of the eddy viscosity are Reynolds-number sensitive, whilst simple measures based on the ratio of modelled to resolved turbulent kinetic energy do not take account of numerical dissipation. The Richardson-extrapolation-based methods, which try to account for numerical dissipation effects, encounter difficulties due to the resolved turbulent kinetic energy sometimes being greater on coarse grids than on fine grids.

Although the various quality measures can provide some limited useful information, at present it appears that the spatial resolution needs to be assessed by performing multiple simulations on different grids with a range of cell sizes, similar to the approach usually taken in RANS simulations. To provide confidence in the LES results, as well as undertaking these tests, additional simulations may need to be undertaken to assess the sensitivity of the predictions to the turbulence model, the numerical treatment and the boundary conditions. Such sensitivity tests are often avoided in industrial studies as they are usually very expensive in terms of computing time. The present work highlights that for indoor-air gas dispersion studies, the current computing power of fast multi-processor desktop PC's is barely sufficient to consider using LES-based techniques. Whilst it may be necessary to use LES if the main parameters of interest are peak values and the statistical spread about the mean, the cost in terms of computing time required to use LES should not be underestimated.

The issue of quality and trust in LES encompasses a huge volume of research and the field is currently developing rapidly. Whilst every effort has been made to provide a reasonably comprehensive and accessible review, by the nature of the subject this report cannot fully cover all of the research carried out in this area and it is likely to become outdated relatively rapidly. In view of the foreseeable use of LES for modelling safety-critical applications in the near future, it is recommended that further work be carried out to help understand LES quality issues.

1 INTRODUCTION

Turbulence is a feature of practically all health and safety related fluid flows. To obtain reliable predictions of the dispersion of a flammable gas or an airborne contaminant (e.g. Figure 1) it is essential that turbulence is modelled to a reasonable degree of accuracy. Computational Fluid Dynamics (CFD) is faced with considerable challenges in modelling turbulence. The difficulty arises from the very wide range of spatial and temporal scales present in turbulent flows. In a typical room, turbulent eddies range in size from the order of millimetres up to tens of metres. The time-scale for an eddy turnover may be just a few tenths of a second but it may also take hours for a full air change in the room. If the CFD model tries to resolve the evolution of every turbulent eddy using a spatial resolution of a few millimetres and a temporal resolution of less than a second, to simulate the flow of air in the whole room would be extremely costly computationally, requiring many weeks or even months of computing time. A recent review paper estimated that based on Moore's Law, this type of direct approach would not be feasible until 2070 [1].

Figure 1 Atmospheric turbulent dispersion on an industrial site

Instead, the most commonly adopted computational modelling approach involves solving for the *mean* flow behaviour. By averaging the flow over a long time or over multiple snapshots, much of the eddy motion is smoothed out and so the resolution required in the simulation, both in space and time, is significantly reduced. This so-called "Reynolds Averaged Navier-Stokes" (RANS) approach has been widely used over the last 20 years for simulating gas dispersion and smoke movement in rooms (e.g. [2-4]) and is the standard approach for industrial CFD. However, it is reliant upon empirical models to account for the effect of turbulence on the mean flow behaviour. These can give rise to inaccuracies under certain flow conditions, such as laminar-turbulent transition and flow impingement, and it is necessary to use different RANS models in different circumstances in order to obtain reliable predictions. The CFD practitioner must therefore have some expertise and knowledge of the capabilities and limitations of the various RANS models and in some circumstances may have to undertake tests to assess the degree of sensitivity in the CFD predictions to the choice of turbulence model.

Advances in computing capabilities in recent years have opened up the possibility of using more sophisticated and potentially more accurate turbulence models. An alternative turbulence treatment called Large-Eddy Simulation (LES) is growing in popularity. LES has been

demonstrated to perform well in a number of flows, notably in simulating gas dispersion in rooms and flow in urban street canyons [5-9]. Instead of averaging over time, LES involves averaging over a small local region of space – a process known as 'filtering'. Effectively, the simulation uses a spatial resolution that is insufficient to capture the motion of all the fine, small eddies in the flow but the large, energy-containing flow structures are resolved fully. Since only the small eddies are modelled, and these account for a small fraction of the total turbulence energy, the dependence of the simulation results on the model is reduced. Moreover, the small turbulent eddies are considered likely to be relatively uniform in structure and it is thought more likely therefore that a single "universal" LES model might be developed.

LES calculations are costly in terms of computing time since they need to resolve the unsteady motion of the large eddies and in most cases it is desirable to have finer spatial resolution than that used with RANS models. The advantage of this, however, is that details of the turbulent fluctuations are resolved and this can be used to provide information on, for example, peak exposure levels, which cannot easily be obtained using RANS models.

Over the last 20 years as the RANS approach has matured, CFD practitioners have come to understand how the quality of RANS simulations can be judged. A major EU-funded project between 2000 and 2004 on "Quality and Trust in Industrial CFD" produced a set of best-practice guidelines that covered most topics of practical interest [10]. The European Research Community on Flow Turbulence and Combustion (ERCOFTAC), which coordinates much of the EU research in turbulence, has developed a website which provides users with advice and best-practice examples[1]. There is also a significant amount of information presented in the literature describing the performance of different RANS models and providing suggestions for how to minimize numerical errors (see Section 2).

In contrast, LES has not yet reached a sufficient level of maturity for quality issues to be well documented. The approach has a number of key underlying differences compared to RANS that makes the issue of quality control more challenging. At present, if two independent CFD groups were asked to perform simulations of the same flow using both RANS and LES models, and the results were compared, the RANS results would be likely to be similar between the two groups, but the LES results would probably be quite different. This issue of repeatability is a key requirement in safety studies, where the accuracy of a model may in some cases be assumed based on its previously reported performance rather than by any direct comparisons with experiments.

Despite the current gap in the knowledge with respect to LES quality, there has been a steady increase in the use of LES for safety-related studies over the last few years. This has particularly been the case in the fire-safety industry, largely due to the increasing popularity of the LES-based code Fire Dynamics Simulator (*FDS*)[2] (e.g. [11, 12]). A recent publication by the OECD [13] has also suggested that LES should be used in assessing nuclear reactor safety, although it acknowledged that there was relatively little experience within the nuclear community on LES.

The purpose of the present work is to survey techniques that provide a means of assessing the quality of large-eddy simulations. To examine the usefulness of these techniques, various measures are used to study the case of a gas release in a ventilated room. The case is typical of a practical scenario investigated as part of an industrial safety study.

This report is split into a number of sections. Following this introduction, Section 2 provides a brief overview of the previous work on CFD quality and reliability: identifying the sources of

[1] http://www.ercoftac.org, *accessed March 2008.*
[2] http://www.fire.nist.gov/fds/, *accessed July 2008.*

errors in CFD simulations, defining some terminology and providing references for useful sources of information. Section 3 sets out the main quality assessment measures for LES that have previously been proposed in the literature. These focus predominately on spatial resolution, which is a critical issue in LES, but also address issues of temporal resolution, the choice of LES model and numerical scheme, and the treatment of walls and inflow boundaries. Section 4 presents the results from applying some of these quality assessment measures to the case of a gas release in a ventilated room. Section 5 provides a general discussion of the issues raised in the preceding sections and Section 6 some overall conclusions.

In presenting this material, it is assumed that the reader is reasonably familiar with the general practises adopted in running steady RANS CFD studies. For background reading, see for example the comprehensive text books [10, 14, 15], and previous HSL publications [16, 17]. A basic description of the standard Smagorinsky LES model is provided in Appendix A which also introduces some of the related terminology. Since the techniques used in assessing LES quality involve mathematical techniques that may be new to the reader, such as spectral analysis and bootstrapping, some useful background information to these topics are provided in Appendices B and C respectively.

2 CFD QUALITY AND RELIABILITY

2.1 BACKGROUND

In the early 1980's, two seminal conference meetings were held at Stanford University in California that aimed to establish the state of the art in simulating complex turbulent flows [18]. Research teams from around the world submitted results from CFD simulations for a number of predefined test cases. The results were then compared against each other and against experimental data, which had been careful vetted for its reliability. The first conclusion from the meetings, known commonly as the Stanford Turbulence "Olympics", was that the quality of the numerical approaches used in the simulations was so poor that it was impossible to draw meaningful conclusions about the relative merits of the different turbulence models [19]. The workshop brought to the fore the importance of numerical accuracy in CFD and provided a catalyst for the developing field of CFD quality and reliability.

In the years since the Stanford Turbulence Olympics there have been significant efforts directed at improving the quality of CFD simulations of turbulent flows. Much of the recent work in this area has been driven by the nuclear and defence industries where the issues of model accuracy are of critical importance. A list of the main organisations involved in this work is given below:

- **European Research Community on Flow Turbulence and Combustion (ERCOFTAC)**: the leading association of research, education and industry groups concerned with the technology of flow, turbulence and combustion in Europe. Its Special Interest Group 101 focuses on "Quality and Trust in Industrial CFD". ERCOFTAC supports the maintenance and development of the Q-Net Knowledge Base[3], an online compendium of CFD test cases and advice. The Knowledge Base was developed largely from a 4-year EU-funded project "Network on Quality and Trust in the Industrial Application of Computational Fluid Dynamics", QNET-CFD, which brought together the expertise of 43 European organisations, principally from industry. In addition, ERCOFTAC supported the book of "Best Practice Guidelines" [10] and the development of the "classic collection" database[4].

- **Advisory Group for Aeronautical Research and Development (AGARD)**: now known as the NATO Research and Technology Organization (RTO)[5]. AGARD was involved in promoting quality and trust in CFD in the late 1970's and 80's [20, 21] and provided support for the development of a database of test cases for validating large-eddy simulations[6]. Current efforts in this area are being led by the NATO Modelling and Simulation Group.

- **Nuclear Energy Agency (NEA)**: part of the international Organisation for Economic Co-operation and Development (OECD). The NEA has recently published a guidance document on best practice use of CFD for design of nuclear reactors [13]. The document was largely based on findings from the three-year EU-funded project: "Evaluation of Computational Fluid Dynamics Methods for Reactor Safety" (ECORA), which involved 12 partners from the nuclear industry and related research

[3] http://eddie.mech.surrey.ac.uk/, *accessed March 2008.*
[4] http://cfd.mace.manchester.ac.uk/ercoftac/index.html, *accessed March 2008.*
[5] http://www.rta.nato.int/, *accessed May 2008.*
[6] http://torroja.dmt.upm.es, *accessed March 2008.*

organisations[7] [22, 23]. The NEA also provides an online data bank of publications relevant for CFD validation[8].

- **International Atomic Energy Agency (IAEA)**: similar to the NEA, the IAEA has a data bank of publications relevant to CFD modelling of nuclear systems[9], including a validation study of thermo-mechanical and thermo-hydraulic codes [24].

- **U.S. Nuclear Regulatory Commission (NRC)**: also similar to the NEA and IAEA, the NRC is involved in verification and validation of CFD codes for nuclear safety applications in the United States. It has recently published a review of fire models[10].

- **American Society of Mechanical Engineers (ASME)**: has a long history of promoting best practice in numerical methods. The journals it publishes adopt rigorous editorial policies aimed at reducing and quantifying numerical errors[11] [25-27]. The ASME Journal of Fluids Engineering recently produced a special issue devoted to issues of verification and validation of CFD codes [28-37] and the ASME Coordinating Group on Computational Fluid Dynamics organised symposia on "Quantification of Uncertainty in CFD" in the 1990's [38-40]. Currently, the investigation of CFD quality issues is being led by the "Performance Test Codes Subcommittee on Verification and Validation in Computational Fluid Dynamics and Heat Transfer" (PTC-61).

- **U.S. National Laboratories**: have been involved in a number of programs and workshops in the field of model validation, verification and uncertainty. Sandia has two departments devoted to "Validation and Uncertainty Estimation" and "Optimization and Uncertainty Estimation", and has organized workshops such as those on heat transfer in pool fires in 2005, the "Model Validation Challenge Workshop" in 2006 [41], and the workshop on fire models and validation in 2007. Los Alamos ran from 2000 to 2004 an Uncertainty Quantification Working Group and organized a conference on sensitivity analysis of model output in 2004[12]. Idaho National Laboratory have also prepared a report on best practice use of CFD for nuclear applications for the U.S. Department of Energy[13].

- **American Institute of Aeronautics and Astronautics (AIAA):** has published guidelines for the verification and validation of CFD models [42, 43] and sponsors the international CFD Drag Prediction Workshops[14], held in the U.S. every two or three years. Participants at the workshops submit in advance the results from their "blind" simulations of aeronautical flows i.e. prior to having access to the experimental data. The workshops aim to provide an open forum where the state-of-the-art in CFD models for drag prediction can be assessed.

- **National Project for Application-oriented Research in CFD (NPARC)**: a partnership between the NASA Glenn Research Center and the Arnold Engineering Development Center that supports the development and maintenance of the CFD code, WIND. The NPARC Alliance has produced an online tutorial on CFD Verification and

[7] http://domino.grs.de/ecora%5Cecora.nsf/pages/Public, *accessed April 2008.*
[8] http://www.nea.fr/html/science/docs/index.html, *accessed March 2008.*
[9] http://www.iaea.org/inis/aws/fnss/abstracts/abst_te_1318_web.html, *accessed May 2008.*
[10] http://www.nrc.gov/reading-rm/doc-collections/nuregs/staff/sr1824/, *accessed May 2008.*
[11] http://journaltool.asme.org/Content/JFENumAccuracy.pdf, *accessed May 2008.*
[12] http://public.lanl.gov/kmh/, *accessed May 2008.*
[13] http://www.inl.gov/technicalpublications/Documents/3480269.pdf, *accessed May 2008.*
[14] http://aaac.larc.nasa.gov/tsab/cfdlarc/aiaa-dpw/index.html, *accessed January 2009.*

Validation[15], based on the AIAA guidelines [42, 43], and has assembled a validation database which focuses on military and aeronautical applications.

- **NAFEMS**: is a worldwide independent association that promotes the use of analysis techniques, including both finite element analysis and CFD. It is focused on the needs of industry and has helped to organise conferences on verification and validation, such as the series of seminars on "Quality and Reliability of CFD Simulations", currently held at Nottingham University. It has a number of publications that provide best-practice advice for industrial CFD users which include the best-practice advice for modelling smoke movement [44].

- **Health & Safety Laboratory (HSL)**: has produced a number of independent reviews of CFD techniques relevant to the health and safety field. Recent examples include a review of fire and explosion models [45, 46], a methodology for validating atmospheric dispersion models for simulating LNG releases [47] and best practice guidelines for undertaking dispersion simulations in gas turbine enclosures [48]. HSL reports are available for download from the Health and Safety Executive website[16].

In addition to the output from these organisations, there is a significant body of peer-reviewed publications on the subject of CFD quality by authors such as Stern [49-51], Obercampf [31, 33, 52-54] and Celik [38, 55-59]. A particularly notable publication by Iaccarino [60], compared the performance of three popular commercial CFD codes and showed that different results could be obtained for the same test case even when the three codes stated that they used nominally the same turbulence models. Various best-practice guides have been produced for specific applications, such as those relating to atmospheric flows in the urban environment [61, 62], indoor-air flows [63] and marine flows[17]. There are useful text books, such as Knupp & Salari [64], the section in the book Ferziger & Perić [14] on error analysis and estimation, and the well-known and comprehensive book on verification and validation by Roache [19]. Most manuals produced for commercial and industrial CFD codes, such as ANSYS-*CFX*/*Fluent*[18], *Star-CD*/*CCM+*[19] and *FDS*, provide guidance on the use of appropriate techniques and models in different circumstances. Finally, there have been numerous conferences and workshops devoted to the issue of CFD quality and trust, such as the mini-symposium on "Advances and Accomplishments in Verification and Validation", part of the 2006 World Congress on Computational Mechanics sponsored by the International Association for Computational Mechanics (IACM), and the Stanford University Center for Integrated Turbulence Simulations Workshop on "Error Estimation, Uncertainty Quantification and Reliability", 22-23 August 2005[20].

Relatively little of this vast body of work on CFD quality and reliability has addressed issues specifically related to large-eddy simulation. In some cases this limitation has deliberately been chosen to limit the scope of works, which would otherwise become so large as to be unmanageable. The aim of the ERCOFTAC Best Practice Guide [10], for instance, was "to offer roughly those 20% of the most important general rules of advice that cover roughly 80% of the problems likely to be encountered". This meant that the discussion of the whole topic of unsteady flows was consigned to just a couple of short paragraphs. Whilst this position was justifiable when the document was published 8 years ago, with the steady improvements in

[15] http://www.grc.nasa.gov/WWW/wind/valid/tutorial/tutorial.html, *accessed May 2008.*
[16] http://www.hse.gov.uk/research/index.htm, *accessed May 2008.*
[17] https://pronet.wsatkins.co.uk/marnet/guidelines/guide.html, *accessed July 2008.*
[18] http://www.ansys.com, *accessed July 2008*
[19] http://www.cd-adapco.com, *accessed July 2008.*
[20] http://www.stanford.edu/group/cits/workshop/tutorials.html, *accessed March 2008.*

cheap computing power and the growth in use of unsteady-RANS and large-eddy simulation for industrial flows in recent years, there is a need to update this guidance.

Current European efforts in the field of LES quality are focussed on the 4-year EU-funded LES-AID project[21] which organised the recent workshop on Quality and Reliability of Large-Eddy Simulations[22] [65] and aims eventually to produce best practice advice for large-eddy simulation. The LES-AID project is an EU-COST action involving 51 partners drawn primarily from academia that provides support for scientists to visit other universities and share expertise, and funds organisers of meetings, but does not provide direct financial support for any ongoing research.

The remaining main sources of information on LES quality issues are the relevant sections in the recent books on LES by Sagaut [66] and Geurts [67], and the proceedings from turbulence modelling workshops and conferences, such as the ERCOFTAC/IAHR/COST workshops on Refined Turbulence Modelling[23] and the Direct and Large Eddy Simulation Workshops [68-73].

2.2 DEFINITION OF TERMS

Verification and Validation

The issue of quality in CFD simulations is often separated into two processes: verification and validation. Roache [19] succinctly defines these two processes as "solving the equations right" (verification) and "solving the right equations" (validation). Verification consists of making sure that the numerical techniques used to solve the underlying model equations are accurate. This includes some consideration of code quality assurance. However, it does not involve testing the code to make sure that the results are physically realistic. A well-verified code that accurately solves the model equations can produce wildly incorrect predictions just because the wrong equations are being solved. Choosing the right equations falls under the heading of "validation", which consists largely of comparing models' predictions against data to determine whether the models have made the right approximations of the physics. More precise definitions of verification and validation are debated at length by Roache, Stern and Obercampf in [50, 74-78] and can be found in the editorial policy statement of the AIAA Journal [42, 43].

Aleatory and Epistemic Uncertainty

Uncertainty in model predictions is sometimes classified as being "aleatory" or "epistemic". Aleatory uncertainty arises from the inherent variability in the physical system or environment being considered. For instance, in atmospheric flows there is a natural aleatory uncertainty in wind speed and direction due to the random nature of atmospheric turbulence. This uncertainty is usually expressed in terms of some statistical representation, such as a probability distribution of the wind speed with associated mean and standard deviation. Although the statistical properties of the variability may be known, due to the irreducible uncertainty of the random physical parameter, it is not possible to predict at any particular instant in time what its exact value will be.

[21] http://lesaid.math.utwente.nl, *accessed May 2008.*
[22] http://www.qles.org/, *accessed May 2008.*
[23] http://tmdb.ws.tn.tudelft.nl/, *accessed May 2008.*

Epistemic uncertainty refers to some lack of knowledge of the system. It is reducible in the sense that if more was known about the system, the uncertainty could be reduced. For example if there was more experimental data available to tune atmospheric turbulence models, in principle a more accurate model could be developed.

More precise definitions are provided in Obercampf [79]. Further information on mathematical techniques that can be used to assess epistemic uncertainty can be found in the Sandia National Laboratories project on epistemic uncertainty[24]. A useful summary of uncertainty analysis specifically aimed at industrial CFD is given by Iaccarino[25].

A Priori and *A Posteriori*

In later discussions in this report and in the literature, the performance of different LES models is assessed using *a priori* and *a posteriori* tests. It is useful to understand what these tests involve in order to appreciate their implications.

A priori tests examine the theoretical behaviour of a model without actually running a full CFD simulation. For example, an *a priori* test could involve taking the velocity field from Direct Numerical Simulation (DNS)[26] or experiments, filtering it to the same resolution as an LES, inputting the filtered field into the LES model equations and using this to predict the resolved stress. The resolved stress, averaged over an appropriate length of time, could then compared back to the DNS or experimental mean stress to see how well it agrees. Since the tests do not involve actually running a simulation, there is no feedback mechanism present between the stress and the velocity. *A priori* tests can therefore avoid some of the problems associated with the interaction of numerical and modelling errors.

A posteriori tests on the other hand consist of actually running a simulation using the LES model and comparing the mean or statistical behaviour to DNS or experimental data. In this respect, they are more akin to how models are actually used in practice in engineering studies. *A posteriori* tests incorporate effects from the interaction of numerical and modelling errors.

Vreman *et al*. [80] and Pope [15] note that a number of studies have shown *a priori* tests to be overly pessimistic about model behaviour; when the models are actually tested in practice the *a posteriori* results showed much better agreement with DNS or experimental data. However, whilst *a posteriori* testing is useful from an engineering perspective, if agreement between the CFD results and the experiments or DNS is poor, it is difficult to identify which aspect of the model (numerics, grid, subgrid model etc.) is actually responsible for the errors.

---

[24] http://www.sandia.gov/epistemic, *accessed May 2008.*
[25] http://www.stanford.edu/dept/ICME/docs/seminars/Iaccarino-2007-03-05.pdf, *accessed May 2008.*

[26] *Direct Numerical Simulations use extremely fine grids to resolve all the turbulent structures in a flow very accurately. The results are therefore considered as representing all the details of the flow and are often used as a substitute for experimental data to tune turbulence models. However, DNS does not, per se, account for uncertainties in boundary conditions, which may be poorly known in environmental flows for example. Whilst DNS obtains a very accurate solution for the specified conditions, the results do not therefore necessarily reflect reality. The computing demands of DNS are extremely high and currently it is used to simulate only relatively simple building block flows (e.g. homogeneous turbulence, channel flow) at relatively low Reynolds number.*

2.3 SOURCES OF ERRORS

There are a number of possible sources of error in CFD simulations of turbulent flows, and specifically large-eddy simulations. In no particular order these include:

Geometrical Simplification

In complex industrial flows it is frequently not possible to include all of the details of the flow geometry. For example, in modelling the dispersion of gas through an oil refinery, the complex arrangement of pipes, ducts and process equipment may be modelled as regions of space with defined porosity, since resolving them by the mesh would be impractical. Walls with small projections that cannot easily be resolved may instead be modelled as surfaces with a certain roughness, or the small projections may be just ignored entirely. The user must also select how far away to place the boundaries of the model, setting the size of the computational domain. Using an inappropriate domain size or simplifying the geometry too much may adversely affect the results of the simulations.

Modelling Errors

For large-eddy simulations modelling errors mainly refers to the approximations made to account for the physical effect of the unresolved Sub-Grid Scale (SGS) turbulence on the resolved flow field. Since the SGS model is a function of the computational grid size, the effect of modelling errors should diminish as the grid is made progressively finer in LES. However, in many industrial CFD studies, it is not possible to use sufficiently fine grids due to the high computational cost this would entail. As a result, flows are often only marginally resolved and modelling errors can be appreciable. A discussion of appropriate LES model choice to minimize modelling errors in certain situations is given in Section 3.4.

Modelling errors may also arise from inappropriate choice of governing equations, such as use of a Boussinesq treatment to account for buoyancy effects when density differences are appreciable.

Boundary and Initial Conditions

The choice of boundary and initial conditions includes consideration of the inlet and outlet flow conditions, the conditions at the walls and the initial state of the modelled flow when the simulation is started. In many safety-related applications, these conditions are poorly specified or even unknown and it may be important to assess the degree of uncertainty by running sensitivity tests to assess how the results change as a function of the boundary conditions. Similarly to RANS, initial conditions in large-eddy simulations may need to be produced by running a pre-calculation to generate fully-developed flow conditions. For example, in a study of an atmospheric release of gas from an oil refinery, the correct wind field across the facility would need to be calculated beforehand, prior to the gas release taking place. One of the specific issues for LES is the treatment of turbulent inflow boundary conditions, which is discussed later in Section 3.7.

Discretization Errors

In CFD, spatial gradients of quantities are calculated by approximating derivatives in terms of nodal values (for an introduction, see Versteeg & Malasekera [81]). The accuracy of the

approximation used to calculate derivatives is usually classified with reference to the Taylor series expansion. A first-order accurate scheme has a leading order term in the truncation error which has a first-order dependence on grid spacing, i.e. the leading error term involves Δx^n with an exponent of $n = 1$, where Δx is the grid spacing. The truncation error provides an indication of the rate at which the error in approximating the gradient reduces as the grid is refined. The magnitude of the error associated with a second-order scheme, such as central differencing, should decrease faster than a first-order scheme as the grid is refined, provided that a sufficiently fine grid is used.

The magnitude of discretization errors is affected by the order of the discretization scheme and the arrangement of the grid nodes. Similarly, the discretization error in time is a function of the temporal discretization scheme and the length of the time-steps. A significant amount of effort has been expended in understanding and describing discretization errors in steady RANS simulations (see, for example, Roache [19]).

Discretization errors are one of the key issues in LES quality. Various studies have shown that the contribution from the discretization error can exceed that of the LES model itself in many cases [80, 82-86]. The issue is complicated by the fact that the size of the grid cell is an input parameter in the LES model. Very few LES studies have attempted to minimize discretization errors and obtain a grid-independent solution in the usual RANS sense [87, 88]. Moreover, it has been shown [67, 89] that the discretization error interacts with the error from the LES model, and in some circumstances this can lead to beneficial results with the two errors partially cancelling each other out. These issues are discussed further in Section 3.3.

Iteration Errors

LES by its nature requires the simulation to resolve the unsteady fluctuations in the flow. The majority of industrial CFD codes use implicit time-discretization and iterate towards a converged solution at each time-step. Depending upon the convergence criteria used, errors may result if an insufficient number of iterations are performed at each time-step. These errors can be reduced at the cost of performing more iterations and increasing the computing time. The quality issues involved in quantifying and minimizing iteration errors are similar in LES to RANS (see Roache [19] and Kornhaas *et al*. [90]).

Aliasing Errors

These are numerical errors that arise from the numerical treatment of the non-linear convection term in the momentum equations. High-wavenumber components are produced in taking the product of velocities in physical space which are "folded back" and appear as lower-wavenumber images contaminating the solution [67, 91]. The problem is a significant issue for LES using high-order or spectral methods for spatial discretization, although it can be avoided by de-aliasing using the "3/2 rule". Various works have shown that aliasing errors are less significant in lower order schemes, such as the second-order central differences commonly used in most industrial LES studies [82, 84, 85], where the primary concern is instead the discretization error. Aliasing errors are mentioned in many early papers on LES, since they were mainly produced using highly specialised spectral-based CFD codes.

Convection Term Treatment

There are a number of different ways in which the convection term in the momentum equations can be expressed: the rotational, divergence, convective or skew-symmetric forms (see [84]).

Analytically, the mathematical forms are all equivalent and they can be transformed from one form into another using simple mathematical rules and physical principles of mass conservation. However, when the different forms are discretized, in order to be coded into CFD software, the different forms of the equations are no longer identical. Tests have shown that the accuracy of LES results and the stability of the calculation can depend upon the particular form of the convective terms used [84-86]. Commercial CFD codes commonly adopt the divergence form (also known as the "conservative" form), which is known to produce fewer unstable fluctuations when there are abrupt changes in flow variables, near shock waves for example [92]. However, both the Fire Dynamics Simulator (*FDS*) code from NIST [93] and the unstructured *Trio-U* code developed by the French nuclear research organisation, the Commissariat à l'Energie Atomique (CEA)[27], use the rotational form. In the case of *Trio-U*, this choice was originally reported to show advantageous behaviour in conserving global kinetic energy [94]. More recently, however, tests have shown that using the conservative form can also conserve well the global kinetic energy provided that the grid is constructed with faces nearly orthogonal to lines connecting cell centres [95, 96]. In *FDS*, central and upwind-biased differencing schemes are used to discretize different parts of the convection term, presumably to maximise numerical stability.

Programming and User Errors

Like any human endeavour, errors can be produced in LES due to mistakes in coding the CFD software and user errors in specifying the problem in the software or post-processing the results.

[27] http://www-trio-u.cea.fr, *accessed July 2008.*

3 ASSESSING LES QUALITY

3.1 INTRODUCTION

As mentioned in the previous Section, the primary areas that distinguish LES quality issues from steady RANS are as follows:

a.) Resolving Flow Unsteadiness

Practical issues related to resolving accurately unsteady flows are not discussed in detail in many previous best practice guides. Relevant issues include: choice of time-step, the accuracy of the numerical scheme used for time discretization, the length of time needed to allow the flow to reach a fully-developed state and the period chosen to average over, in order to produce time-averaged statistics. Such issues are common to unsteady-RANS, LES and hybrid RANS-LES models.

b.) Grid dependence

In RANS simulations, it has long been recommended that a grid dependence study be undertaken to assess the magnitude of numerical errors. Solutions are usually obtained using three or more different meshes with increasing grid densities and the results are considered adequately grid independent when they no longer show significant change with further grid refinement. In more rigorous studies, the results on different grids may be used to determine a Grid Convergence Index (GCI).

In LES, the cost of running the calculations is often so high that users try to minimize the number of sensitivity tests as far as possible. In many cases, this has resulted in LES results being published with no grid-sensitivity analyses. The situation is further complicated by the fact that the LES model behaviour is inextricably linked to the mesh size. LES results can therefore show greater sensitivity to the grid than RANS models.

c.) Choice of LES Model

There are two classes of LES models: implicit and explicit. The former uses a discretization scheme that provides sufficient numerical viscosity to account for the effect of the unresolved small-scale turbulence, while the latter involves an explicit subgrid-scale (SGS) model based on some physical considerations. The present work considers only explicit SGS models, which are used in the majority of industrial LES studies. For information on implicit models, such as the MILES approach, see for example [97].

Since the principle of LES is that most of the large energy-containing turbulent eddies are resolved and only the more isotropic smaller eddies modelled, the LES model should only account for a small fraction of the total turbulent kinetic energy and the results should be less sensitive to the details of the LES model than in RANS, where all of the turbulence energy is modelled. However, due to the high cost of running LES calculations and the high Reynolds numbers featured in many industrial flows, the grid resolution may be marginal at best, in which case the LES model may take on greater significance. The choice of the Smagorinsky constant and the treatment of transitional flows are also important considerations in choosing an appropriate LES model.

d.) Wall Treatments

In a turbulent flow as a wall is approached the size of the turbulent eddies decreases. Resolving most of the turbulence energy near walls therefore becomes very costly due to the fine mesh required. For most high-Reynolds-number flows this makes wall-resolving LES prohibitively expensive. Over the last ten years a number of techniques have been suggested to overcome this problem. Generally these have involved either adopting a coarse near-wall mesh and a "wall function", which assumes some properties of the flow behaviour close to the wall, or a hybrid RANS-LES model which treats the flow near the wall using RANS and uses LES elsewhere.

e.) Inflow Conditions

Many flow simulations involve turbulent fluid entering the domain through one or more inlets. In steady RANS simulations, it is reasonably straightforward to assign boundary conditions at these inlets, usually by prescribing profiles of the mean velocity and turbulence statistics (such as the turbulent kinetic energy, k, and dissipation rate, ε). In LES, however, it may be necessary to create physically realistic turbulent fluctuations within the flow entering the domain.

f.) Numerical Schemes

The majority of industrial and commercial CFD codes use unstructured computational grids in order to simulate complex geometries. As a consequence, the range of numerical schemes is usually limited to first- and second-order accurate upwind biased and second-order central schemes in space. Similarly in time, only first and second order accurate schemes are usually available in commercial and industrial codes. For RANS-based turbulence models, upwind-biased schemes are usually recommended to maximise numerical stability, but central schemes are preferred in LES since they produce less numerical dissipation and have improved energy-conservation properties.

The present review focuses on topics (a.) and (b.), although some discussion is provided on topics (c.), (d.), (e.) and (f.), and pointers are provided for where to find further information.

It has previously been mentioned that there are two classes of LES models: implicit and explicit. In addition, there are also implicit and explicit *filtering* approaches. Filtering is the fundamental process of averaging over a localised spatial area that is used to derive the LES transport equations. It can be shown that the process of discretizing the Navier-Stokes equations and integrating fluxes over cell faces, which is an inherent part of the Finite-Volume Method (FVM), is equivalent to a filtering process [67]. Nearly all commercial and industrial CFD codes use FVM and implicit filtering. Explicit filters tend instead to be used mainly in academic CFD codes which rely on spectral or other high-order finite-difference methods. Lund [88] showed that explicit filtering can improve LES results by reducing numerical error, but at a significant computational cost. Instead of devoting the additional computing time required to use explicit filters, the commonly-adopted position is that it is more efficient to use the computing time to run the implicitly-filtered LES with a finer mesh, which should increase the accuracy of the simulation due to the improved resolution of small scales (this is discussed further in Section 3.3). For these reasons, the present work only considers LES based on implicit filtering.

3.2 FLOW UNSTEADINESSS

In many industrial applications, the main parameters of engineering interest are time-averaged values and sometimes a measure of the fluctuation about the mean. To calculate these quantities in time-varying CFD simulations of statistically stationary turbulent flows it is important to ensure that the simulations have first reached a fully-developed state and that once this condition has been met, that the statistics are gathered over a sufficiently long time period[28].

A commonly-used approach to judge when a simulation has reached a fully-developed state is to monitor the main parameter of interest, for example a gas cloud volume, and plot its variation over time. The flow can be considered to be fully-developed once the parameter is not exhibiting a general trend to increase or decrease over time. When it has reached this stage, statistics are commonly averaged over around ten or more of the longest cycles and then the calculation is stopped. An example of this is shown in Figure 3.1.

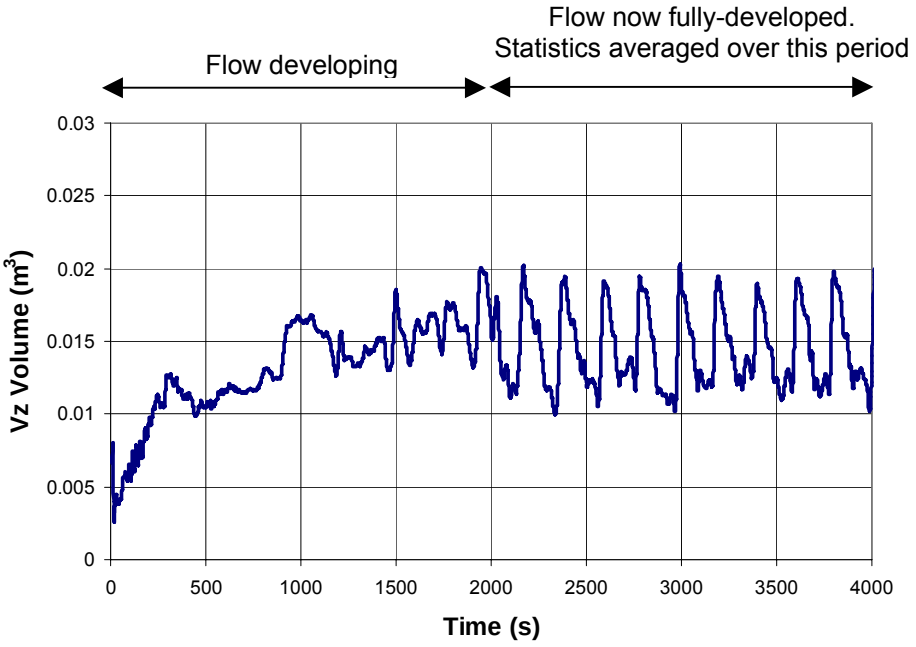

Figure 3.1 Variation of predicted gas cloud volume over time

A more rigorous approach is to calculate the running average of the parameter once the flow has reached a fully-developed state and stop the calculation once the mean value holds a steady value for a "reasonable" length of time. In some flows, the time over which the average is taken can be related to a physical time-scale of the flow to help assess what is meant by "reasonable". In internal flows, such as simple channel flows, the number of flow-through times may be used, in buoyant flows the characteristic plume puffing frequency, and in bluff body flows the eddy-shedding frequency. Then, if the mean parameter remains unchanged over, say, ten or more flow-through times, the mean value could be considered adequately converged. Estimates of the

[28] *If the flow is not statistically steady, such as a starting plume, multiple simulations can be performed and the results ensemble-averaged to calculate the equivalent mean values.*

characteristic timescales for jets and plumes can be found for example in Cetegen & Kasper [98] and List [99].

In many industrial applications, the flows considered are more complex than these simple scenarios and involve interactions from many underlying flow elements (e.g. a plume impinging onto a bluff body in a cross flow). As a consequence, there may be subtle long-time-period oscillations that are difficult to characterise in terms of a single frequency. To provide a first step towards a mathematical framework to address this issue, Celik *et al*. [59] proposed that statistical convergence be judged using Confidence Intervals (*CI*).

3.2.1 Confidence Intervals

The definition of confidence intervals can be found in statistical text books such as Crawley [100] and is best explained by considering an example. Let us assume that we want to assess the *CI* of the mean velocity at a particular point in space based on the velocity obtained from a CFD simulation. Although the velocity is monitored continuously over time (from one time-step to the next), the standard method used to calculate the *CI* requires that the data is uncorrelated (i.e. stochastically independent). The first step is therefore to sample the velocity signal at intervals in time spaced sufficiently apart that the individual samples are uncorrelated. To do this, an appropriate time interval needs to be calculated. A statistical approach for calculating the integral time-scale, τ, is described in detail in Section 8. For the velocity time-trace shown in Figure 3.2, the value of τ calculated using this method is around 11 seconds. Uncorrelated samples taken at interval of 2τ are shown in Figure 3.2 as red dots. Whilst the original velocity signal was composed of 5000 data points recorded at 1 s intervals, the uncorrelated data is composed of 227 samples at 22 s intervals.

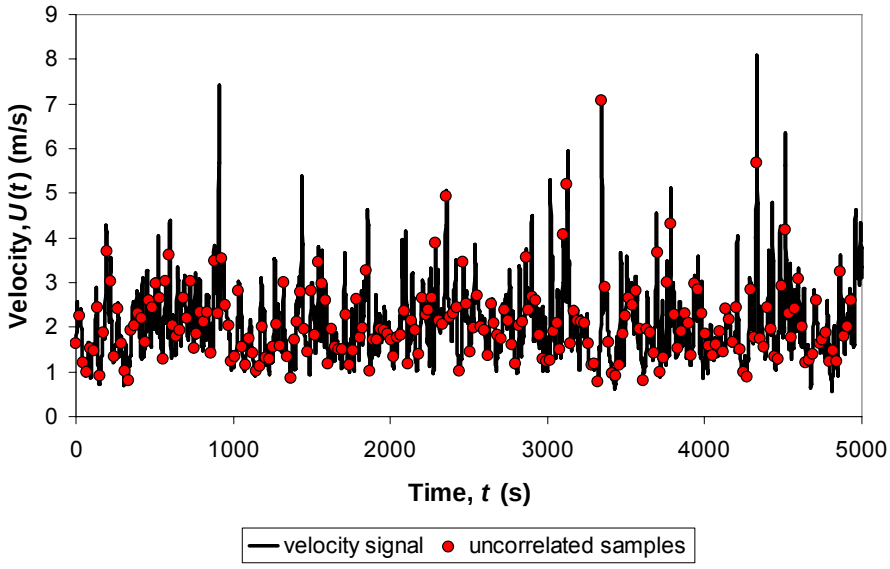

Figure 3.2 Turbulent velocity signal and uncorrelated samples taken at intervals of twice the integral time-scale. The data is taken from DNS of a channel flow.

The mean, U, and variance, $\overline{u^2}$, of the uncorrelated velocity samples are then evaluated from:

$$U = \frac{1}{n}\sum_{i=1}^{n}\tilde{u}_i \quad ; \quad \overline{u^2} = \frac{1}{n-1}\sum_{i=1}^{n}\left(\tilde{u}_i - U\right)^2 \tag{3.1}$$

where n is the number of samples and $\tilde{u}_i$ is the sampled velocity. The confidence levels are then calculated from:

$$CI = \left[U - k\sqrt{\frac{\overline{u^2}}{n}}, U + k\sqrt{\frac{\overline{u^2}}{n}}\right] \tag{3.2}$$

For the example shown in Figure 3.2 the mean velocity, U, is 2.07 m/s and the CI for $k = 1$ and $k = 2$ are [2.01 m/s, 2.13 m/s] and [1.94 m/s, 2.19 m/s] respectively.

The confidence intervals can also be expressed in terms of a fractional statistical error, e_s, defined as:

$$e_s = \frac{k\sqrt{\overline{u^2}/n}}{U} \tag{3.3}$$

where for $k = 1$ and $k = 2$ the fractional errors are 2.8% and 5.5% respectively

So what exactly do these confidence intervals tell us? The notion of the CI is based on the central limit theorem which states that: "if a random variable can be expressed as the sum of a large number of approximately independent components, and none of these components is much larger than the others, then the sum will be approximately a normally distribution" [100]. In other words, the mean of a sample of random variables approaches a Gaussian distribution as the number of samples goes to infinity.

To go back to the example, if we took the velocity signal and calculated the average velocity based on a number of discrete samples and then repeated the calculation with different samples many times, and then plotted a graph of the mean velocity against the occurrence of that mean velocity (i.e. a probability distribution), the graph would look more and more like a Gaussian distribution as the number of samples was increased to infinity, see Figure 3.3.

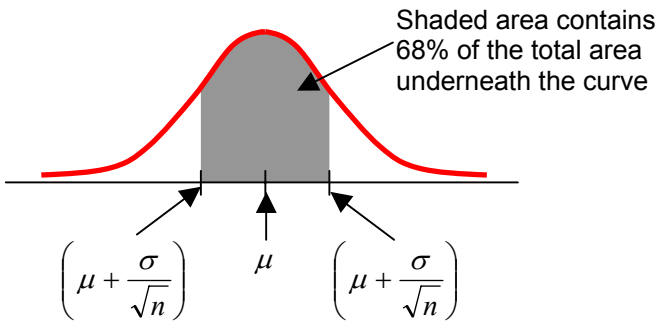

Figure 3.3 Gaussian distribution.

Since it is assumed that the mean velocity distribution is Gaussian, we can define certain regions. The area underneath the curve between the limits of $\mu \pm \sigma / \sqrt{n}$, where μ is the mean and σ the standard deviation, is known by definition to contain 68% of the total area under the graph (see Figure 3.3). In our example, μ is the mean velocity (U) and the standard deviation is the square-root of the variance ($\sigma = \sqrt{\overline{u^2}}$). Therefore, the confidence intervals with k = 1 are the upper and lower limits on x-axis in the graph shown in Figure 3.3. We can say then from our *CI* calculation that we are 68% confident that the mean velocity lies between 2.01 and 2.13 m/s.

Similarly, the area underneath the curve between the limits of $\mu \pm 2\sigma / \sqrt{n}$ is known to contain 95% of the total area under the graph. So from our example, we can say that we are 95% confident that the mean velocity is between 1.94 and 2.19 m/s.

We can also express the *CI*'s in terms of fractional errors, so we can say that we are 68% confident that the mean velocity is 2.07 ± 2.8% and we are 95% confident that the mean velocity is 2.07 ± 5.5%.

Confidence intervals are useful since they take into account both the spread in values about the mean and the number of samples taken. So, in our example, if the turbulence intensity had been higher, the velocity variance would be larger and hence the fractional error in the k = 1 confidence interval would be greater. To obtain the same fractional error as before we could then increase the number of uncorrelated samples, n. Since the *CI* is proportional to the inverse square-root of n, if the intensity of the u-velocity fluctuations ($I = \sqrt{\overline{u^2}} \big/ U$) doubled from 5 to 10%, the number of uncorrelated samples would need to increase by a factor of four to keep the same confidence levels.

Celik *et al*. [59] suggested that confidence intervals should be reported in discussing the averaged results of transient CFD simulations to provide useful information for readers. They also provided an example, based on LES simulations of a free plane jet by Klein [101], with fractional errors of 1 or 2% for confidence levels in the mean velocity of 68 and 95% respectively.

In addition to calculating confidence intervals based on the mean velocity, it is possible to calculate confidence intervals based on the velocity variance or standard deviation. Details of the calculation method are provided in [59].

3.2.2 Bootstrapping Methods

There are a number of problems associated with evaluating confidence intervals using the standard statistical method outlined in the previous section. Firstly, the method relies on the data being uncorrelated in order for it to produce a normal distribution and for the underlying principle of the central limit theorem to apply. This requires that the data from the LES be sampled at intervals spaced sufficiently apart in time, a process that throws away a considerable amount of information.

Secondly, the time-scale used to sample the signal to obtain uncorrelated data is poorly defined. In the example in the previous section the velocity signal was sampled at intervals of 2τ, where τ is the integral time-scale calculated using a method described in Section 8. This method consists of calculating the velocity autocorrelation, and then integrating the area beneath the autocorrelation between a time-lag of zero and the point where the autocorrelation first reaches

zero, as shown by the shaded area in Figure 3.4. The choice of this time-scale is essentially arbitrary, however. In the literature, other choices for τ include the time-lag at which the autocorrelation falls to a value of e^{-1}, or where it reaches a value of zero, or where it reaches its first minimum [102-104]. Based on the data shown in Figure 3.4, this can lead to sampling intervals of 2τ varying between 22 and 100 seconds, which produces fractional statistical errors for the 95% confidence interval of between 5.5 and 10.9 %. A further alternative method of estimating the integral time-scale based on time series analysis is also given in [105].

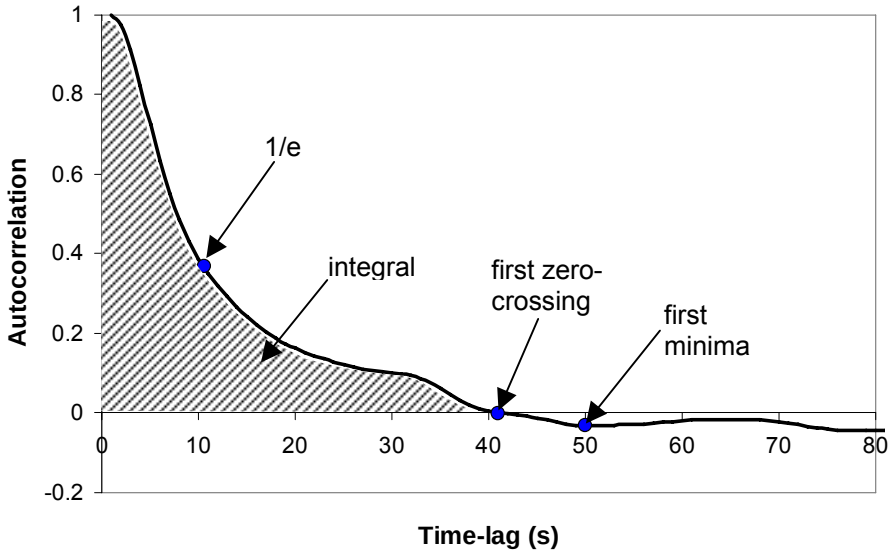

Figure 3.4 Autocorrelation of the velocity data in Figure 3.2 showing four different time-scales that can be used to represent the signal.

The confusion over the choice of appropriate time-scale, τ, is particularly critical for LES since calculations tend to be lengthy and it is desirable to minimise the computing time by calculating statistics over as short a time-period as possible. To overcome the limitations of the standard methods, Theunissen *et al*. [106] suggested an alternative approach for calculating confidence intervals based on "bootstrapping", a technique long used by statisticians but only recently applied to the field of turbulence and fluid mechanics [107]. One of the advantages of the bootstrapping approach used by Theunissen *et al*. [106] is that it can handle correlated data and hence all of the data is used.

In brief, the method consists of calculating a "block" length using a certain algorithm, where the block length is smaller than the signal. If we take the signal shown in Figure 3.2 which is composed of 5000 individual measurements of velocity, the block length is around 80. The velocity signal is then sampled by selecting a block of data at a random position within the signal *with replacement* (i.e. individual measurements can be selected more than once where blocks overlap). The sampled blocks of data are then joined end to end to produce a reconstructed signal or "bootstrap" of similar length to the original signal. In this case, each bootstrap would comprise 63 blocks each of length 80. This process is repeated many times to obtain a large number of bootstraps (typically 10,000 [108]) and the mean velocity from each bootstrap is calculated. A histogram of the mean velocities from 10,000 bootstraps of the data shown in Figure 3.2 is shown in Figure 3.5, which demonstrates that the distribution is Gaussian. The overall mean velocity from the bootstraps is calculated in the usual way, by adding all the means and dividing by their number (Equation 3.1) The upper and lower

confidence intervals can be determined from the percentile method: the 10,000 mean velocities from the bootstraps are ranked in order of magnitude from small to large and the 68% confidence intervals picked out by selecting the values 34% above and below the middle value (i.e. the 1,600th and 8,400th entries in the ordered sequence). The 95% confidence intervals are similarly the 250th and 9,750th entries.

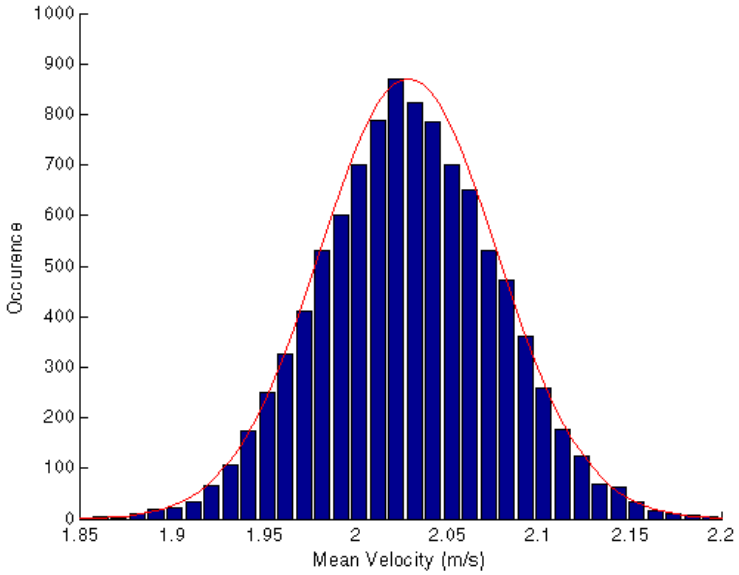

Figure 3.5 Probability distribution of mean velocities from applying the bootstrapping method to the data shown in Figure 3.2 using 10,000 bootstraps; the red line shows a Gaussian distribution for reference.

Details of the algorithm used to determine the block length are provided in Appendix C together with references for useful papers and sample MatLab code. Table 3.1 provides a summary of the mean and 95% confidence intervals calculated using the standard statistical methods described in the previous section and the bootstrapping approach described here. The data is also plotted graphically in Figure 3.6 with confidence intervals shown as error bars. The mean velocity calculated from the bootstrapping approach is the same as that obtained by averaging all of the velocity data and the confidence intervals of 4.6% are lower than any of the standard statistical approaches.

Table 3.1 Summary of means and confidence intervals calculated using standard statistical methods and bootstrapping, based on the data shown in Figure 3.2.

Calculation Method	*Sampling Interval, 2τ (sec)*	*Mean and 95% Confidence Intervals*
All data	-	2.03 ± ?
Integral	22	2.07 ± 5.5%
1/e	22	2.07 ± 5.5%
First zero-crossing	82	1.89 ± 10.5%
First minima	100	2.06 ± 10.9%
Bootstrapping	-	2.03 ± 4.6%

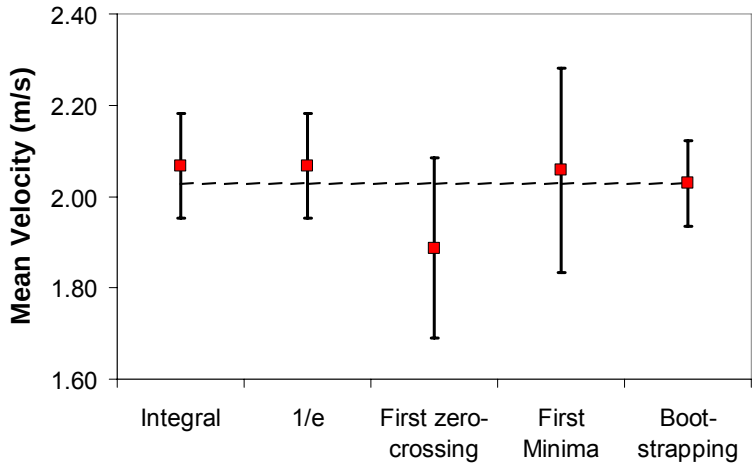

Figure 3.6 Mean velocities and 95% confidence intervals calculated using standard statistical methods and bootstrapping, based on the data shown in Figure 3.2. The dashed line indicates the mean of all the data.

The advantages of the bootstrapping method are that it can be used on both correlated or uncorrelated data. If the data is completely uncorrelated the block length algorithm returns a block length of one. Theunissen *et al*. [106] demonstrated for uncorrelated data that the bootstrapping and standard statistical methods produce identical results. The bootstrapping approach is also fully-automatic in the sense that there are no freely chosen variables, unlike the standard approach where one has to select a sampling frequency. The only variable in the bootstrapping approach described here is the number of bootstraps and this is chosen to be sufficiently large that increasing its value further has no affect on the results. Figure 3.7 shows how the mean and 95% confidence intervals vary as a function of the number of bootstraps. Using 10,000 bootstraps is a reasonable choice and produces results which are independent of the bootstrap count. Computing time could be saved by using fewer bootstraps, but such savings would be negligible in comparison with the computing time needed to run the LES calculations. The MatLab code used to generate the data shown in Figure 3.7 took only a few minutes to run on a desktop PC. A further advantage of bootstrapping is that it can be used to assess the confidence intervals on any statistic including the mean, variance, standard deviation and higher-order moments.

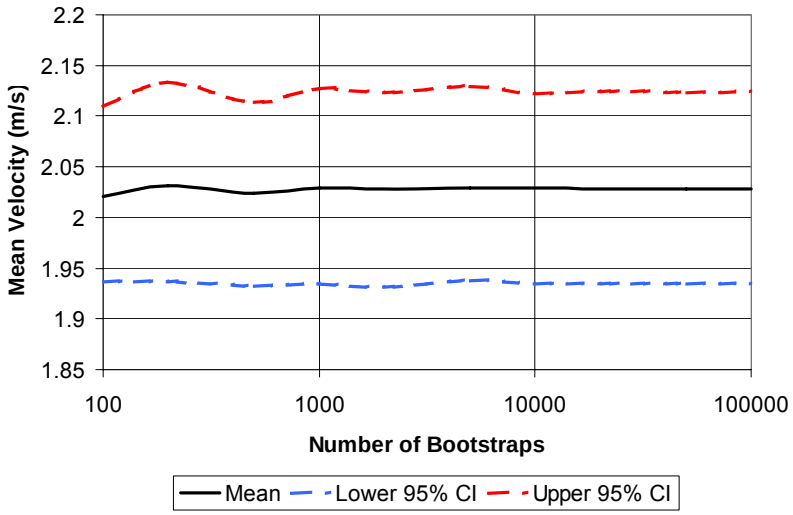

Figure 3.7 Mean and upper and lower 95% confidence intervals calculated using the bootstrapping method as a function of the number of bootstraps for the velocity data given in Figure 3.2.

3.3 GRID DEPENDENCE

The sensitivity of CFD model predictions to the computational grid resolution is one of the key quality issues for large-eddy simulation. A number of independent studies have shown that the effect of numerical errors related to grid resolution can be of similar magnitude or even larger than the effect of the turbulence model itself [80, 82-86].

It is possible to obtain a grid-independent LES solution by refining the grid (i.e. decreasing the cell size, h) whilst keeping constant the filter width, Δ, used in the Smagorinsky SGS model. This approach has been tested for homogeneous turbulence and mixing layers in [67, 89] and a channel flow in [83, 109]. Geurts [67, 89] refers to the ratio between the filter width and the mesh size (Δ/h) as the "SGS resolution". Increasing the SGS resolution increases the number of grid nodes spanning the filter width and correspondingly decreases the spatial discretization error. Geurts [110] reports that between 4 and 6 nodes are required to produce a grid-independent solution. In practice most commercial CFD codes assume instead that $\Delta = h$, a choice which is largely driven by the high computational cost of increasing the SGS resolution: every doubling of the SGS resolution for a given filter width leads to a factor of 16 increase in the computational cost [111].

The classical approach to LES, and indeed most CFD practices, is to minimize numerical errors and construct models that approximate as accurately as possible physically realistic behaviour. Whilst this approach may be desirable, Geurts *et al*. [67, 89] and Brandt [83, 109] have shown in simulations using the Smagorinsky model and implicit filtering that numerical and modelling errors dynamically interact with each other. In trying to minimise the numerical error by increasing the SGS resolution, the accuracy of the LES solution can actually become worse. In the cases they examined the numerical and modelling errors partially cancelled each other out to the benefit of the overall results.

Meyers, Geurts and Baelmans [67, 110, 112, 113] have recently studied this phenomena in simple building block flows (mixing layers and homogenous turbulence) and have developed an approach to tune the Smagorinsky model constant in order to minimise the total error,

accounting for the fact that the grid will itself introduce some numerical error. The practical advantage of their approach is that if one is limited to a certain grid resolution, based on the computational cost of the simulations, it should be possible to tune the turbulence model to obtain the best accuracy. They also suggest that accurate results could be obtained faster by performing a number of simulations on a relatively coarse grid by optimising the turbulence model rather than just performing one LES using the finest grid possible. Their "optimum refinement strategy" was constructed on the basis that an exact solution was already known from a previous DNS, although they suggest that experimental data or theoretical predictions could be used in other cases. A methodology for generalising this to the case where reference DNS or experimental data is not available is given in Klein *et al*. [114].

The works discussed above show that it is not generally advantageous to minimise numerical errors by increasing the "SGS resolution". The quality of the LES predictions are, however, clearly linked to the resolution of the grid. Whilst the works of Geurts *et al*. [67, 110, 112, 113] have shown that there are complex interactions between numerical and modelling errors, and that using a finer grid can in some circumstances even degrade the solution, it is well established that an overly coarse grid will produce erroneous predictions. It should generally be the case that a finer grid should produce more reliable LES results and in the limit of a very fine grid, the results should tend to those of a DNS. The central issue that therefore needs to be addressed in the industrial context is how to determine when the LES grid used is sufficiently fine.

The following few sections describe a number of possible approaches that have been reported in the literature to assess grid resolution in LES. Following Celik *et al*. [59], these approaches can broadly be classified into four groups:

- Rules of thumb
- Techniques based on prior RANS results
- Single-grid estimators
- Multi-grid estimators

As the names suggest, single-grid estimators require one LES calculation while multi-grid estimators involve a number of LES calculations and usually some form of Richardson extrapolation.

3.3.1 Rules of Thumb for Plumes

The manual for the Fire Dynamics Simulator (*FDS*) [93] provides some rules of thumb for the appropriate grid resolution in modelling fire plumes that can be used to design the LES grid prior to undertaking any simulations. It suggests that the grid resolution can be assessed relative to the characteristic fire diameter, D^*, which is calculated from:

$$D^* = \left(\frac{\dot{Q}}{\rho_\infty c_p T_\infty \sqrt{g}} \right)^{2/5} \qquad (3.4)$$

where $\dot{Q}$ is the total heat release rate, ρ_∞ is the ambient density, T_∞ is the ambient temperature, c_p is the specific heat capacity and g is the gravitational constant. The *FDS* manual [93] reports that grid sensitivity studies have shown that reasonably accurate results are produced provided

that the ratio of D^* to the grid cell size, h, is sufficiently large, i.e. that there is a sufficient number of cells within the fire region. A small value of D^*/h indicates that the fire is under-resolved.

Although the *FDS* manual does not clearly state what constitutes the limits of "large" and "small" values of D^*/h, the inverse of this ratio has been investigated as an indicator of grid resolution in fire simulations by Ma & Quintiere [115]. They defined a resolution parameter, R^*, as:

$$R^* = \frac{\max(\delta x, \delta y, \delta z)}{D^*} \qquad (3.5)$$

where δx, δy, and δz are the grid cell dimensions. In various fire plumes, they found that the best predictions of the flame height were obtained with a resolution, R^*, of 0.05 (i.e. 20 cells spanning the characteristic fire diameter). A finer grid overpredicted the flame height and a coarser grid underpredicted it. Although these recommendations provide a useful starting point for the design of the computational grid, the results appear to have shown an undesirable degree of grid dependency.

Similar findings to those of Ma & Quintiere [115] were reported by Bounagui *et al*. [116]. A discussion of grid dependence in forced and natural convection flows is given by Smardz [117] and in small and large fires in enclosures by Petterson [118]. Further information can be obtained from the *FDS* validation website[29] and a discussion of grid-dependence issues in helium plumes is given in the works of Tieszen *et al*. [119, 120].

3.3.2 Turbulence Length Scales and Cell Size

Turbulence is often described using two characteristic length scales: the Kolmogorov and the integral length scales. The Kolmogorov length scale, η, relates to the smallest dissipative turbulent eddies while the integral length scale, L, is related to the largest eddies.

The cost of performing a steady RANS simulation is significantly less than performing an LES, usually by an order of magnitude or more. It is therefore not unreasonable for CFD practitioners to first investigate a flow by performing a steady RANS simulation before proceeding to try LES. One of the benefits of first performing a RANS simulation is that it can be used to provide an estimate of the turbulence length scales in the flow, which can help design the grid for the LES.

This approach was adopted in the work of Addad *et al*. [121] who examined a buoyancy-opposed wall jet flow. They designed their LES grid to have cells of width, h, between 2 and 5 times smaller than the turbulence length scale, l_m, in the main free-jet region of the flow. The turbulence length scale was calculated from the RANS model as follows:

$$l_m = c_\mu^{3/4} \frac{k^{3/2}}{\varepsilon} \qquad (3.6)$$

where $c_\mu = 0.09$, k is the turbulent kinetic energy and ε the dissipation rate. They based this choice of grid resolution on the earlier work of Baggett *et al*. [122] who suggested that modelling errors could be minimised by using an LES filter width of $\Delta \approx L_\varepsilon/10$, where L_ε is the

[29] http://www.fire.nist.gov/fds/, *accessed June 2008.*

integral dissipation length scale equal to $\left(\overline{u_i u_i}\right)^{3/2} / \varepsilon$. Near the walls, Addad *et al*. [121] reduced the cell size to around 10% of the value in the free-jet region.

A similar approach was tested in Van Maele & Merci's [123] recent simulations of tunnel fires using *FDS* and *Fluent*. They suggested that a suitable LES grid should have a filter width of $\Delta \approx l_I/12$, where the integral turbulence length scale was calculated from $l_I = k^{3/2}/\varepsilon$. This is equivalent to the larger of the grid sizes suggested in the earlier Addad *et al*. [121] study.

A more fundamental discussion on appropriate LES cell sizes as a function of the integral length scale was provided by Pope [15]. Based on analysis of homogeneous isotropic turbulence, it was shown that in order to resolve 80% of the turbulent kinetic energy, the filter width should be approximately 12 or 17 times smaller than the integral length scale, l_I, according to whether a sharp spectral cutoff or Gaussian filter was used.

Further analysis was provided by Jiménez & Moser [124], who showed that in simulations of a channel flow using the dynamic Smagorinsky model, good results could only be achieved if the subgrid shear stress represented a negligible fraction of the total stress. They showed that in order to have an error of 1% in the core of the channel away from the walls, the filter width should be 5 – 10% of the integral dissipation length scale.

A summary of the grid resolutions mentioned in the papers discussed above is given in Table 3.2.

Table 3.2 Ratios of the integral length scale $\left(k^{3/2}/\varepsilon\right)$ to the filter width (Δ) suggested in the literature.

Reference	$(k^{3/2}/\varepsilon)/\Delta$
Baggett *et al*. [122]	3.5
Jiménez & Moser [124]	3.5 – 7
Pope [15]	12 – 17
Addad *et al*. [121].	12 – 30
Van Maele & Merci [123]	12

Further analysis is provided in the literature comparing the LES filter width to the Kolmogorov turbulence length scale, which is calculated from:

$$\eta = \left(\nu^3 / \varepsilon\right)^{1/4} \qquad (3.7)$$

where ν and ε are the kinematic viscosity and turbulence dissipation rate. Celik *et al*. [58] recommended as a rough rule of thumb that the ratio of the filter width to the Kolmogorov length scale (Δ/η) should be less than 25, although they acknowledged that the value should be a function of the turbulence Reynolds number and the ratio of the filter width to the grid size (Δ/h). Pope [15] showed that in high-Reynolds-number turbulence most of the dissipation of turbulence energy occurred at length scales between 8 and 60 times the Kolmogorov length scale, and the demarcation between dissipative and inertial regions of the energy spectrum occurred at length scales of around 60η. In their recent simulations of an impinging jet, Hadžiabdić & Hanjalić [125] used four different meshes with a maximum spacing of approximately 21η. Despite using such fine grids their results still showed some sensitivity to the cell size. A summary of these grid resolutions is provided in Table 3.3.

Table 3.3 Ratios of the filter width (Δ) to the Kolmogorov length scale (η) suggested in the literature.

Reference	Δ/η
Celik *et al.* [58]	< 25
Pope [15]	~ 60
Hadžiabdić & Hanjalić [125]	< 21

The above approaches to assess the LES grid size based on predicted length scales from prior RANS simulations are also alluded to in the OECD Best Practice Guidelines for the Use of CFD in Nuclear Reactor Safety [13] where it notes: "As a general rule of thumb either the code logic or the user should ensure that 4 to 5 mesh cells are available to span (in each direction) the smallest eddy resolved by the Navier-Stokes solution."

A fuller discussion of near-wall grid resolution is given in Section 3.5.

3.3.3 Magnitude of the Subgrid-Scale Viscosity

It is useful to be able to assess whether the LES grid is sufficiently fine on the basis of just a single trial LES calculation. There are a number of suggestions for how this could be achieved in the literature. Celik *et al*. [59] refer to these methods as "single grid estimators". The simplest of these is the magnitude of the turbulent viscosity relative to the molecular viscosity, ν_t/ν.

Celik *et al*. [59] suggest that as a rough rule of thumb the ratio of effective viscosity to the molecular viscosity (ν_{eff}/ν) is approximately 20 for good LES and 1.0 for DNS, where ν_{eff} is the sum of the turbulent, numerical and molecular viscosities ($\nu_{eff} = \nu_t + \nu_{num} + \nu$). They do not define how to calculate the unknown numerical viscosity although they suggest that it could be estimated from the turbulent viscosity, since both terms should scale with the grid size. It will also be a function of the ratio of the filter width to grid size Δ/h. In an earlier paper, Celik *et al*. [58] suggested that numerical effects could be approximated as contributing 50% of the unresolved turbulent kinetic energy, i.e. $\nu_{num} = \nu_t$. They also noted that the ratio (ν_{eff}/ν) is dependent upon the Reynolds number. Based on analysis of homogeneous isotropic turbulence they show that for a high turbulence Reynolds number, Re_t, of 1200 the ratio (ν_{eff}/ν) would be approximately 20, while for a low Re_t of 300 the ratio (ν_{eff}/ν) would be 5. Here, the turbulence Reynolds number can be calculated from:

$$Re_t = \frac{k^2}{\nu\varepsilon} \qquad (3.8)$$

where k is the turbulent kinetic energy and ε the dissipation rate. In many LES results presented in the literature the value of the ratio (ν_t/ν) is presented. For example, in simulations of a plane jet and at Reynolds number of 4,000, Klein [101] obtained reasonably good predictions with (ν_t/ν) reaching a maximum of 3. In the recent impinging jet simulations of Hadžiabdić & Hanjalić [125] at a Reynolds number of 20,000 the maximum (ν_t/ν) was also around 3.

3.3.4 Relative Effective Viscosity Index

The Relative Effective Viscosity Index, *LES-IQ*$_v$, is another single grid estimator and one of a number of quality indices proposed by Celik *et al*. [58]. It is derived by comparing the LES grid resolution to the Kolmogorov length scale, and is calculated from:

$$\text{LES-}IQ_\nu = \frac{1}{1+\alpha_\nu\left(\frac{\nu_{eff}}{\nu}\right)^n} \qquad (3.9)$$

where constants α_v = 0.05 and n = 0.53 are derived from studying homogeneous isotropic turbulence. A value of *LES-IQ*$_v$ greater than 0.8 is suggested as indicating a good LES and a value greater than 0.95 a DNS. The effective viscosity is calculated from the sum of the model, numerical and molecular viscosities ($v_{eff} = v_t + v_{num} + v$). As mentioned previously, Celik *et al*. [58] suggested that based on an intuitive approximation the numerical dissipation could be considered as contributing to 50% of the total unresolved energy budget, i.e. $v_{num} = v_t$.

There are no actual applications of *LES-IQ*$_v$ shown in the works of Celik *et al*. [58, 59] although the theoretical variation of *LES-IQ*$_v$ with the ratio of the grid size to the Kolmogorov length scale and the viscosity ratio (v_{eff}/v) is presented for homogeneous isotropic turbulence.

3.3.5 Subgrid Activity Parameter

Another quality index loosely based on the magnitude of the turbulent viscosity is the "subgrid activity parameter", devised by Geurts & Fröhlich [89], which is defined as:

$$s = \frac{\overline{\varepsilon_t}}{\overline{\varepsilon_t} + \overline{\varepsilon_\mu}} \qquad (3.10)$$

where ε is the dissipation, subscripts μ and t refer to molecular and turbulent values respectively, and the overbar represents time-averaging. The molecular and turbulent dissipation are defined as:

$$\varepsilon_\mu = \nu S_{ij}\frac{\partial U_i}{\partial x_j} \quad ; \quad \varepsilon_t = -\tau_{ij}\frac{\partial U_i}{\partial x_j} \qquad (3.11)$$

where τ_{ij} is the SubGrid-Scale (SGS) stress, $\partial U_i/\partial x_j$ the velocity gradient, v the kinematic viscosity and S_{ij} the strain rate. Definitions of the strain rate and SGS stress are provided in Appendix A. Since the strain rate is a symmetric tensor ($S_{ij} = S_{ji}$), Equation (3.11) can be written:

$$\varepsilon_\mu = \frac{1}{2}\nu S^2 \quad ; \quad \varepsilon_t = \frac{1}{2}\nu_t S^2 \qquad (3.12)$$

where the strain invariant is $S = \left(2S_{ij}S_{ij}\right)^{1/2}$ and v_t is the subgrid-scale eddy viscosity. The subgrid activity can therefore be calculated from:

$$s = \frac{\overline{\nu_t S^2}}{\overline{(\nu + \nu_t) S^2}} \qquad (3.13)$$

No approximations have been needed in transforming Equations (3.10) and (3.11) into (3.13) but the latter is easier to calculate in commercial CFD codes which typically store S as part of the standard calculation procedure.

The subgrid activity parameter measures the importance of the subgrid scales in the flow. A value of s of zero indicates that the LES filter width is so fine that the modelled component is negligible and the simulation is in effect a DNS, while a value of one indicates that the simulation is a high Reynolds number LES, where the magnitude of the molecular dissipation is negligible in comparison to the modelled term. In tests where the grid size is varied independently of the filter width, Geurts & Fröhlich [89] and Brandt [109] showed that s is related primarily to the filter width Δ and shows little sensitivity to the grid resolution, h. Geurts [67] also suggested that simulations with $s < ½$, are operating in the dissipation range while $s > ½$ are operating in the inertial range.

Brandt [109] presented examples where the subgrid activity parameter was used to assess the grid resolution in a channel flow with turbulence Reynolds number $Re_t = 395$. Relatively coarse meshes with 52,000 and 175,000 cells produced peak subgrid activity values of 0.5 and 0.3 respectively.

Celik *et al*. [58] showed that the subgrid activity could be approximated as:

$$s = \frac{\nu_t}{\nu + \nu_t} \qquad (3.14)$$

and commented that since in most applied LES studies the turbulent viscosity is significantly larger than the molecular viscosity ($\nu_t \gg \nu$), the value of s will nearly always be close to unity. This was illustrated by a practical example of the wake behind a destroyer at a Reynolds number of the order 10^6, where the value of s was indeed nearly one. They argued that the definition of s is not sufficiently sensitive to the grid resolution and instead proposed a modified subgrid activity parameter, s^*:

$$s^* = \frac{\nu_t + \nu_{num}}{\nu_t + \nu_{num} + \nu} \qquad (3.15)$$

where ν_{num} is the effective viscosity introduced from the numerical scheme. The disadvantage of this expression is that ν_{num} cannot readily be determined, although Celik *et al*. [58] suggest that as a first approximation it can be taken as equal to the subgrid-scale eddy viscosity, ν_t. If this approach is taken, however, the modified subgrid activity parameter will be even closer to unity than the original version proposed by Geurts & Fröhlich [89].

3.3.6 Turbulence Spectra

Turbulence is composed of a range of spatial scales which are usually classified in order of size from large to small into: an energy containing range, an inertial subrange and a dissipation range [15]. The smallest scales are considered to be nearly isotropic and exhibit universal behaviour

while the large structures carry most of the turbulence energy. In an ideal LES, the grid is sufficiently fine to capture all of the energy containing range and part of the inertial subrange, but model the smaller eddies.

The universal behaviour of small scales in turbulent flows has been demonstrated in a number of complex flows including channels flows, boundary layers, jets and wakes behind cylinders and aircraft [15, 126, 127]. Typical experimental data are shown in Figure 3.8, where the horizontal axis is the wavenumber[30], κ, normalized with the Kolmogorov length scale, η, and the vertical axis is the streamwise energy $E_{11}(\kappa_1)$ normalised by $\left(\varepsilon\nu^5\right)^{1/4}$, where ε is the dissipation rate and v is the kinematic viscosity. The figure shows how the energy of the turbulence decreases as the eddies reduce in size. For $\kappa\eta > 0.1$ (the dissipation range) all of the experimental data points lie on a single curve, demonstrating the universal behaviour of high-wavenumber spectra. The inertial subrange extends from $\kappa\eta < 0.1$ where the data follow a line with constant slope of -5/3, i.e. $E_{11} \propto \kappa^{-5/3}$. The sloping region of the graph extends to higher energy for higher Reynolds number flows indicating a greater separation between large and small scales. The large energy-containing range is not universal and is specific to the large scales of the particular flow.

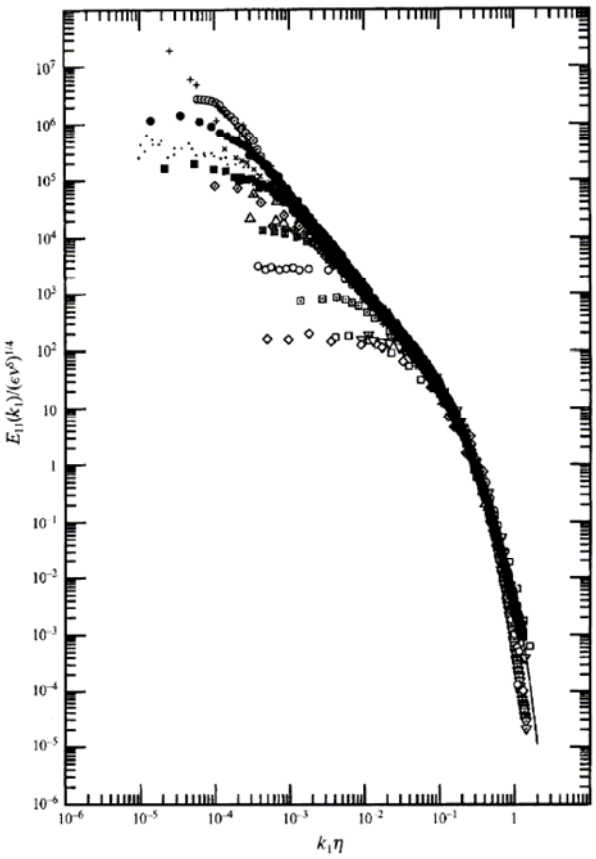

Figure 3.8 Kolmogorov's universal scaling for one-dimensional longitudinal power spectra compiled by Saddoughi & Veeravalli [74], reproduced with permission from Cambridge University Press.

[30] *The wavenumber is equivalent to a frequency but expressed in terms of distance instead of time, where* $\kappa = 2\pi / l$ *and l is the length scale of the wave.*

Similar graphs such as this are often produced in LES studies to examine the energy spectrum of the turbulence and investigate whether the flow is sufficiently well resolved. An example, shown in Figure 3.9, is taken from the studies of forced plumes by Zhou *et al*. [128, 129]. Similar examples are presented by Ilyushin & Krasinsky [130] for jets and Tutar *et al*. [131] for wakes. In each of these cases, it is demonstrated that the energy spectra at the smallest scales (highest wavenumber) exhibits a -5/3 power-law scaling.

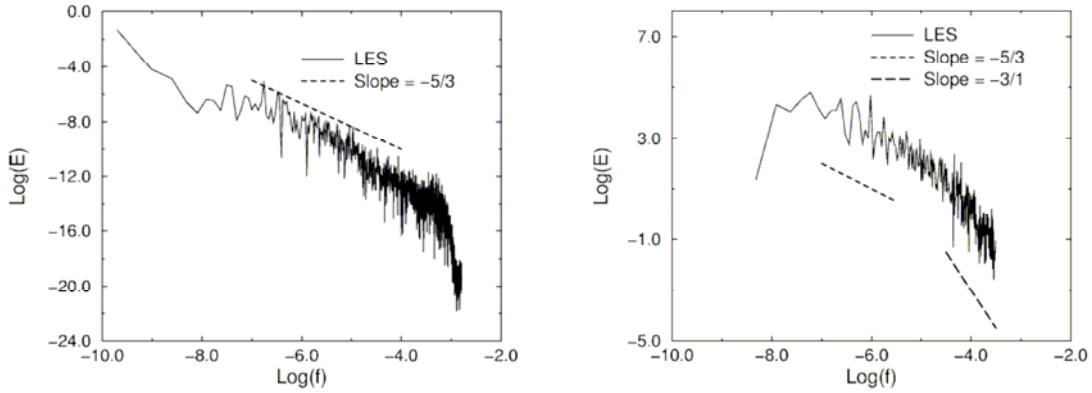

Figure 3.9 Temporal power spectra based on centreline velocity (left) and temperature (right) from the large-eddy simulations of plumes by Zhou *et al*. [76] (reproduced with permission from Elsevier)

Details of how to calculate the temporal power spectra are given in Appendix B. In practical terms, it requires the CFD program to store the relevant parameter such as a velocity component, temperature or concentration at a point in the flow at each time-step. The time-history is then processed to produce the energy spectrum using a short MatLab program, or if this is not available, one of the freeware equivalents, SciLab or Octave. A sample MatLab program is provided in Appendix B.

One of the limitations of the energy spectrum approach to assess LES grid resolution is that the separation of scales is related to the Reynolds number of the flow. The results shown in Figure 3.8 are for Taylor Reynolds numbers in the range 30 to 3,000 which corresponds roughly to bulk flow Reynolds numbers of between 500 and 10^6. At the lower end of this range there is considerable overlap between the energy containing and dissipation ranges, and the inertial range in effect disappears. Assessing grid resolution is therefore only possible using this approach at reasonably high Reynolds numbers, not in transitional flows.

To assess the separation of turbulence length scales and whether a distinct inertial subrange exists, Van Maele & Merci [123] calculated the ratio of the integral length scale ($l_I = k^{3/2} / \varepsilon$) to the Kolmogorov length scale $\left(\eta = \left(\nu^3 / \varepsilon \right)^{1/4} \right)$ in a tunnel fire using an initial RANS simulation. In their case, the ratio was smaller than 600 which was taken as implying that there was no fully-developed turbulent energy spectrum.

Mydlarski & Warhaft [132] have also shown that for Reynolds numbers of magnitude commonly experienced in indoor-air flows ($Re \approx 10{,}000$), the power-law exponent in the inertial subrange is reduced to around -3/2 instead of -5/3.

The slope of the concentration or temperature spectra is modified in buoyant flows. Various studies of buoyant plumes have shown that the slope in the inertial subrange may increase to -3

[133-135] (see Figure 3.9). Elicer-Cortés *et al*. [136] also identified three distinct regions in the spectra: a production region characterised by a slope of 2, a buoyancy-affected inertial subrange with slope of -3 and a dissipation region at very high frequencies with a slope of -7.

A further limitation of using the energy spectrum as a means of assessing LES grid resolution is that it cannot easily be used over the entire flow field to produce, for example, contour plots of grid resolution quality. Instead, it can only be determined at discrete points that need to be carefully chosen.

3.3.7 Resolved vs. Modelled Turbulent Kinetic Energy

In large-eddy simulations, the turbulent kinetic energy can be decomposed into three components: the turbulent kinetic energy from the resolved velocity fluctuations (k_{res}), the component from the subgrid-scale turbulence model (k_{sgs}) and the component that is damped or modelled implicitly by the dissipative numerical scheme (k_{num}):

$$k_{tot} = k_{res} + k_{sgs} + k_{num} \qquad (3.16)$$

It has been suggested that large-eddy simulations should aim to resolve at least 80% of the turbulence kinetic energy [15, 137]. One means of assessing the LES grid resolution is therefore to calculate the ratio of the resolved to the total turbulent kinetic energy, k_{res} / k_{tot}, and ensure that its value is maintained above 0.8.

The resolved turbulent kinetic energy, k_{res}, can be calculated by taking the square of the fluctuating velocity component in the three coordinate directions (*uu*, *vv* and *ww*) and averaging them over time to find the resolved Reynolds stresses $\overline{u^2}$, $\overline{v^2}$ and $\overline{w^2}$. These are then summed to calculate k_{res}, as follows:

$$k_{res} = \frac{1}{2}\left(\overline{u^2} + \overline{v^2} + \overline{w^2}\right) \qquad (3.17)$$

There is no generally accepted way to calculate the modelled turbulent kinetic energy, k_{sgs}, in LES using the Smagorinsky model. Three different proposed methods were examined by Gant [17]:

$$k_{sgs} = \frac{3}{2}\left(\frac{\nu_t}{\sqrt[3]{Vol}}\right)^2 \qquad (3.18)$$

$$k_{sgs} = 3.6\left(\frac{\nu_t S^2 (Vol)^{1/3}}{\pi}\right)^{2/3} \qquad (3.19)$$

$$k_{sgs} = \frac{l^2 S^2}{C_E} \qquad (3.20)$$

where *Vol* is the cell volume, *S* is the strain invariant, ν_t is the subgrid-scale eddy viscosity, C_E is a constant stress-energy ratio which is assumed to have a value of 0.3 and *l* is the Smagorinsky length scale ($l = C_s \Delta$, where C_s is the Smagorinsky constant). The first of these expressions (3.18) was derived by assuming that the turbulent viscosity is the product of a velocity and a

length scale, where the velocity scale is given by $\sqrt{2k_{sgs}/3}$ and the length scale Δ. The second (3.19) was taken from Pope [15] for an idealised LES of high Reynolds number turbulence with a sharp spectral cutoff, and the last (3.20) was from Mason & Callen [138]. It was shown in [17] that, assuming the Smagorinsky constant C_s was 0.1 and the filter width was twice the grid spacing ($\Delta = 2h$) these three formulae could be rearranged to give respectively:

$$k_{sgs} = 0.0006\Delta^2 S^2 \qquad (3.21)$$

$$k_{sgs} = 0.049\Delta^2 S^2 \qquad (3.22)$$

$$k_{sgs} = 0.033\Delta^2 S^2 \qquad (3.23)$$

Two further estimates for k_{sgs} were described by Klein [101]. The first of these was based on the work of Lilly [139]:

$$k_{sgs} = \frac{\nu_t^2}{(C_s\Delta)^2} \qquad (3.24)$$

where the Smagorinsky constant C_s was assumed to be 0.094. Based on the same assumptions as before, this is equivalent to:

$$k_{sgs} = 0.011\Delta^2 S^2 \qquad (3.25)$$

The second was to evaluate k_{sgs} from the trace of the subgrid-scale stress, τ_{ii}, evaluated from the scale similarity model:

$$k_{sgs}^{ssm} = \frac{1}{2}\tau_{ii} \qquad \text{with} \qquad \tau_{ij} = \langle U_i U_j \rangle - \langle U_i \rangle \langle U_j \rangle \qquad (3.26)$$

where $\langle\ \rangle$ indicates filtered quantities using a filter twice the width of the computational grid.

These two approaches were used by Klein [101] to estimate the fraction of the turbulent kinetic energy modelled from:

$$\frac{k_{res}}{k_{tot}} = \frac{k_{res}}{k_{res} + k_{sgs}} \qquad (3.27)$$

The first approach (3.24) was found to consistently underpredicted k_{sgs} whilst the second (3.26) overpredicted k_{sgs} in both *a priori* and *a posteriori* tests of a plane jet flow using three different grids. The errors with the first approach were so great that even changing the value of C_s within a reasonable range could not significantly improve the results. The data from Klein [101] was re-analysed by Celik *et al.* [59] using Equation (3.24) assuming[31] $C_s = 0.05$. It was found that in the fully-developed turbulent region of a plane jet using a fine grid, the modelled turbulent kinetic energy was approximately 10% of the resolved turbulent kinetic energy ($k_{sgs} \approx 0.1\ k_{res}$).

[31] *There appears to be an error in Celik et al. [59], Equation (17) which has k_{sgs} instead of ν_t.*

In another example, Kempf *et al*. [140] used Equations (3.24) and (3.27) to estimate the fraction of the turbulent kinetic energy modelled in a bluff-body stabilized non-premixed flame. The results indicated that 84% of the total turbulence energy was resolved. The authors noted that although this did not provide proof of adequate grid resolution it was still useful for comparison purposes.

The difficulties described above in calculating the modelled turbulent kinetic energy can be avoided if, rather than using the Smagorinsky model, an alternative turbulence model is used which solves a transport equation for the subgrid-scale turbulent kinetic energy, k_{sgs}, for example, the one-equation model of Krajnović & Davidson [141].

The SST-based DES model used in Section 4 also solves a transport equation for the turbulent kinetic energy, k, in addition to one for the eddy frequency, ω. Using this model, certain parts of the flow are resolved in "LES mode" and other parts in "RANS mode" (see discussion in Section 3.5). In the LES region, the modelled k can be interpreted as the subgrid-scale value, k_{sgs}, whilst in the steady RANS region k accounts for the turbulent kinetic energy across all scales.

There are two main drawbacks to using the ratio of the resolved to the total turbulent kinetic energy to assess LES quality. Firstly, the approach assumes implicitly that as the grid is refined the proportion of turbulent kinetic energy resolved increases until it reaches a value of 100%, when the LES becomes essentially a DNS. However, it has been shown that in some cases the resolved turbulent kinetic energy actually decreases as the grid is refined. This implies that the resolved turbulent kinetic energy is not a reliable indicator of grid resolution. Secondly, the approach does not account for the numerical dissipation which in many situations is of the same order or even larger than the modelled dissipation.

3.3.8 Richardson Extrapolation Methods

Systematic grid convergence studies are commonly used in steady RANS simulations and are probably the most reliable ways of assessing numerical uncertainty [19].

Richardson extrapolation is based on representing the CFD solutions as a Taylor series expansion on the grid spacing, h:

$$\phi = \phi_{exact} + g_1 h + g_2 h^2 + g_3 h^3 + ... \qquad (3.28)$$

For a second-order numerical method, such as the central differencing scheme commonly adopted in LES, $g_1 = 0$. At its simplest level, Richardson extrapolation involves running two simulations with different grid spacings, h_1 and h_2, and using these to obtain a more accurate estimation of ϕ. For a simulation using second-order numerical discretization, the solutions are assumed to be represented sufficiently accurately by the truncated expressions:

$$\phi_1 = \phi_{exact} + g_2 h_1^2 \qquad (3.29)$$

$$\phi_2 = \phi_{exact} + g_2 h_2^2 \qquad (3.30)$$

where there are two unknowns (ϕ_{exact} and g_2) and two equations. The equations are rearranged to obtain an estimate of ϕ_{exact} from:

$$\phi_{exact} = \frac{h_2^2 \phi_1 - h_1^2 \phi_2}{h_2^2 - h_1^2} \tag{3.31}$$

or alternatively:

$$\phi_{exact} = \phi_1 + \frac{\phi_1 - \phi_2}{r^2 - 1} \tag{3.32}$$

where r is the refinement ratio given by $r = h_2 / h_1$. There is a lengthy discussion on Richardson extrapolation and the order of accuracy of the approximations in the book by Roache [19]. The approach is only appropriate if the numerical error decreases monotonically with the grid spacing, h. This assumption is not valid for coarse meshes where the numerical errors are not in the asymptotic range of grid spacing, and possibly other situations. Richardson extrapolation can be applied to both field values (e.g. mean velocity, temperature) and parameters such as the lift coefficient or gas cloud size. Since it is a simple extrapolation, the resulting value of ϕ_{exact} may not satisfy certain constraints such as boundedness.

In most situations, Richardson extrapolation is not used to improve upon the actual predictions but instead used to help identify the level of grid convergence of the solution. The relative error between grids 1 and 2 is defined as:

$$\varepsilon = \frac{\phi_2 - \phi_1}{\phi_1} \tag{3.33}$$

and the estimated fractional error:

$$E_1 = \frac{\varepsilon}{r^p - 1} \tag{3.34}$$

where p is the order of the numerical scheme. The Grid Convergence Index (GCI) is used to relate the error obtained from Equations (3.33) and (3.34) to the error that would be expected from a doubling of the grid with a second-order method (where r = 2 and p = 2). For the same estimated fractional error, the relative error or GCI is calculated from:

$$GCI = F_s \frac{\varepsilon}{r^p - 1} \tag{3.35}$$

where F_s = 3. This can alternatively be written:

$$GCI = F_s \left| \frac{\phi_{ext} - \phi_1}{\phi_1} \right| \tag{3.36}$$

In deriving the GCI, the choice of a doubling of the grid and second-order accurate approach which leads to the F_s "factor of safety" value of 3 is somewhat arbitrary. Roache [19] recommended the value as being suitable for grid convergence studies using only two grids but suggested that to avoid over-conservatism a lower value of 1.25 could be used for carefully performed grid convergence studies involving three or more grids. The GCI is a relative error and typically for reasonably well-resolved meshes it should have a value of a few percent.

If three grids are used (coarse, intermediate and fine), the GCI can be calculated from the coarse to the intermediate (GCI_{12}), and from the intermediate to the fine (GCI_{23}). If the grids are within the asymptotic range the following relation should hold:

$$GCI_{12} = r^p GCI_{23} \tag{3.37}$$

With three or more solutions on different grids, a more accurate estimate of the extrapolated value can also be obtained from cubic splines or approximate error splines to calculate the GCI [56, 57].

Celik & Karatekin [142] proposed a similar measure to the GCI called the Extrapolated Relative Error (ERE), given by:

$$ERE = \left| \frac{\phi_{ext} - \phi_1}{\phi_{ext}} \right| \tag{3.38}$$

Examples of GCI and ERE error estimators being used in URANS and DES simulations are given in Celik *et al*. [59]. Further examples of Richardson extrapolation being applied specifically for the resolved turbulent kinetic energy in LES are discussed below.

3.3.9 LES "Index of Quality"

The "LES Index of Quality", *LES-IQ*$_k$, proposed by Celik *et al*. [58] is based on the same principle of assessing the proportion of turbulent kinetic energy resolved as examined in Section 3.3.7 but estimates the total turbulent kinetic energy from Richardson extrapolation. To find the *LES-IQ*$_k$ requires two or more LES solutions on different grids.

The *LES-IQ*$_k$ proposed by Celik *et al*. [58] is calculated from:

$$LES\text{-}IQ_k = \frac{k_{res}}{k_{tot}} = \frac{k_{res}}{k_{res} + a_k h^p} \tag{3.39}$$

where k_{res} is the resolved kinetic energy, k_{tot} is the total kinetic energy, h is the grid size, a_k is a constant to be determined and p is the order of accuracy of the numerical scheme. The necessary steps in order to calculate *LES-IQ*$_k$ are as follows:

1. Perform LES calculations using two separate grids: coarse and fine. Hereafter subscript "1" refers to coarse mesh results and subscript "2" to fine mesh results.

2. Calculate the resolved turbulent kinetic energy with both grids, i.e. find k_1^{res} and k_2^{res}, from Equation (3.17).

3. Calculate the characteristic grid cell dimension, h, for both grids. For structured meshes using:

$$h = \sqrt[3]{(\Delta x \Delta y \Delta z)} \tag{3.40}$$

where Δx, Δy and Δz are the cell dimensions, and for unstructured meshes:

$$h = \sqrt[3]{(Vol)} \tag{3.41}$$

where Vol is the cell volume.

4. Calculate the *LES-IQ*$_k$ on the fine grid from:

$$LES\text{-}IQ_k^f = \frac{1}{1+\left(1-\frac{k_1^{res}}{k_2^{res}}\right)\left[\frac{1}{\left(\alpha^p-1\right)}\right]} \tag{3.42}$$

and on the coarse grid from:

$$LES\text{-}IQ_k^c = \frac{1}{1+\left(\frac{k_2^{res}}{k_1^{res}}-1\right)\left[\frac{\alpha^p}{\left(\alpha^p-1\right)}\right]} \tag{3.43}$$

where $\alpha = h_1/h_2 > 1$ is the ratio of the grid-cell dimensions on the coarse and fine meshes and p is the order of accuracy of the numerical scheme (in most cases, $p = 2$).

In most commercial CFD codes, the filter width, Δ, is assumed to be equal to the grid size, h. If an alternative approach is used, such as that proposed by Geurts & Fröhlich [89], the total turbulent kinetic energy must be calculated using Richardson extrapolation on both Δ and h, requiring three separate simulations with different grid sizes and filter widths.

Celik *et al*. [58] also presented formulae for determining *LES-IQ*$_k$ in which the total turbulent kinetic energy is obtained from DNS or experiments instead of Richardson extrapolation. This approach was used to help judge whether Richardson extrapolation provided a sufficiently accurate means of assessing this quantity.

The *LES-IQ*$_k$ criteria was initially tested in six cases by Celik *et al*. [58] including: flow around a square cylinder, a turbulent mixing layer, channel flow, ship wake flow, surface piercing flat-plate boundary layer and a vertical buoyant jet flow. In all of these cases, the *LES-IQ*$_k$ gave results in accord with the anticipated results, i.e. when grids were used that were known to well resolve the flow the *LES-IQ*$_k$ was of the order 80 – 95%. There was also good agreement between the *LES-IQ*$_k$ based on Richardson extrapolation and that calculating using the total turbulent kinetic energy from experiments. However, further tests by Celik *et al*. [59] found that *LES-IQ*$_k$ gave overly optimistic results in a shear layer with forced excitation at the inlet. The *LES-IQ*$_k$ was around 80 – 90% while the actual results appeared to show strong grid dependence.

In the mixing layer tests, Celik *et al*. [58] found that the resolved turbulent kinetic energy from the LES exceeded that of the DNS. This is contrary to the anticipated behaviour of LES where the additional model and numerical dissipation is expected to damp the velocity fluctuations and lead to a lower resolved turbulent kinetic energy than in the DNS. Celik *et al*. [58] also found other examples of similar behaviour in the literature and noted that in their channel flow tests near the wall, the coarse-grid k_{res} exceeded the fine-grid and DNS values. A discussion of this anomalous behaviour was provided in the Appendix to their paper [58] where Jordan noted that in the wake of bluff bodies the peak turbulence intensities from LES can be twice the correct values. Klein [101] also reported this behaviour in a plane jet and channel flow.

A number of explanations for the cause of k_{res} exceeding the true turbulent kinetic energy are discussed by Celik *et al.* [58]. It was noted that insufficient resolution in channel flows can lead to the slope of the mean velocity profile adjacent to the wall being poorly predicted, which can cause inaccuracies in the calculated pressure gradients which have a knock-on effect on the strain rates and hence the turbulence kinetic energy. Errors are convected and diffused, which can lead to changes in the flow behaviour, for example changing the location of transition, separation or reattachment locations in complex flows. This is further complicated when hybrid RANS/LES models are used, where the location of the RANS and LES regions may also change as the grid is refined.

To account for the fact that k_{res} may be larger than the DNS turbulent kinetic energy, Celik *et al*. [58] proposed a correction to the formula for *LES-IQ*$_k$:

$$LES\text{-}IQ_k = 1 - \frac{\left|k_{tot} - k_{res}\right|}{k_{tot}} \qquad (3.44)$$

In regions where the k_{res} is less than k_{tot} this reverts to the original equation for *LES-IQ*$_k$, see Equation (3.39).

A further limitation of *LES-IQ*$_k$ was identified by Klein [101], who showed that it appeared to produce misleading results near to the orifice in a plane jet flow. Here the *LES-IQ*$_k$ gave unrealistically low values where it was known that the grid was resolving 80% of the turbulent kinetic energy. Klein suggested that this behaviour was a consequence of the turbulent kinetic energy being very low in this region of the flow, so that small changes in k_{res} produced significant shifts in *LES-IQ*$_k$. It was therefore recommended that *LES-IQ*$_k$ should not be used for laminar or transitional flows.

3.3.10 Grid and Model Variation

Klein [101] proposed an alternative approach to the LES Index of Quality, also based on Richardson extrapolation, where instead of just refining the grid, both the grid and the effect of the subgrid scale model are varied. The approach is based on the principle that the difference between the mean velocity field from an LES and the exact solution can be approximated by:

$$u_\Delta - u = c_n h^n + c_m \Delta^m + O\left(\Delta^{n+1}, \Delta_S^{m+1}\right) \qquad (3.45)$$

where n is the order of the numerical method, m is the order of the modelling error, h is the grid size, Δ is the filter width, u_Δ is the mean LES solution, u is the exact solution and c_n and c_m are constants. The first term on the right-hand-side, $c_n h^n$, is the first-order numerical error, and the second term, $c_m \Delta^m$, is the first-order SGS model error. The above decomposition is based on a Taylor series expansion where it is assumed that the numerical and modelling errors are independent.

In Klein's approach, the higher order error terms are ignored and it is assumed that the SGS model acts like a second-order dissipation term so that, with a second-order accurate numerical scheme, $n = m = 2$, thereby requiring just three simulations to produce an estimate of the errors[32]. The three simulations involve a standard calculation, a repeat of the standard

[32] *In a later publication from the same group, Celik et al. [59] recommended that a value of 2/3 be used for the exponent m, although they also noted that a higher value could be used for moderate Reynolds number flows.*

calculation with the effect of the subgrid model reduced by a factor α (i.e. reducing Δ)[33] and a repeat of the standard calculation with the grid size reduced by a factor β (i.e. reducing h). This leads to three versions of Equation (3.45):

$$u_1 - u = c_n h^n + c_m \Delta^m \quad (3.46)$$

$$u_2 - u = c_n h^n + c_m (\alpha\Delta)^m \quad (3.47)$$

$$u_3 - u = c_n (\beta h)^n + c_m \Delta^m \quad (3.48)$$

These three simultaneous equations are then solved for the three unknowns, u, c_n and c_m. Klein [101] reduced both the model contribution and the mesh size by a factor of two. In some circumstances reducing h by a factor of two in all directions could lead to an overly coarse mesh and a smaller change may be more appropriate.

Encouraging results were obtained by Klein [101] in channel flows where the approach indicated that errors were highest near the wall which coincided with the region where the LES predictions showed poor agreement with DNS data. In a plane jet flow, analysis of the error contributions indicated that the numerical and model errors were of similar magnitude but opposite sign which was in agreement with previously published analyses.

The grid and model variation approach was tested independently by Brandt [83, 143] in a fully-developed channel flow. Brandt compared the error estimated from Klein's approach against the actual error by comparing LES to DNS results. This showed that the error estimated from the grid and model variation was significantly different from the true error. Different meshes were tested to see whether this was the cause of the problem, but this did not resolve the issue. Further simulations were performed in order to estimate the order of the numerical and modelling errors (terms n and m). These showed that while m was approximately 2 in the fully-turbulent log-law region of the flow, closer to the wall in the viscous sublayer the term underwent significant change, varying between -2 and 4. Furthermore, the order of the numerical error, n, varied from 4 near the wall to -8 in the buffer layer and -4 in the log-law region. This was taken to indicate that for the particular grid resolution used, the accuracy of the numerical scheme could not be described by just the first term in the Taylor series expansion, i.e. the resolution was not in the asymptotic range.

Overall, Brandt [83, 143] concluded that despite the promising results shown by Klein, the use of Richardson extrapolation in LES is not straightforward and its accuracy is highly dependent on the applied grid resolution. The work also raises similar questions over the accuracy of the LES Index of Quality proposed by Celik *et al*. [58] which uses a Richardson extrapolation based on turbulent kinetic energy.

3.3.11 Summary

Table 3.4 provides a short summary of each of the approaches for assessing grid resolution described above together with their advantages and disadvantages. Approaches numbered 3 – 7 are single-grid estimators requiring just one LES calculation while approaches 8 – 10 are multi-grid estimators requiring several LES calculations.

---

[33] *Klein [101] actually controlled directly model contribution, $(C_s\Delta)^2$, instead of the filter width, Δ, but the two are equivalent except for the power of α in Equation (3.47). The approach presented here is taken from Brandt [83].*

Another single-grid estimator which is not included in this list was published very recently by Kuczaj & Komen [144]. In large-eddy simulations of turbulent mixing in a T-junction, they found that results were grid-independent provided that the cell size was of the order $\lambda/3$, where λ is the Taylor microscale.

Table 3.4 Summary of the advantages and disadvantages of grid quality measures

Ref.	*Grid Quality Measure*	*Advantages*	*Disadvantages*
1	Rules of thumb for grid resolution in plumes (Section 3.3.1)	• Provides basic guidance on mesh resolution for plumes	• Recommendations largely anecdotal based on using just one CFD code, *FDS* • Does not account for LES model used or discretization errors directly
2	Ratio of grid size to the integral length scale or Kolmogorov length scale (Section 3.3.2)	• Cheap and easy to compute from prior RANS simulation • Can be used to generate grid before running LES	• Accuracy of RANS length scales uncertain • Some dispute over recommended ratios • Does not account for LES model or discretization errors • Cannot be used in transitional or laminar regions
3	Ratio of turbulent to laminar viscosity, ν_t/ν (Section 3.3.3)	• Easy to compute • Provides initial estimate of quality based on performing just one LES	• Recommended ratio is dependent on the Reynolds number • Does not account for effects of numerical dissipation
4	Relative effective viscosity index, $LES\text{-}IQ_\nu$ (Section 3.3.4)	• Provides initial estimate of quality based on performing just one LES	• Few examples of its application in the literature • Assumes effect of numerical dissipation is the same as modelled dissipation
5	Subgrid Activity Parameter, s (Section 3.3.5)	• Shows importance of subgrid scales in the flow • Requires just one LES	• Requires calculation of additional time-averaged parameters • Relatively insensitive to grid resolution, in many cases $s \approx 1$ • Depends on Reynolds number
6	Turbulence Spectra (Section 3.3.6)	• Identifies the range of resolved turbulence scales directly • Involves identifying the inertial subrange with -5/3 slope.	• Complex to calculate • Only "spot" values calculated, not a field so difficult to use to help design grid. • Problems with no distinct inertial subrange at low Reynolds number • Slope of temperature or concentration spectra modified in buoyancy affected flows

Table 3.4 (cont.) Summary of the advantages and disadvantages of grid quality measures

Ref.	*Grid Quality Measure*	*Advantages*	*Disadvantages*
7	Ratio of resolved to total turbulent kinetic energy, k_{res} / k_{tot} (Section 3.3.7)	• Shows the proportion of turbulence energy is resolved • Requires just one LES	• Requires calculation of additional time-averaged parameters • Does not account for discretization errors • Underlying assumption that $k_{tot} > k_{res}$ is incorrect in some flows
8	Grid convergence index (GCI) and extrapolated relative error (ERE) (Section 3.3.8)	• Can be used to assess grid-sensitivity of any parameter of interest • Approaches well documented	• Requires two or more simulations on different grids • Reliability depends on grid resolution being within asymptotic range • Debate over appropriate "factor of safety" in GCI
9	Index of Quality, *LES-IQ*$_k$ (Section 3.3.9)	• Uses Richardson extrapolation to determine how much turbulent kinetic energy is resolved. • Reasonably good accuracy reported in some flows	• Requires two or more LES on different grids • Assumes effects of numerical errors second order • Problems associated with $k_{tot} < k_{res}$ in some flows • Reliability depends on grid resolution being within asymptotic range • Ratios of the cell size on different grids can be discontinuous • Possibility of obtaining values greater than 100% and negative values
10	Grid and Model Variation (Section 3.3.10)	• Accounts for model and numerical errors independently	• Requires three or more LES using two different grids • Problems associated with $k_{tot} < k_{res}$ in some flows • Reliability depends on grid resolution being within asymptotic range

3.4 LES MODEL CHOICE

There does not yet exist a universal LES model to account for the effect of the unresolved subgrid-scale (SGS) turbulence on the resolved scales in LES that provides unsurpassed accuracy in all flows. Instead there is a range of SGS models of different complexity that perform better or worse in different flows and have their own advantages and disadvantages in terms of simplicity, accuracy and economy. To provide a full discussion of the merits of all the different SGS models would be a significant undertaking in itself and several recent reviews have been carried out [15, 66, 67, 145]. The majority of industrial LES studies currently use two relatively simple SGS models: the standard and dynamic forms of the Smagorinsky model.

These two models are available in most commercial and industrial CFD codes. Details of the standard Smagorinsky model are presented briefly for reference in Appendix A.

Experience with RANS models has shown that industrial CFD users are very reluctant to adopt more complex turbulence models, even when these have been shown to outperform simpler models in some flows. For example, the standard k-ε RANS model which was developed in the 1970's [146, 147] is still in widespread use today, despite the fact that it is well known to produce anomalous behaviour near stagnation points [148, 149] and has significant shortcomings in flows involving rotation, flow curvature and boundary layer separation [150, 151]. It seems likely therefore that industrial users will continue to use the standard and dynamic Smagorinsky models for the foreseeable future. Hybrid RANS-LES models are discussed separately in Section 3.5.

The primary issue for industrial LES users is therefore to identify the shortcomings of the common standard and dynamic Smagorinsky models and understand their accuracy limitations in different flows. There is a huge amount of information on this subject in the literature, which includes hundreds of examples of the models applied to different flows (e.g. [68-73]). Despite this wealth of information, there are difficulties in collating and interpreting the LES results, not least because there is no generally accepted guidance on numerical errors and grid resolution unlike with RANS models (see Section 2). It is therefore often unclear whether the poor performance of a model in one flow is a consequence of inadequate grid resolution, numerical errors or the model itself. This issue was also highlighted in the findings from the Rottach-Egern workshop on LES of bluff body flows [152].

Notwithstanding these difficulties, a number of shortcomings of the standard and dynamic Smagorinsky models have been documented over the last 20 years, which are described briefly below. This is not intended to be an exhaustive discussion, for more detail see for example Pope [15], Sagaut [66], Geurts [67] or the succinct discussion in Park & Mahesh [153].

3.4.1 Dissipation and the Smagorinsky Coefficient

The standard Smagorinsky model [154] is generally recognised as being overly dissipative, i.e. it damps too great a proportion of the velocity fluctuations. To overcome this problem, the model constant, C_s, is often reduced from the value of 0.17, which was determined in *a priori* tests with homogeneous turbulence [155], to a value of 0.1, which has been shown to produce good results in channel flows [156] and mixing layers [89]. Moin & Kim [157] used a value as low as 0.065 in their early channel flow work. Most commercial CFD codes use a default value of C_s = 0.1, although the Fire Dynamics Simulator (*FDS*) code from NIST[34] uses C_s = 0.2. Using the commercial code *Star-CD,* Addad [158] showed that it was appropriate to decrease the model constant to a value of 0.0594 in order to compensate for the effects of numerical dissipation.

In a laminar flow, the unresolved turbulent SGS stress should be zero. The standard Smagorinsky model does not produce this result unless C_s is manually set to zero. This means that the model should not be used in transitional flows where there are both laminar and turbulent regions [159]. Moreover, C_s must be modified near walls in order to capture the correct asymptotic behaviour, where the turbulent shear stress should vary with the cube of the wall distance and decay to zero in the viscous sublayer. Commonly a correction is made to the Smagorinsky model in the form of van Driest damping function (e.g. [157]). Near-wall damping

[34] http://www.fire.nist.gov/fds, *accessed April 2008.*

functions are usually included by default in commercial and industrial CFD codes, with the exception of *FDS*.

The problems associated with setting ad-hoc values of the Smagorinsky coefficient and near-wall damping functions are overcome with the dynamic Smagorinsky model [160-162] which calculates an appropriate value of the model coefficient based on the local flow field. It correctly predicts C_s to be zero in laminar flows and obtains the cubic shear stress distribution near walls without any special near-wall treatment.

3.4.2 A Priori Tests and Physical Modelling

The standard and dynamic Smagorinsky models perform poorly in *a priori* tests [163]. The models both assume that the subgrid stress is perfectly correlated with the resolved strain rates, but in real flows this correlation is weak. The dynamic model also assumes scale invariance in the inertial range, but in low Reynolds number flows there is no well-defined inertial range. Jiménez & Moser [124, 164] provided a detailed discussion of the performance of the dynamic Smagorinsky model and examined its performance in both *a priori* and *a posteriori* tests. They noted that despite the poor *a priori* performance, the model performs well in *a posteriori* tests. They attributed this good performance to the fact the dynamic model automatically corrects the simulation when there is an accumulation of energy at high wavenumbers (i.e. small length scales) and thus prevents the pile-up of energy contaminating the resolved larger scales. Because of this built-in sensor, the model was reported to be relatively robust in how it responds to errors in the physics. They also noted that although the model provides a relatively poor representation of some of the physics, provided that a sufficiently fine grid is employed the effect of the model on the stresses and hence the resolved velocity field should be limited.

3.4.3 Backscatter

The classical view of turbulent flows involves a cascade of scales with large eddies breaking-up into smaller and smaller eddies which are eventually dissipated by the action of viscosity. This view is consistent with the mean flow behaviour. On an instantaneous level, however, there are times when locally the cascade works in reverse, a process known as “backscatter”, where energy is fed from smaller to larger scales. The standard Smagorinsky model only accounts for energy transfer from the resolved to the modelled scales and does not account for any backscatter effects. The absence of backscatter in the model is also partly responsible for the poor results in *a priori* tests [15, 67]. The dynamic model is, however, able to account for some backscatter effects although this depends upon the approach taken to smooth the model constant (see below). It is not clear how significant the effects of modelling backscatter are on the mean flow predictions. DesJardin *et al*. [165] commented that backscatter may be important for laminar to turbulent transition. For further information, see Piomelli *et al*. [166] or da Silva & Métais [167].

3.4.4 Averaging and Clipping the Dynamic Model Constant

As noted above, due to the way in which the dynamic model constant is calculated, it can become negative or take very large values. Negative values are sometimes interpreted as modelling the effects of backscatter but can seriously compromise numerical stability. To overcome these problems, it is common practice to average the constant over space or time, or

limit its minimum value such that the effective viscosity ($\nu + \nu_t$) is always positive. Spatial averaging is often applied in directions of local flow homogeneity if these exist, for example in planes parallel to the wall in channel flow. Temporal averaging can take the form of under-relaxation between values at one time-step and the next (e.g. see Addad [158]).

In most industrial flows, the geometry is complex and there are rarely directions of flow homogeneity, so spatial averaging cannot easily be performed. Unfortunately, not all studies reported in the literature provide details of the particular approach taken to stabilise the dynamic model which can make direct comparisons difficult. A model has been developed which avoids the difficulties associated with not having directions of spatial homogeneity by averaging over local flow path-lines [168], but this has not yet become widely used.

3.4.5 Marginal Resolution

The Smagorinsky models are based on the premise that the unresolved turbulent scales are isotropic and that the production and dissipation of turbulent kinetic energy are in balance, a condition known as local equilibrium. This is true provided that the grid is sufficiently fine and the unresolved scales are within the inertial subrange, but in many industrial applications of LES the grid resolution is likely to be marginal at best. More sophisticated SGS models attempt to account for the structure of the unresolved turbulent scales with some solving additional transport equations to account for the non-local-equilibrium effects. For details, see [66, 167].

A number of the limitations described above for the standard and dynamic Smagorinsky models have been addressed in alternative SGS models. Vreman [169] has developed a model which is no more complicated than the standard Smagorinsky model yet which correctly reduces the SGS stress near-walls and in transitional regions and does not require any clipping procedures to maintain numerical stability. Similarly, the Wall-Adapting Local Eddy-viscosity (WALE) model of Nicoud & Ducros [170] is relatively simple to implement and reproduces the correct near-wall behaviour.

3.5 WALL TREATMENTS AND HYBRID RANS/LES MODELS

One of the greatest challenges that must be overcome if the use of LES is to become more widespread in industrial CFD is the issue of turbulent flows near solid boundaries. The size of turbulent eddies decreases near walls and their structure becomes more anisotropic, exhibiting characteristic streaks, bursts and hairpin vortices [171, 172]. In order to continue to resolve 80% of the turbulence energy near walls, the size of the grid cells must be decreased significantly. Typically, the recommendations are for cell sizes in terms of wall units[35] of (x^+, y^+, z^+) < (100, 2, 20) in the (streamwise, wall-normal, spanwise) directions [173, 174]. Recent work by Hadžiabdić & Hanjalić [125] has shown that in complex flows involving flow impingement, these guidelines may be overly optimistic and smaller cell sizes may be necessary. In their studies, they found that even with cell sizes of $y^+ < 1$, the results exhibited grid sensitivity.

[35] *The wall unit is a length scale based on the local friction velocity and viscosity which is commonly used to non-dimensionalise length scales near walls. The wall unit is calculated from ν / U_τ, where ν is the kinematic viscosity and U_τ the friction velocity. Length scales made dimensionless in this way are usually given the superscript '+', for example: $y^+ = y\, U_\tau / \nu$.*

In some situations it may be critically important to resolve the unsteady fluctuations near solid surfaces, for example to model the effect of riblets used for drag reduction on ship hulls. However, in many other situations it may not be important to resolve the unsteady fluctuations within the boundary layer in order to predict the overall flow behaviour. In these cases, simplifications can be adopted to reduce the computational expense of wall-resolving LES.

There are two main approaches commonly used with LES to reduce the cost of resolving the fine-scaled structure of turbulent boundary layers: wall functions and hybrid RANS-LES. The wall function approach uses empirically derived profiles of velocity (and temperature, where relevant) to approximate the flow behaviour near the wall. The near-wall grid is relatively coarse, with wall-adjacent cells sizes typically in the range $10 < y^+ < 100$. Calculations using wall functions are typically one or two orders-of-magnitude faster to compute than comparable calculations using the wall-resolution approach. However, the assumed profiles used in wall functions are only valid for flows close to equilibrium, such as plane channel flows and zero-pressure gradient boundary layers. For more complex flows involving flow impingement, boundary layer separation and buoyancy effects, wall functions may give erroneous results [175].

Hybrid RANS-LES models are currently the subject of much research interest. The aim of these approaches is to model the near-wall regions using RANS and use LES in the core of the flow away from walls. Rather than specify the RANS and LES zones manually, most models switch automatically between the two zones based on the ratio of the turbulent length scales to the grid size or wall distance. The grid resolution and time-step constraints are less stringent for hybrid models than for wall-resolving LES which provides significant savings in computing times, but there are significant difficulties to overcome in matching the LES and RANS solutions at zone boundaries.

Commercial and industrial CFD codes commonly include variants of the most popular hybrid RANS-LES model called Detached-Eddy Simulation (DES) [176] or variants upon it, such as SST-based DES model [177] and the Delayed Detached-Eddy Simulation (DDES) model [178].

The quality issues for hybrid RANS-LES are similar to those discussed above for pure LES models, particularly with respect to grid resolution in the LES region of the flow domain. Additional quality issues for hybrid models include the extent of the RANS and LES regions, the behaviour of the models in the transitional RANS/LES region, and the asymptotic behaviour of the RANS and LES models. Commonly, upwind-biased numerical schemes are used in the RANS region and central differencing in the LES region. Different approaches may be taken to switch the numerical scheme from those used to switch the turbulence model, which introduces some further quality concerns.

Hybrid RANS-LES modelling is still evolving rapidly and readers are recommended to review the recent literature. The results from a number of case studies are provided in recent conference proceedings [72, 73, 179] and there is shortly to appear a summary report of the outcome from the EU-funded *DESider* project[36] which examined the performance of various hybrid RANS-LES models. A comprehensive guide to the design of computational grids for DES is given by Spalart [180] and best-practice guidance on the use of hybrid RANS-LES methods has recently been presented at an ERCOFTAC seminar in October 2008[37].

Menter *et al*. [181] have recently developed a new RANS model called 'Scale-Adaptive Simulation' (SAS) which decreases the eddy-viscosity under certain conditions so that unsteady

[36] http://cfd.mace.manchester.ac.uk/desider, *accessed April 2008.*
[37] http://www.ercoftac.org, *accessed August 2008.*

flow behaviour is resolved. The model is mentioned in the report by the OECD on CFD for nuclear reactor safety [13] and it is claimed that since the model is not based on LES, it exhibits less grid-dependence. To date there has been relatively little published data in the literature examining the performance of the model in a wide range of flows compared to that of DES. The behaviour of both the SAS and DES models are explored in the case study, presented in Section 4.

3.6 NUMERICAL SCHEMES

3.6.1 Spatial Differencing

In most industrial CFD studies, the geometry is complex and unstructured meshes are commonly used. The computational stencil used to determine gradients of functions in practically all unstructured codes is limited to one cell either side of the cell in which the derivative is being calculated due to the prohibitive cost of finding neighbours of the neighbouring cells. As a consequence of this limited stencil, spatial differencing is usually limited to second-order-accurate central or bounded upwind-biased schemes.

It is generally recommended that central differencing schemes are used with LES in order to minimize numerical dissipation [67]. One of the limitations, however, of central differencing is that it can produce unbounded values and give rise to spurious undershoots and overshoots when the cell Peclet number exceeds a value of two [182]. The Peclet number expresses the ratio of the magnitude of convection to diffusion and is calculated from:

$$Pe = \frac{\rho U}{\Gamma/\Delta x} \qquad (3.49)$$

where ρ is the density, U the velocity, Γ the diffusivity and Δx the cell width in the same direction as the U-velocity.

The condition for boundedness ($Pe \leq 2$) with central differences is usually not rigorously enforced in LES for two main reasons. Firstly, $Pe \leq 2$ is a sufficient but not necessary condition for boundedness of a solution [14], and secondly, it is commonly assumed that any numerical artefacts resulting from the central differencing scheme will be small compared to the physical unsteady turbulent fluctuations. Such numerical errors resulting from the use of central differences are usually only readily apparent in laminar steady flows, where it might be appropriate to switch to a bounded upwind-biased scheme. For parameters such as temperature and concentration, where unbounded values (such as negative concentrations) have no physical meaning, bounded central schemes are commonly employed (e.g. DesJardin *et al*. [165]).

Grid refinement provides a means of reducing the Peclet number by reducing Δx, although there may also be a corresponding decrease in the effective viscosity (Γ) from the dependence of the turbulence model on the filter width.

Further discussion of different spatial differencing schemes and the way these can interact with grid resolution and turbulence model constant in large-eddy simulations is provided in Geurts [67, 110]. For a discussion of the suitability of upwind-biased schemes, see also Mittal & Moin [183].

3.6.2 Temporal differencing

Many commercial and industrial CFD codes are limited to relatively simple temporal discretization schemes: usually first and second-order implicit schemes. First-order schemes tend to diffuse steep temporal gradients in a similar manner to first-order upwind spatial differencing schemes and should therefore be avoided. Second-order implicit Euler schemes have no strict limit on the time-step for stability, but can in some circumstances produce non-physical oscillations in the solution.

For LES it is recommended to use a temporal discretization of at least second-order accuracy, preferably Crank-Nicolson [14], with a time-step, Δt, chosen to keep the Courant number less than one. The Courant number is calculated from:

$$C = \frac{U\Delta t}{\Delta x} \qquad (3.50)$$

Physically, a Courant number less than one means that disturbances travel a distance less than one whole grid cell in a single time-step. The condition $C < 1$ is also known as the Courant-Friedrichs-Levy (CFL) condition and is a prerequisite for stability using explicit temporal discretization schemes. In some situations, it may be difficult to maintain $C < 1$ across the whole flow domain. If this is the case, it is useful to document the proportion of cells with Courant number greater than one and explore the effects of changing the time-step.

The COST Report on CFD for Urban Dispersion [61] and the best practice guidelines from the ECORA project [22] suggest an alternative means of determining the time-step which involves estimating the highest frequency of turbulent fluctuations likely to occur in the flow field and resolving these with at least 10 – 20 time-steps per period. Empirical correlations for the eddy-shedding frequencies for jets and plumes can be found in the literature, see for example Cetegen & Kasper [98] or List [99]. Further information on appropriate time-step sizes are given by Kornhaas *et al*. [65].

3.6.3 Kinetic Energy Conservation

As noted previously, the aim of explicit LES is to use a subgrid-scale model to account for the effect of the unresolved turbulence and to use non-dissipative numerical schemes to minimize any artificial dissipation. To this end, the ability of different CFD codes to conserve global kinetic energy has been investigated by a number of researchers. Both *a priori* and *a posteriori* tests have been undertaken, the former by means of discretizing the equations by hand and examining the overall conservation properties [14, 184]. *A posteriori* tests have involved running simulations of hypothetical nature, such as an inviscid Taylor-Green vortex flow. The analytical solution is known for this flow and since it is inviscid there is no physical damping. The only cause for the vortex to decay is therefore solely from the particular choice of numerical treatment. The approach provides a useful indicator of the overall CFD model performance, accounting for the interaction of the spatial and temporal discretization, the choice of mesh elements (tetrahedral, hexahedral, polyhedral), the pressure-velocity coupling and the choice of collocated or staggered storage locations for pressure and velocity.

Recent tests of Taylor-Green vortex flow by Laurence [95] using the commercial code *Star-CD* showed that the energy conservation of hexahedral and polyhedral cells was good and nearly equivalent, whereas that of tetrahedral cells was poor. The reason for polyhedral cells conserving kinetic energy well was explained as being related to the fact that lines connecting nodes were nearly orthogonal to cell faces (see also Moulinec *et al*. [96]) . Polyhedral cells have

much greater flexibility in terms of meshing complex geometry than hexahedra, and are currently used in a number of commercial and industrial codes including ANSYS-*Fluent*, *Star-CD*/*CCM+*, EDF's Code *Saturne*[38] and *OpenFOAM*[39].

Most commercial and industrial CFD codes use collocated storage locations where pressure, velocity and scalar parameters are all stored at cell centres. Using central differencing and Cartesian meshes this can introduce checkerboard oscillations where the pressure field develops a pattern of alternating high and low values at neighbouring nodes. To avoid these problems, a modification is commonly applied to the pressure interpolation, known as the Rhie-Chow correction [185], which removes the problems of checkerboarding but also introduces a systematic but small energy loss. This is undesirable in the context of LES and Laurence [95] noted that the Rhie-Chow correction does dissipate some energy in inviscid test cases, but also found that it made little difference in viscous LES predictions. The CEA code *Trio-U* uses staggered locations for velocity and pressure and thereby avoids problems with checkerboard oscillations.

3.6.4 Iterative Convergence

Most industrial LES uses implicit temporal discretization in which multiple "inner" iterations are performed for each time-step. The solution may contain errors if an insufficient number of iterations are performed and the solution is not well-converged. Judging what constitutes a "sufficient" number of iterations is not always straightforward and can be difficult to predict in advance. In most cases, CFD practitioners base their approach on values of the dimensionless residuals. Celik *et al*. [59] suggest that the solution be judged to be converged when residuals have fallen by 3 or 4 orders of magnitude at each timestep. This is likely to be a function of the time-step size, however, with a smaller time-step requiring fewer inner iterations and producing a smaller drop in residuals to reach a converged state. In an ideal situation, the significance of convergence errors would be assessed by repeating the LES with a tighter convergence criteria. This is rarely performed in practice however, due to the significant costs involved in repeating an LES.

The issue of iterative convergence errors in LES is similar to that faced in steady CFD simulations, which is discussed at length in Ferziger & Perić [14] and Roache [19]. Further information on convergence errors in LES can be found in Kornhaas *et al*. [65].

3.7 INFLOW CONDITIONS

In RANS simulations, flows of turbulent fluid into the computational domain are usually characterised in terms of their velocity and mean statistical properties, such as a turbulence intensity and dissipation rate. Whilst it may be necessary to express these as profiles across the width of an inlet, in most cases they are constant in time. In LES, however, it is often necessary to specify time-varying inlet conditions that are characteristic of the turbulent fluctuations.

There have been a number of proposals for how to specify turbulence characteristics for LES inflow conditions, some of which have been incorporated into commercial and industrial CFD codes. These include techniques based on assumed turbulent spectra where the velocity fluctuations are determined by taking inverse Fourier transforms of the velocity field described in spectral space, and other approaches based in physical space using assumed eddy properties

[38] http://rd.edf.com/code_saturne or http://www.cfdtm.org/Saturne/, *accessed July 2008*
[39] http://www.opencfd.co.uk, *accessed July 2008*

(size, shape and distribution) [131, 186-190]. Simple uncorrelated random "white-noise" fluctuations have been shown to be ineffective [191].

In some situations it may not be necessary to impose unsteady turbulent inflow conditions. For example, in some jet or plume flows the energetic shear layer at the edge of a jet, or buoyancy induced instabilities in the plume, generates the vast majority of turbulence within the flow domain, and the small-scale fluctuations in the pipe leading to the jet have little effect [121, 165].

4 GAS RELEASE IN A VENTILATED ENCLOSURE

4.1 INTRODUCTION

The flow investigated in this work involves a low-pressure jet of gas released into a ventilated small room. The configuration was previously examined by the Health and Safety Laboratory (HSL) as part of a joint Health and Safety Executive (HSE) and industry sponsored project to examine the implications of new hazardous area classification legislation. A comprehensive report on this earlier work [192] is available from the HSE website[40]. As part of this study, experiments were undertaken to validate the CFD model, which are also described briefly below.

The original interest in examining this flow was to predict the likely size of the flammable gas cloud produced by the jet. In the field of hazardous area classification, the size of the flammable cloud is commonly assessed using three different measures:

1. **100% LEL volume:** the volume of gas that is above the lower explosive limit of the gas. This is directly related to the volume of gas that would be expected to take part in an explosion. Note that the volume of gas above the Upper Explosive Limit (UEL) is not subtracted from the 100% LEL volume because it is likely to be relatively small and it is possible that during an explosion this gas could become diluted and therefore also take part in the explosion. For methane, the LEL is 4.4% vol/vol.

2. **50% LEL volume**: the volume of gas above half LEL (i.e. for methane, above 2.2% vol/vol). This is the volume that is often used as part of a risk assessment to allow for uncertainty in the calculation of the 100% LEL volume. It takes into account the fact that even when the mean concentration is below LEL, the instantaneous concentration may be above LEL.

3. $\mathbf{V_z}$: this is defined in BS EN 60079:10 [193] as the volume of gas that has an average concentration of half LEL. The boundary of the gas cloud is undefined in BS EN 60079:10. Here it is assumed that the cloud boundary is at a constant concentration. This concentration will be less than ½ LEL and will typically be around one third LEL although it will vary from case to case.

An indication of the relative size of the 100% LEL, 50% LEL and Vz cloud volume is shown in Figure 4.1.

In the CFD results shown subsequently, the discussion will focus on the predicted 50% LEL and Vz gas cloud volumes. Since the size of the gas clouds cannot be directly measured experimentally, there is no direct validation of the CFD model predictions of the 50% LEL and Vz values. Validation is instead obtained by comparing predicted against measured gas concentrations at certain predefined locations in the room.

[40] http://www.hse.gov.uk/research/publish.htm, *accessed June 2008.*

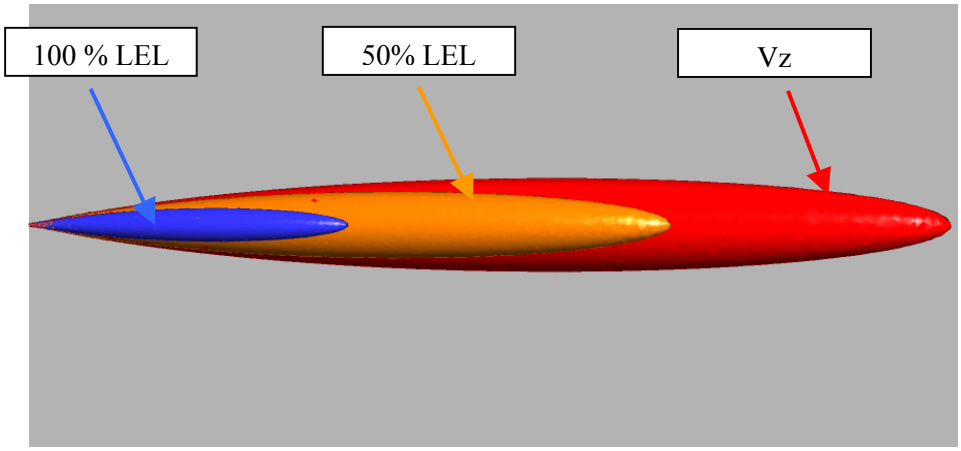

Figure 4.1 Relative sizes of gas cloud volumes for a free jet

4.2 EXPERIMENTS

The experiments were conducted using an enclosure with internal dimensions $4 \times 4 \times 2.92$ m high, located within a climate controlled laboratory (Figure 4.2). The enclosure had two ventilation inlets and two outlets with dimensions 0.4 m by 0.4 m located 0.5 m from the sidewalls, one at 2.3 m and one at 0.3 m from the floor, positioned diagonally opposed on opposite walls, as shown in the schematic in Figure 4.3. A negative pressure was maintained at the ventilation outlets to achieve a room ventilation rate of 12 air-changes-per-hour (ach), equivalent to a face velocity at the outlets of 0.47 m/s. A combination of perforated plates, porous foam and honeycomb were used to generate uniform flow across the face of the ventilation inlets.

Figure 4.2 Photo of the test enclosure during commissioning showing ventilation extracts on the near side

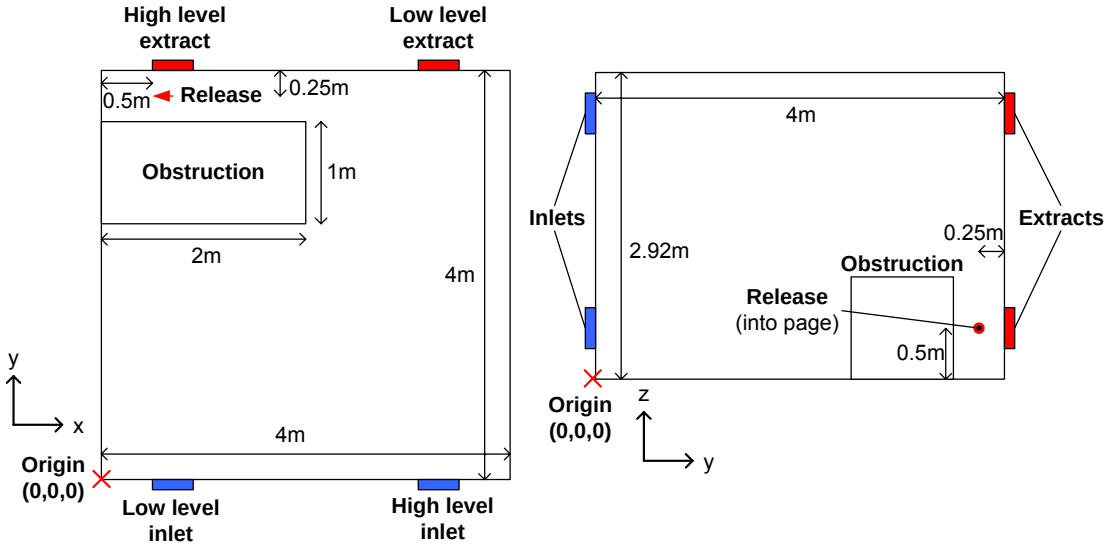

Figure 4.3 Test enclosure layout and tracer release position for configuration 3, plan view (left) and side view (right)

Although the objective of this study was to assess the behaviour of natural gas releases in enclosures, to avoid generating a flammable atmosphere a tracer gas comprising a mixture of 1% isobutylene (iso-C_4H_8), 48% nitrogen and 51% helium was released which had the same mean molecular mass and density as methane. The circular nozzle cross-sectional area was 2.5 mm^2 and the mass release rate of gas was fixed at 0.86 g/s. This would be equivalent to low-pressure gas release through a 2.5 mm^2 orifice at a stagnation pressure upstream of the nozzle of 1 barg assuming that the orifice had a discharge coefficient of unity. The nozzle was located in one corner of the room in a narrow cavity formed between two of the enclosure walls and a 2 × 1 × 1 m box obstruction. A series of CFD simulations undertaken as part of the earlier study [192] showed that this configuration of obstruction and jet location was likely to give rise to a relatively large gas cloud for the given gas release rate and ventilation rate within the enclosure.

Gas concentrations were recorded at in total 14 positions. A photo showing the nozzle and the nearby sampling positions is presented in Figure 4.4. Gas was pumped from the predetermined positions for ten minutes into gas sample bags. After the sampling period the concentration in each bag was measured to determine the mean concentration of tracer gas at each point. Before sampling of the tracer gas, the gas concentrations in the enclosure were allowed to reach equilibrium. To determine when steady state conditions had been reached, gas concentrations were measured in real-time at two positions, one in the lower extract duct and the second inside the enclosure at Position 11 (see Figure 4.4).

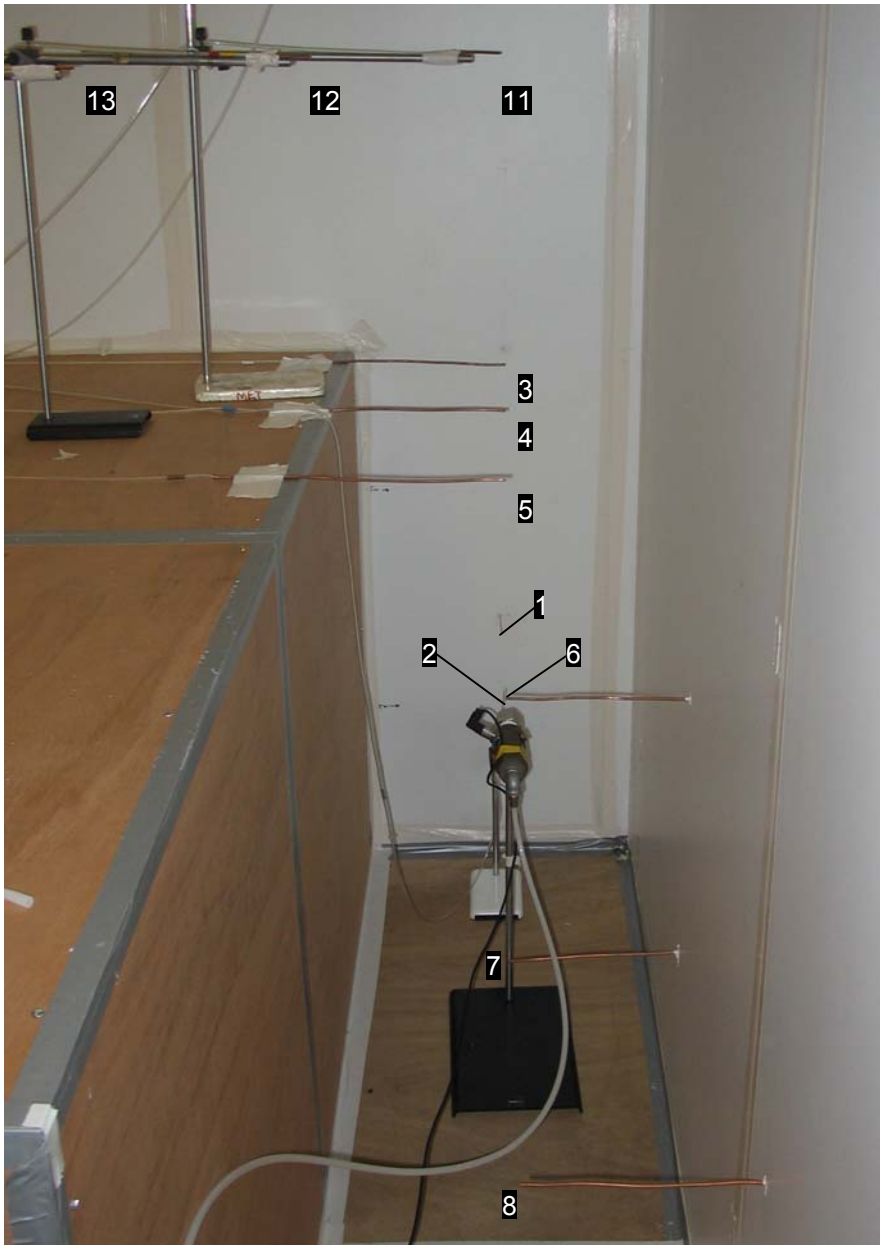

Figure 4.4 Photo of the nozzle and sampling positions. Position 6 is vertically above the nozzle, Position 7 vertically below and Position 8 horizontally behind the nozzle. Positions 1 and 2 face the gas jet with Position 2 closer to the nozzle. See also Figure 4.6.

4.3 CFD METHODOLOGY

The following sections describe the details of the CFD models used to simulate the gas dispersion in the ventilated room. All of the simulations in this study were performed using the commercial CFD code ANSYS-*CFX*, version 11.

4.3.1 Geometry

The geometry for the modelled configuration is shown in Figure 4.5. The effect on the flow of the sampling lines and fixtures present in the experiments (Figure 4.4) were ignored. Gas concentrations were monitored in the CFD model at the same locations where samples were taken in the experiments, as shown in Figure 4.6.

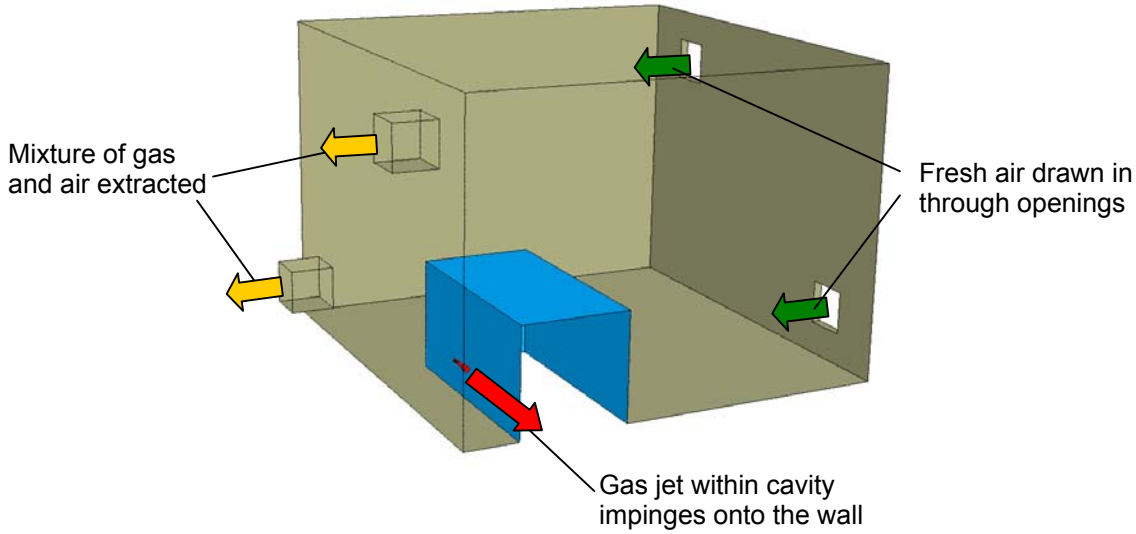

Figure 4.5 CFD model geometry and boundary conditions

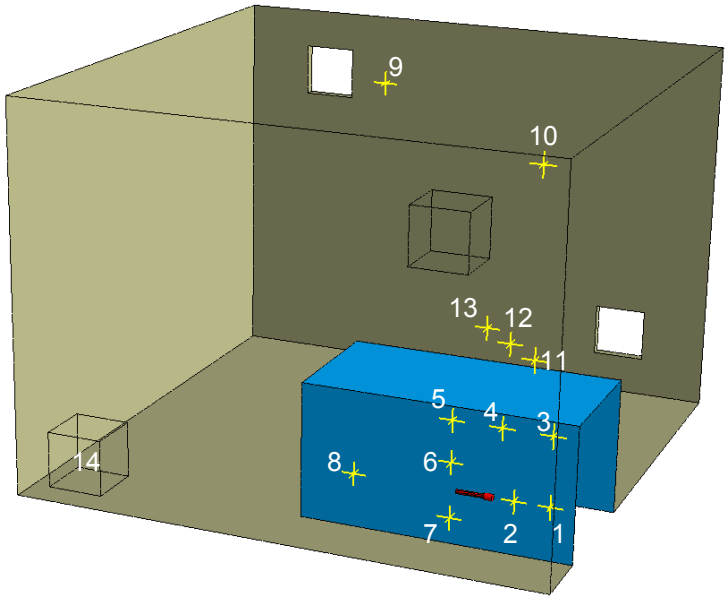

Figure 4.6 Locations of the gas concentration monitoring positions used in the experiments and the CFD model, indicated by yellow crosses.

4.3.2 Boundary Conditions

To match the experimental arrangement, the ventilation velocity was specified at the face of the extract ducts and air was pulled into the room through the two inlets. All of the walls were treated as adiabatic (i.e. perfectly insulated) and air entered the room at a temperature of 20 °C with an assumed turbulence intensity of 5 % and eddy viscosity ratio of 10%.

At a pressure of 1 barg the gas flow through a 2.5 mm^2 circular orifice is under-expanded or "choked". Close to the orifice, the flow features a complex pattern of shockwaves. Rather than attempt to resolve these complex small-scale flow features in the CFD simulation, a pseudo-source approach was used. The gas was released in the model at the speed of sound at the point where the pressure had dropped to ambient. Though this point in reality would occur at a very short distance downstream from the nozzle, the distance is so small that for the case considered here it has been ignored. Due to the expansion of the gas between the actual nozzle and the point where the pressure reaches ambient, the orifice through which the gas was released in the CFD model was 2.7 mm^2, instead of the actual nozzle diameter of 2.5 mm^2. A close up view of the modelled nozzle is shown in Figure 4.7. The gas was released at a temperature of -18 °C, which was calculated assuming isentropic expansion, and the turbulence intensity and eddy-viscosity ratio were assumed to be 5 % and 10% respectively. Further details of the pseudo-source approach used to model the gas release can be found in Ivings *et al.* [3], where the methodology is referred to as a "resolved sonic source".

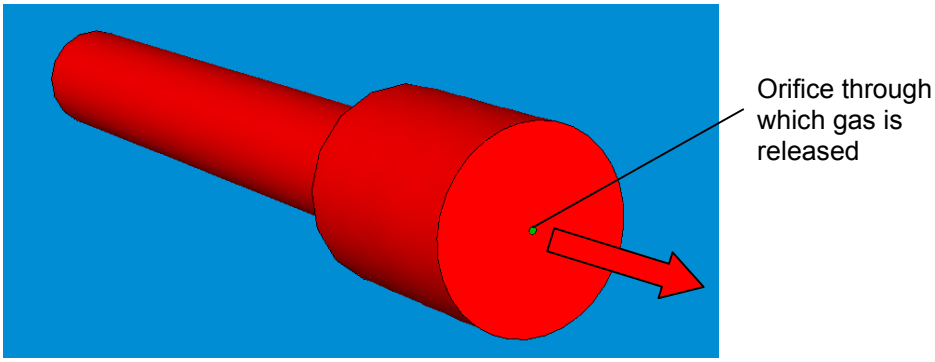

Figure 4.7 Close-up view of the modelled nozzle and orifice

4.3.3 Turbulence Models

Four different turbulence treatments were tested in the present work: steady RANS, unsteady RANS, Scale-Adaptive Simulation (SAS) and Detached Eddy Simulation (DES). LES calculations could not be performed because of the nature of the high-speed flow near the orifice (see discussion in Section 4.3.6). The steady and unsteady RANS calculations used the Shear Stress Transport (SST) model of Menter [194] which was combined with an automatic wall treatment that switches smoothly from low-Reynolds-number model to a wall-function treatment near surfaces. The SAS model used was that proposed by Menter *et al.* [181, 195, 196] which comprises a modified SST model that reduces the eddy-viscosity in certain regions of the flow as a function of the von Kármán length scale in order to resolve flow unsteadiness.

The DES model was the SST-based version of Strelets [177] which switches from a RANS model near walls to LES in the core of the flow according to the local value of the turbulence length scale and the size of the computational grid cell. The original formulation of the DES model was used from [177] without the more recent "Delayed-DES" modifications suggested in Spalart *et al*. [178] that increase the thickness of the region modelled by RANS in order to reduce the model's sensitivity to grid-induced boundary-layer separation.

With both the SAS and DES models a spatial discretization scheme was used that switched from an upwind biased second-order to a central differencing scheme in regions where flow unsteadiness was resolved, using a blending function described in Strelets [177]. The extent of the region modelled using central differencing is shown in Figure 4.8. In the high-speed jet region, near the solid surfaces and in a laminar region on the opposite side of the room from the jet the upwind-biased scheme was active but the remainder of the room was modelled using central differencing.

The standard buoyancy corrections were adopted in the two turbulence transport equations in all of the models used. Compressibility effects were also accounted for by solving a transport equation for the total enthalpy together with the ideal gas law.

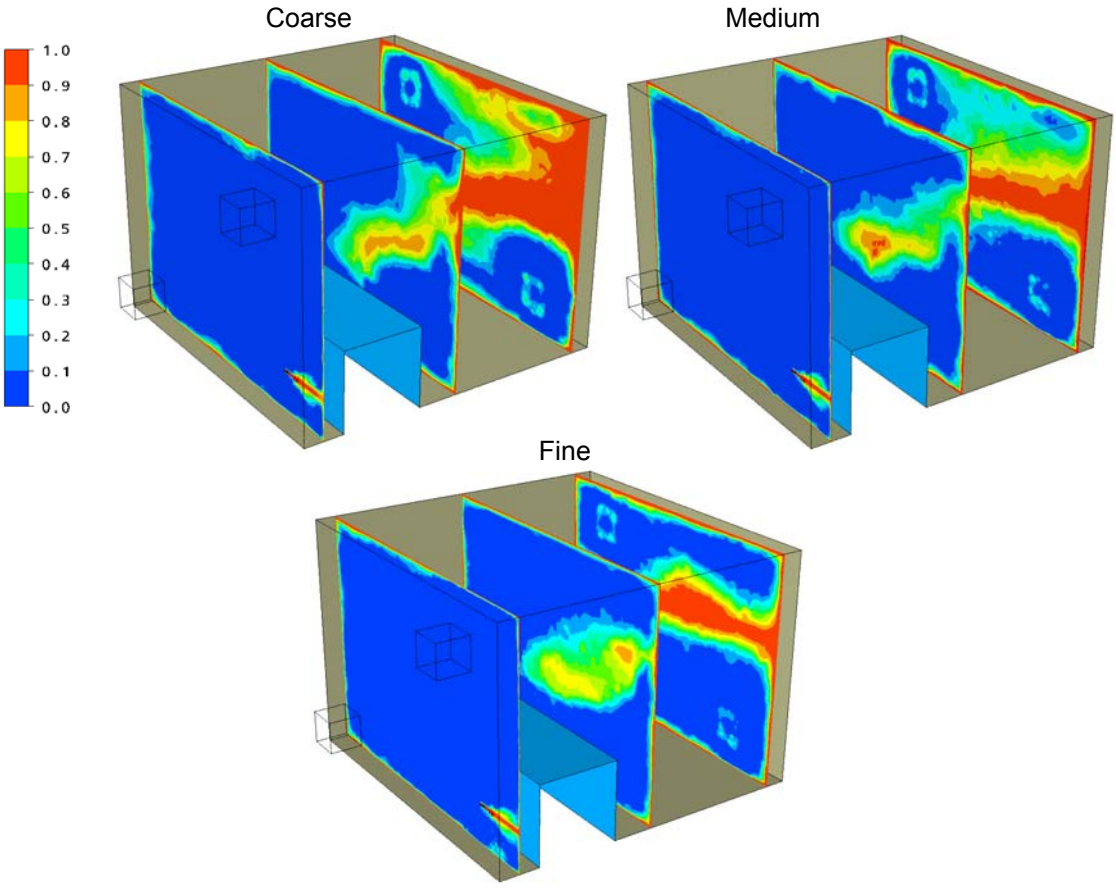

Figure 4.8 Time-averaged blending function used for the three different grids, where a value of 0 indicates central differencing and 1 an upwind-biased second-order scheme.

4.3.4 Computational Meshes

Three computational grids were used in the present study: coarse, medium and fine, comprising 224,000, 412,000 and 660,000 nodes respectively. The fine grid represented the maximum grid resolution that could practically be used given the available computing resources. The DES calculations on the fine grid took in total 45 days to compute using three processors on a fast desktop PC.

The grids mainly comprised tetrahedral cells with prism layers on each wall. Cells were refined in the regions where gradients were anticipated to be large: near the gas jet, the ventilation inlets and outlets, and near walls. Figure 4.9 shows cross-sections through the three grids on the mid-plane through the gas jet. In all three grids, the number of nodes used to resolve the jet source was held constant at 51.

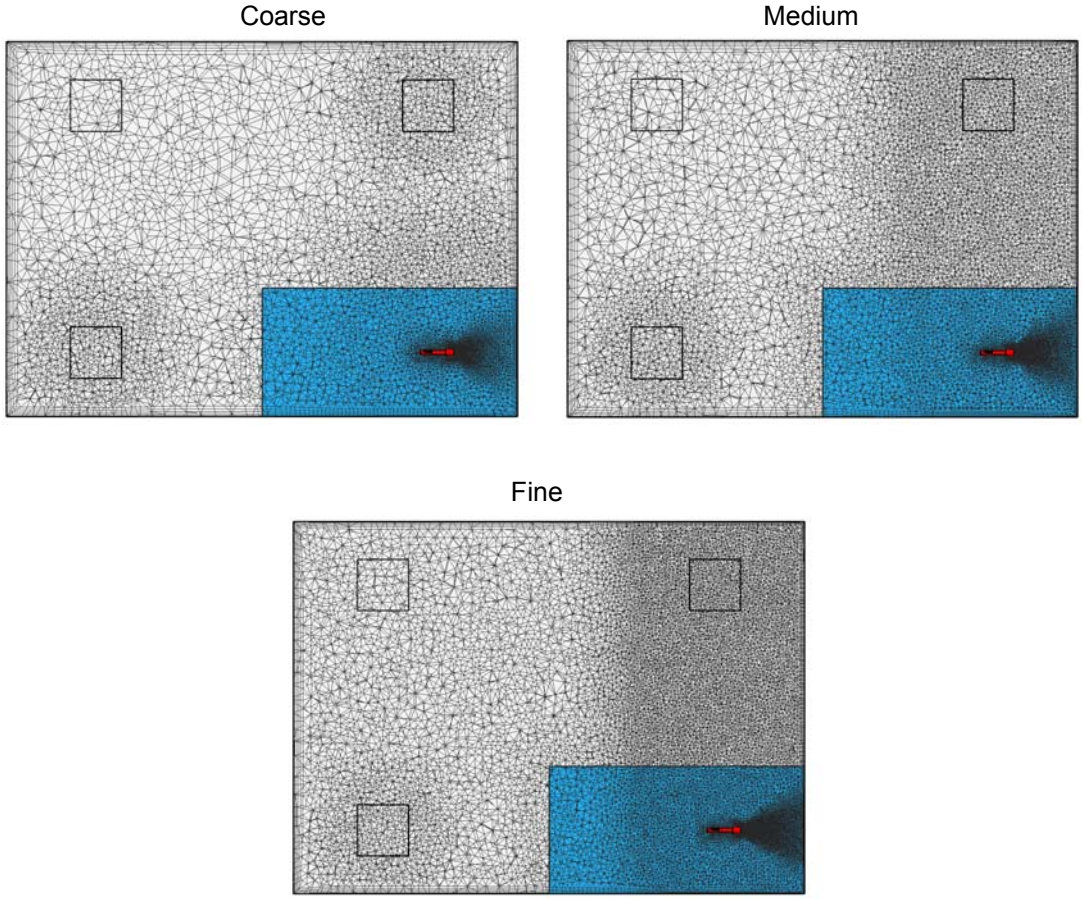

Figure 4.9 Cross-sections through the coarse, medium and fine meshes showing the arrangement of grid cells.

Figure 4.10 shows the y^+ distribution on the walls of the enclosure for the three grids from the steady RANS calculations. The maximum y^+ values occurred in the high-shear region close to the jet impingement. For the coarse, medium and fine meshes, the maximum y^+ values were 110, 93 and 53 respectively. In the attached plume region vertically above the jet, the y^+ varied between approximately 10 and 30 and elsewhere the y^+ was mostly below 20, 15 and 10 in the coarse, medium and fine meshes respectively. To resolve the boundary layers on walls, the y^+ should be less than 2 and hence these values are not ideal. They are, however, the lowest values

that could be achieved within the limits of the available computing capabilities and they reflect the range of values likely to be used in many industrial LES calculations.

The y^+ values with the unsteady RANS model were practically identical to those from the steady RANS. The DES and SAS models showed some slight differences, predominantly in the impingement region where y^+ was around 80 with the fine grid.

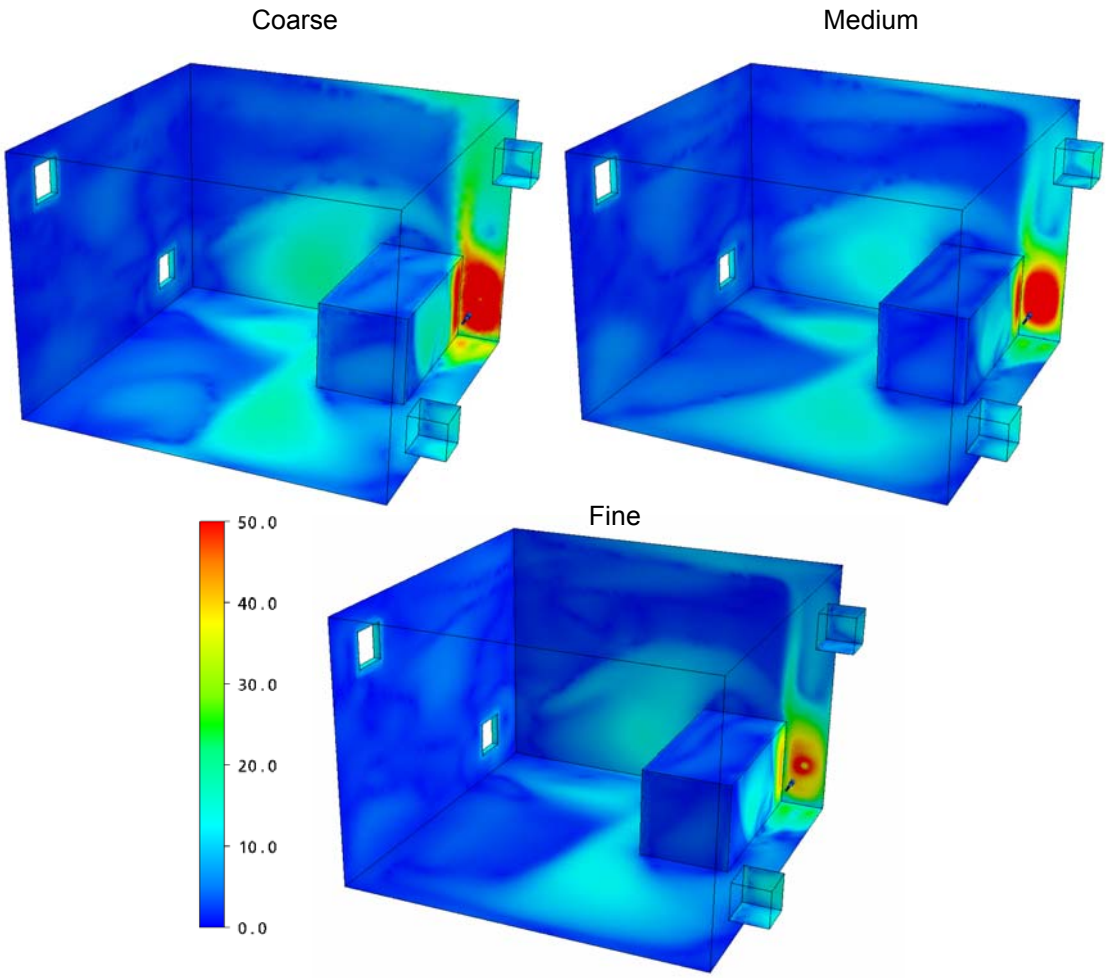

Figure 4.10 Dimensionless cell sizes (y^+) for the wall-adjacent cells from steady RANS simulations with the coarse, medium and fine meshes.

4.3.5 Overview of Flow Behaviour

To aid the subsequent discussions and identify certain underlying characteristics of the flow in the room, Figure 4.11a shows the predicted streamlines from a steady RANS simulation. This shows that part of the ventilation air "short-circuits" the room, passing directly from the upper ventilation inlet to the lower extract without much mixing taking place in the room. The fresh air from the lower ventilation inlet, however, impinges onto the sidewall of the box and produces a more disordered flow pattern. Also clearly visible is the jet impinging at high velocity into the corner of the room between the box and the adjacent walls.

Figure 4.11b shows the Vz cloud produced in the steady RANS simulation. As noted previously, this is the cloud defined such that its mean concentration is half the Lower Explosive Limit (LEL) or 2.2% methane by volume. The gas jet impinging onto the nearby wall causes the flow to be redirected by the adjacent walls such that gas is re-entrained into the jet flow, giving rise to locally high gas concentrations. The natural buoyancy of this gas-rich cloud generated within the cavity then produces a low-momentum plume which rises towards the ceiling. The large V_z cloud extends from the cavity where the jet is located, all the way to the ceiling and across the ceiling to the far corner of the room.

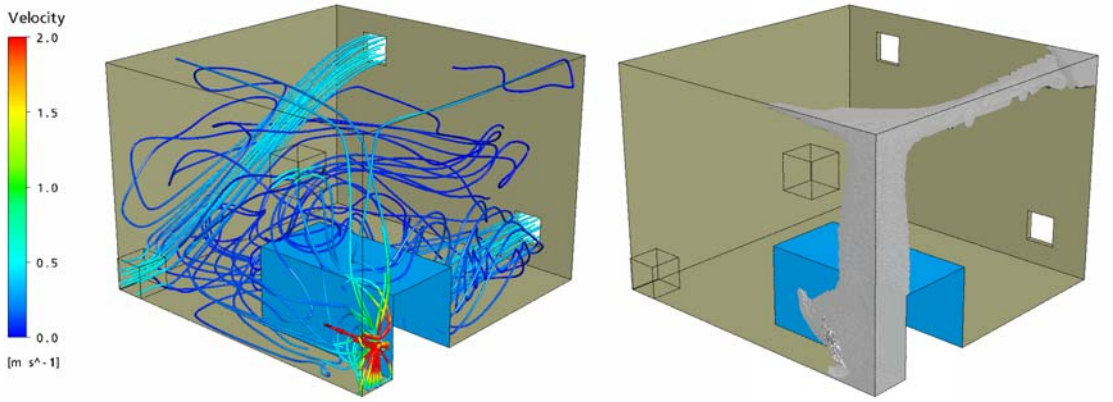

Figure 4.11 Overview of flow behaviour predicted by the steady RANS model; a.) streamlines coloured by mean velocity; b.) Vz gas cloud

4.3.6 Temporal Discretization and Averaging

The ventilated room shown in Figure 4.11 contains a number of underlying flow elements which each have their own characteristic turbulent time-scales. The main flow elements include: the gas jet, the jets produced by the fresh air entering the room through the ventilation inlets, and the buoyant plume of gas. In addition, the rate at which the room is ventilated, in terms of air changes per hour, also provides another characteristic time-scale.

A review of jet experiments presented by List [99] found that the frequency, f, of vortices produced in the jets was characterised by a Strouhal number, $St = fD/U$, of between 0.3 and 0.5. For the methane jet considered here, the diameter, D, and velocity, U ,of the source conditions are 1.9 mm and 415 m/s respectively. This suggests that the vortex frequency is between 66 and 109 kHz, or a time-scale of approximately 10^{-5} seconds.

Similarly, for the ventilation inlets the square cross-section ducts have sides of length 0.4 m, and the inlet velocity is 0.47 m/s. Based on the Strouhal number, $St = fD/U$, of between 0.3 and 0.5, the frequency range is between 0.3 and 0.6 Hz, i.e. time-scales of 2 to 3 seconds.

For plumes, Cetegen & Kasper [98] found the characteristic pulsation frequency to be given by the relation $St = 0.8\, Ri^{0.38}$ where the Richardson number, Ri, is given by:

$$Ri = \left[\left(\rho_\infty - \rho_p\right)gD\right] / \rho_\infty U^2 \qquad (4.1)$$

where ρ is the density and subscripts ∞ and p refer to the ambient and plume values respectively. If the average velocity and density are taken over a horizontal section in the corner

of the room where the gas plume rises, the Richardson number calculated from Equation (4.1) is 1.5. A value of *Ri* less than around 0.1 would indicate that the flow is momentum dominated and a value greater than ten that it is buoyancy dominated. The value of 1.5 suggests that overall the flow is mixed in nature or weakly buoyancy driven. The Strouhal number for the plume is 0.94, indicating that the instabilities have a frequency of around 0.3 Hz or a time-scale of around 3 seconds. It should be noted that the plumes considered by Cetegen & Kasper [98] were "free" plumes rising unimpeded in free space, whereas in the case considered here the plume rises in one corner of the room and is bounded for the most part on two sides by walls. This could affect the frequency of the turbulent fluctuations.

The air change rate in the room is 12 ach, so the volume flow rate of fresh air is sufficient to fill the entire room volume every 5 minutes. Due to the non-uniform distribution of the flow within the room, however, there are regions which are refreshed faster or slower than this value.

The various time-scales for the flow in the room are summarised in Table 4.1. The difference between the smallest and largest time scales is over 7 orders of magnitude. Ignoring even the general room ventilation, the time-step size in the CFD simulations would need to be around five orders of magnitude smaller to resolve the temporal instabilities of the jet than those of the plume. In practical terms, this means that it is not possible to resolve both jet and plume fluctuations in the same calculation. Performing more than 10^5 time-steps for a simulation involving a reasonably fine computational grid is not achievable on current desktop computers within a realistic time frame. Instead, a pragmatic approach has been taken here. By using the DES model, the rapid temporal instabilities in the jet-region are modelled using RANS while the plume instabilities are resolved by LES.

Table 4.1 Approximate turbulent time-scales for the various flow elements in the room

Flow Element	***Approx. Time-Scale (s)***
Sonic gas jet	10^{-5}
Fresh air inlets	2 – 3
Plume	3
Room ventilation	300

The time-step used in the CFD simulations must be of the order of one second or less to resolve the fluctuations in the plume and the inlet ventilation flow. Following a series of tests, a time-step of 0.1 seconds was selected as offering the best compromise between the length of time needed to converge the solution at each time step and the overall computing time. The average Courant number achieved using this time-step with the DES model on the fine grid is shown in Figure 4.12. In the cavity between the box and the adjacent wall, the Courant number is above 2 and in the jet region above 5, but in the majority of the plume it is around 1.0 to 1.5 and elsewhere in the room, mainly below 0.5. The same time-step was used in the unsteady RANS, SAS and DES simulations. All of the unsteady calculations used second-order backward Euler differencing in time.

Mean residuals were converged to a value of 10^{-5} at each time-step, which was generally achieved within five inner iterations. Maximum residuals were of the order 5×10^{-4} and occurred in close proximity to the jet. The ANSYS-*CFX*11 manual [197] suggests that this maximum residual level should provide a reasonable level of convergence.

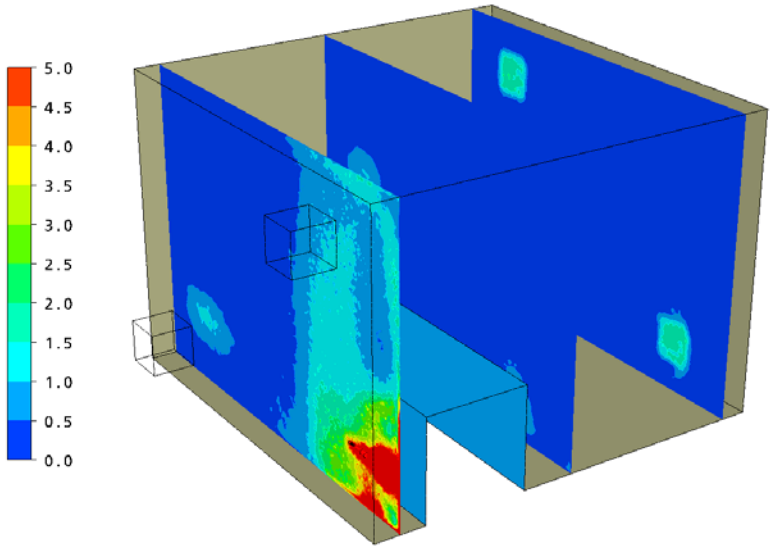

Figure 4.12 Average Courant number for the DES model with the fine grid

4.4 ASSESSMENT OF LES QUALITY

4.4.1 Grid Resolution Determined from Prior RANS

In Section 3.3.2 it was noted that one means of assessing the adequacy of grid resolution in LES was to compare the size of the computational grid cells to the integral length scales calculated from a RANS simulation. Figure 4.13 shows the ratio of the integral length scale to the cell size, calculated from $\left(k^{3/2}/\varepsilon\right)/\Delta$, where Δ is the cube-root of the cell volume. The literature reviewed in Section 3.3.2 suggested that it was desirable to have a ratio greater than 3.5 although some had suggested that it should be as high as 30. Figure 4.13 shows that the coarse, medium and fine grids are at the lower end of this range of recommended values (i.e. relatively coarse). The ratio is highest above the jet where in the plume region with the fine mesh it is around 8. The ratio is smaller elsewhere in the room and falls to around one or less near the wall on the opposite side of the room from the gas jet. The ratios are generally smaller for the medium and coarse grids, which have values in the plume region of around 6 and 4 respectively.

Care should be exercised in interpreting these results as the flow in the room is not fully turbulent. In the region furthest from the jet, the turbulence intensity, plotted in Figure 4.14, shows that the flow is practically laminar. Since the turbulence levels are so low in this region, the turbulence length scale will be close to zero, and therefore the ratio of this length scale to the grid size no longer provides a meaningful indication of grid resolution.

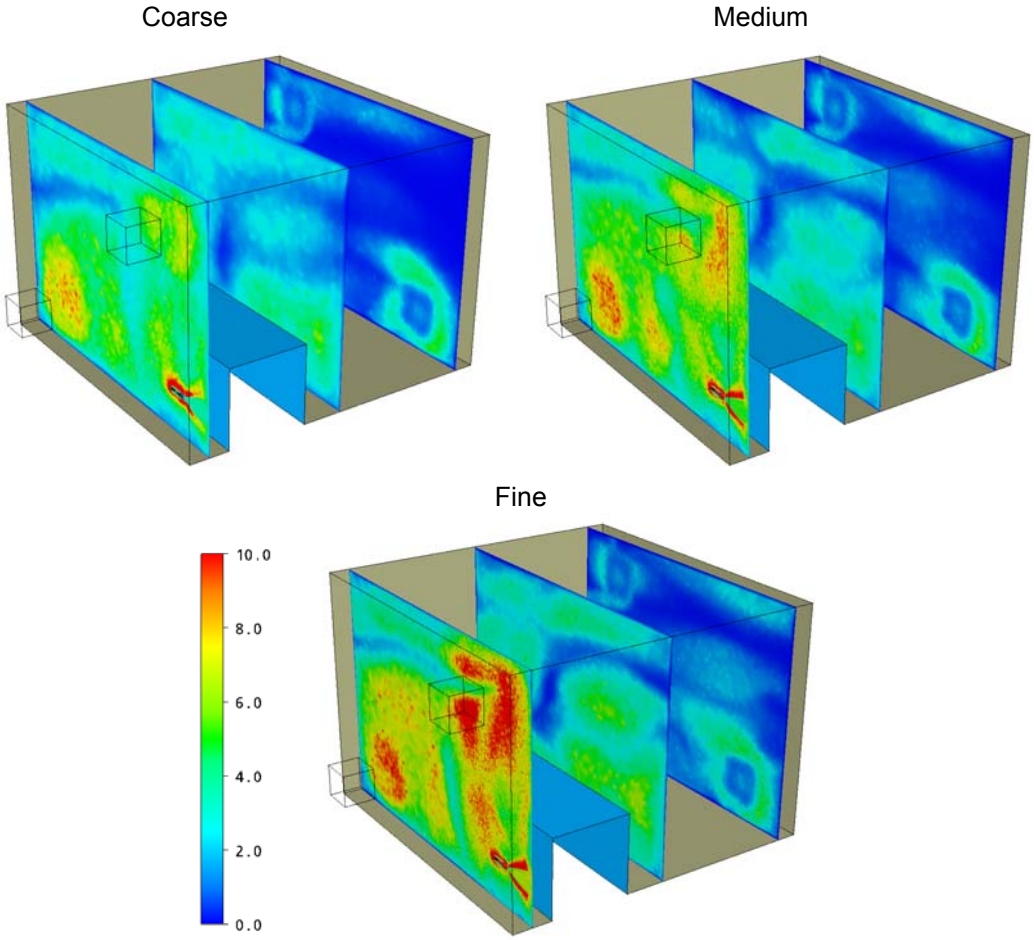

Figure 4.13 Ratio of the integral length scale to the computational grid cell size calculated using steady RANS on three different meshes

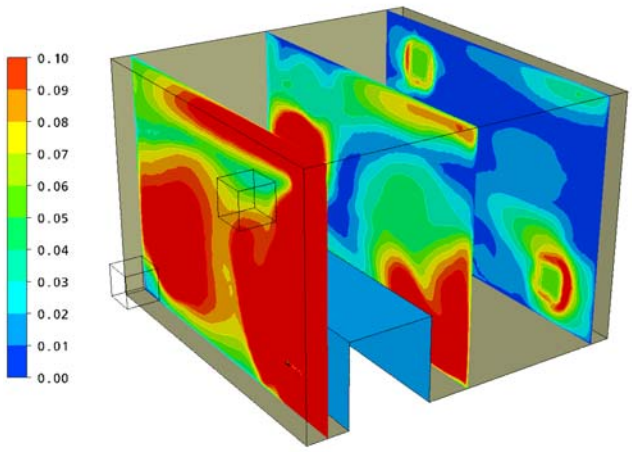

Figure 4.14 Contours of turbulence intensity calculated based on the turbulent kinetic energy from steady RANS and the ventilation inlet velocity of 0.47 m/s

A further means of assessing grid resolution suggested in Section 3.3.2 was to examine the ratio of the grid cell size to the Kolmogorov length scale, Δ / η. The literature reviewed suggested that this ratio should be maintained at a value of around 25 or less. Figure 4.15 shows that in the plume region, the coarse grid has a ratio of over 60, whilst the medium and fine grids have ratios of around 50 and 40 respectively. On the opposite side of the room from the gas jet, the ratio in all three grids falls to below 10. The flow here is nearly laminar and the turbulence dissipation rate, ε, close to zero. As a consequence, the Kolmogorov length scale, η, is very large (since it is related to the inverse of ε) and the ratio of grid size to Kolmogorov length scale correspondingly small.

These grid resolution indices based on prior RANS simulations indicate that, overall, the regions near the jet and in the plume immediately above it are under-resolved even using the fine grid. Ideally, the cell size would have been halved in this region, although to do so would require roughly a factor 8 increase in the number of grid nodes and a corresponding decrease in the time-step in order to satisfy the CFL condition. Further away from the jet the grid resolution appears to be reasonably good, although since the turbulence levels are low in these regions the RANS based measures are less reliable.

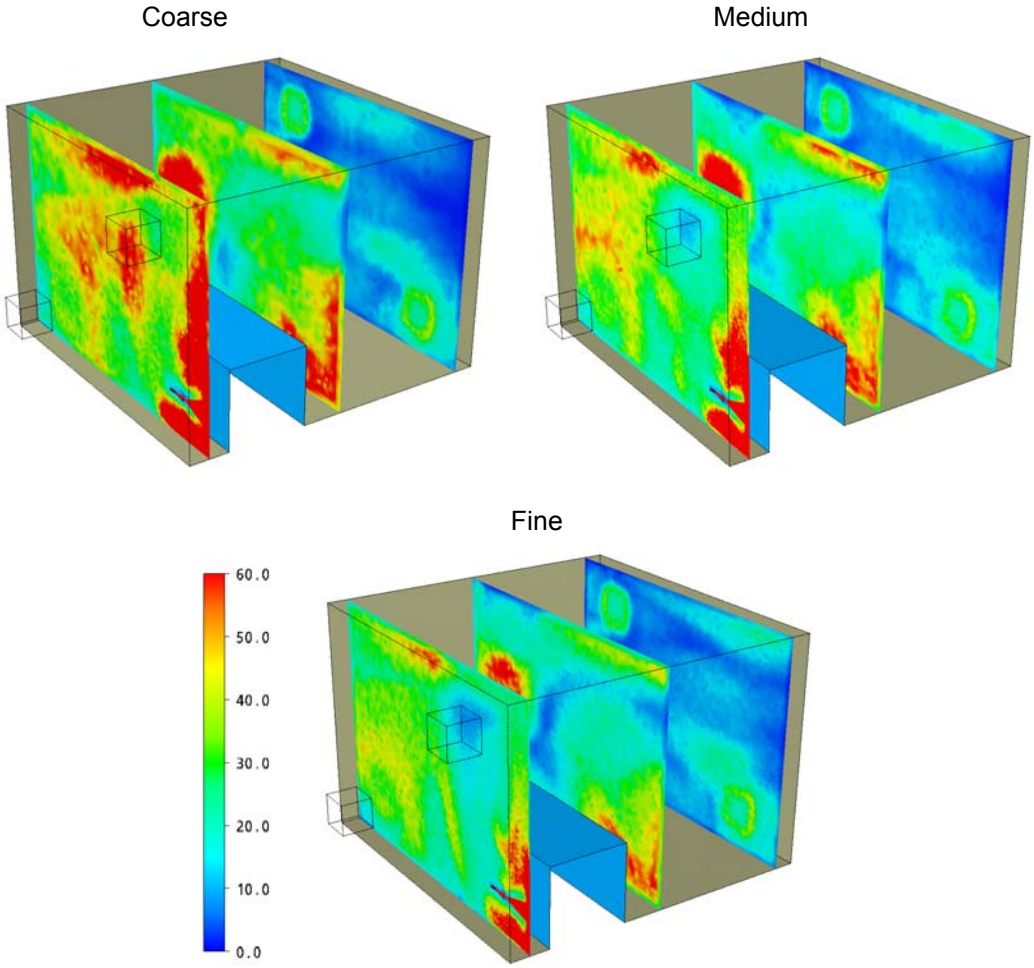

Figure 4.15 Ratio of the grid cell size to the Kolmogorov length scale predicted by the steady RANS model on three different grids

4.4.2 Single-Grid Estimators

A number of measures for assessing LES quality were described in Sections 3.3.3 - 3.3.7 which required just one LES calculation, so-called single-grid estimators. The simplest of these is the ratio of the mean turbulent to the laminar viscosity, ν_t / ν. Figure 4.16 and Figure 4.17 plot this measure for the DES and SAS models with the coarse, medium and fine grids. With both the DES and the SAS model, the viscosity ratio decreases as the grid is refined. The DES values are generally lower than the corresponding SAS model values, although the distribution is different in the two cases. The SAS values are generally higher in the plume region whereas the DES values are higher behind the gas jet and in the shear layers around the ventilation fresh-air jets. With the fine mesh, the DES viscosity ratio is around 15 – 40 in the plume region while the with SAS model it is higher at around 100 – 200. This is still less than that predicted by the URANS and RANS models which have viscosity ratios of 200 – 300 in the plume. Away from the jet and plume regions, in the core of the room both DES and SAS models have viscosity ratios less than 20.

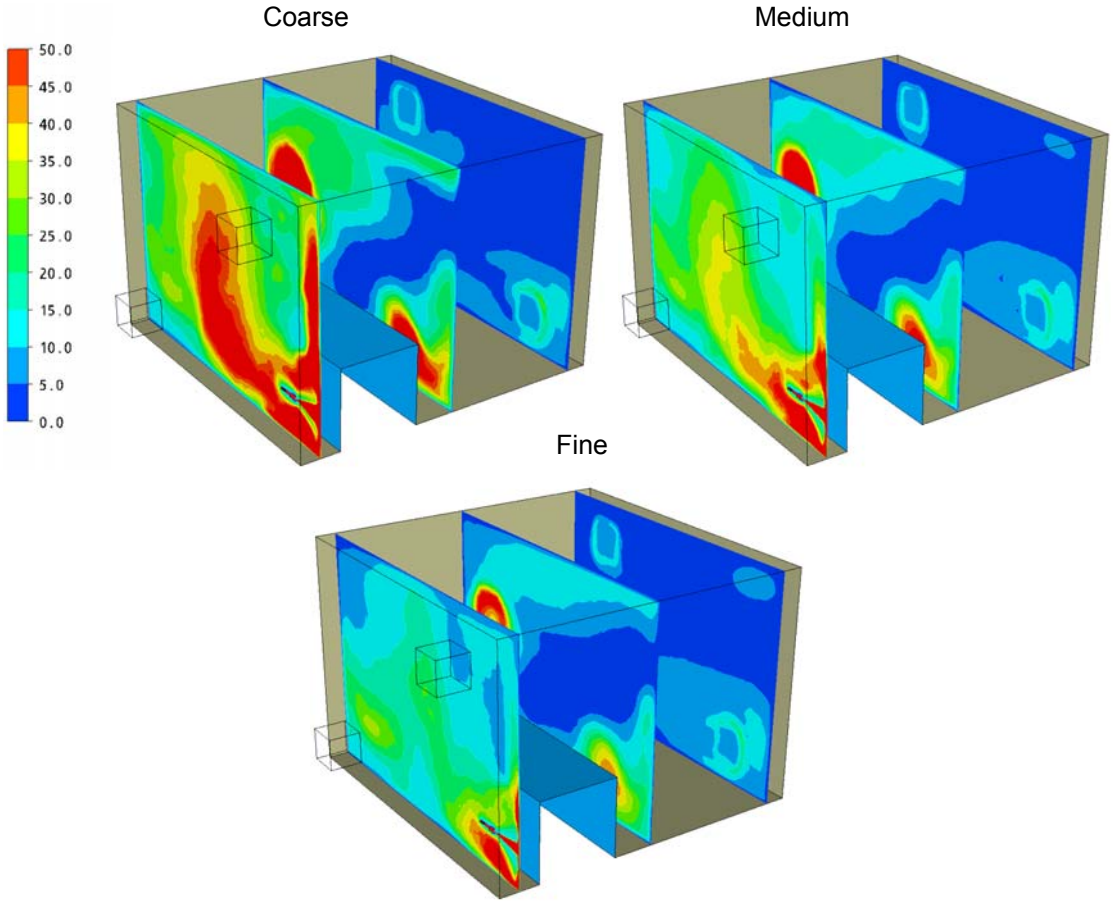

Figure 4.16 Ratio of the mean turbulent to the laminar viscosity, ν_t / ν **,** for the DES model

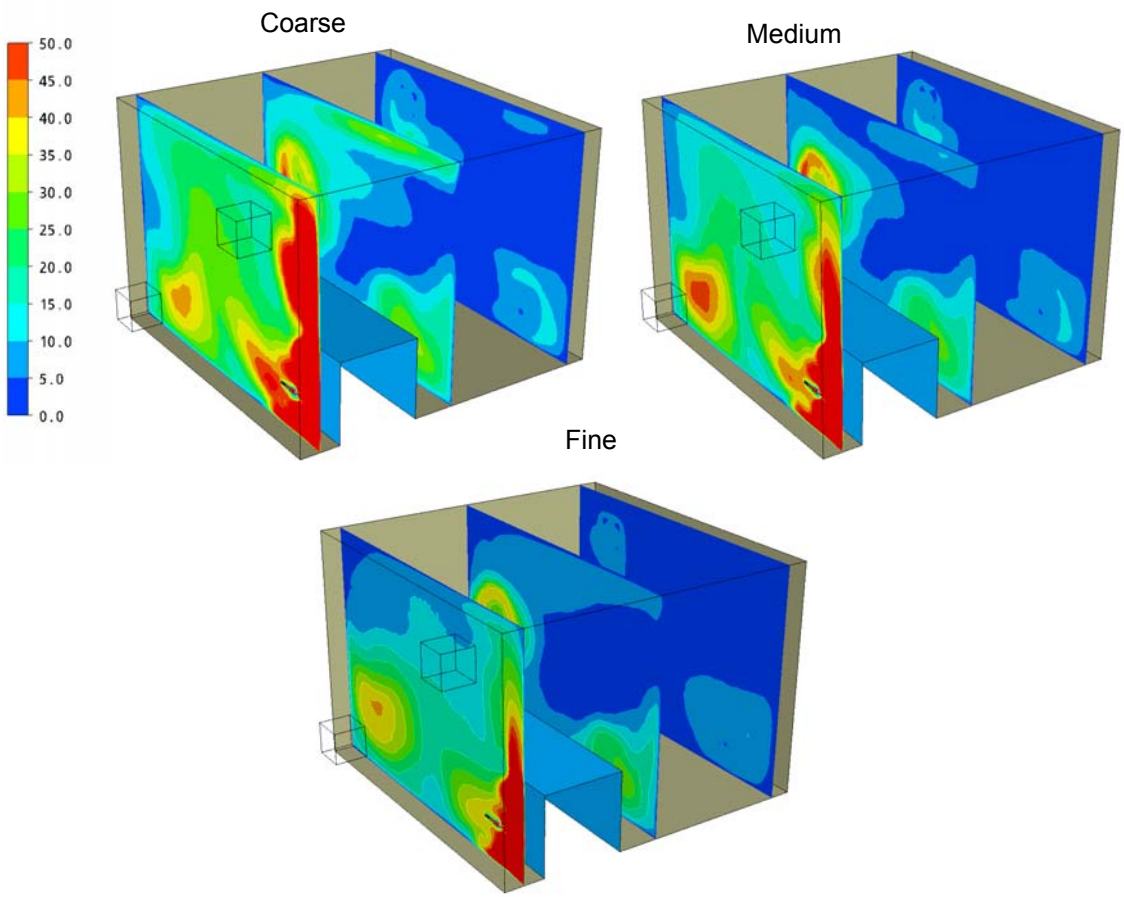

Figure 4.17 Ratio of the mean turbulent to the laminar viscosity, ν_t/ν **,** for the SAS model

The viscosity ratios with the DES model in the regions where it behaves primarily as LES (see Figure 4.8) are high compared to the values recommended in the literature. For example, Celik *et al*. [58] suggested that ν_t / ν should be around 20 in highly turbulent regions where the turbulence Reynolds number, $Re_{t,}$ is around 1200 and around 5 in less turbulent regions where Re_t is around 300. The turbulent Reynolds numbers for the RANS model are presented in Figure 4.18, which shows that in the plume region Re_t is approximately 2000.

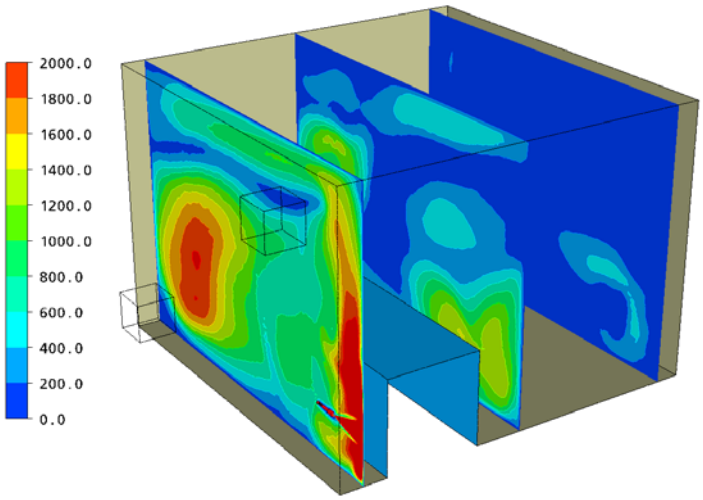

Figure 4.18 Turbulent Reynolds number from the steady RANS model on the fine grid.

Another single grid estimator proposed by Celik *et al*. [58] called the Relative Effective Viscosity Index, *LES-IQ*$_v$, is shown in Figure 4.19. According to Celik *et al*. [58], a value of *LES-IQ*$_v$ greater than 0.8 indicates a good LES and a value greater than 0.95 a DNS. The values for the fine-grid DES near the jet are between 0.6 and 0.7, in the plume region between 0.7 and 0.8. Elsewhere in the room where the flow is less turbulent, the *LES-IQ*$_v$ is generally above 0.8. This suggests that even the finest grid used in this study is only marginally resolved.

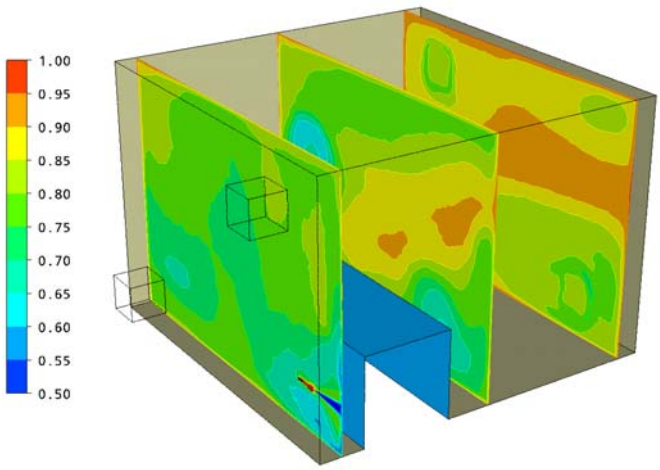

Figure 4.19 *LES-IQ*$_v$ calculated from Equation (3.9) for the DES on the fine grid

The subgrid activity parameter, devised by Geurts & Fröhlich [89], is shown in Figure 4.20 for the DES model on the medium and fine meshes. The parameter indicates the importance of the subgrid scales in the flow where a value of zero is in effect a DNS and a value of one a high Reynolds number LES. The DES results shown in Figure 4.20 have subgrid activity close to one across a large part of the room. The parameter also shows relatively little sensitivity to the grid resolution. Celik *et al*. [58] noted that this behaviour would be common in many engineering

flows where the turbulent viscosity is significantly larger than the molecular viscosity. The modified subgrid activity parameter that they proposed instead is plotted in Figure 4.21 for the fine grid, which shows practically identical results to the original proposed parameter.

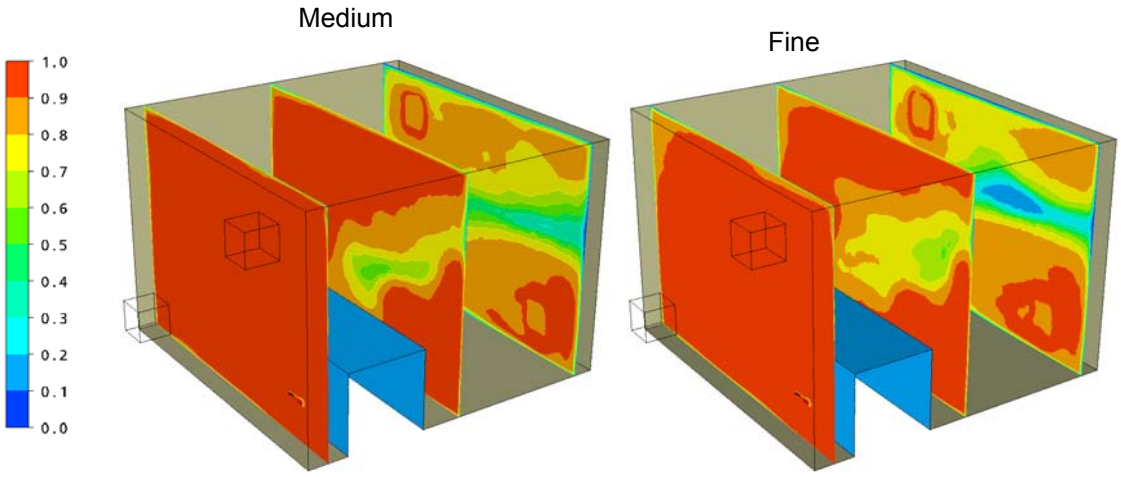

Figure 4.20 Subgrid Activity Parameter calculated from Equation (3.13) for the DES

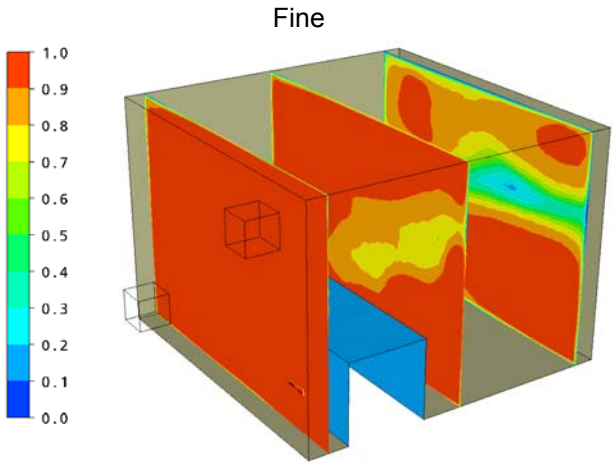

Figure 4.21 Modified Subgrid Activity Parameter calculated using Equation (3.15) for the DES.

Another single-grid estimator is the ratio of resolved to total turbulent kinetic energy, which is shown for the fine-grid DES and SAS models in Figure 4.22. The total turbulent kinetic energy is calculated from the sum of the resolved kinetic energy and the modelled kinetic energy, where the modelled k is taken at a single instant in time rather than a time-averaged value. The results presented in Figure 4.22 show that the DES model resolves a slightly greater proportion of the turbulent fluctuations near the source and in the plume region than the SAS model, although both models have a resolved component which accounts for 70 to 90 % of the turbulence energy in the majority of the plume region. This suggests that the grid resolution is reasonable.

The fact that a steady velocity has been used to model the flow entering the room through the ventilation inlets is also clearly visible. Due to the absence of turbulent structures in the flow, the resolved turbulent kinetic energy is practically zero near the inlets.

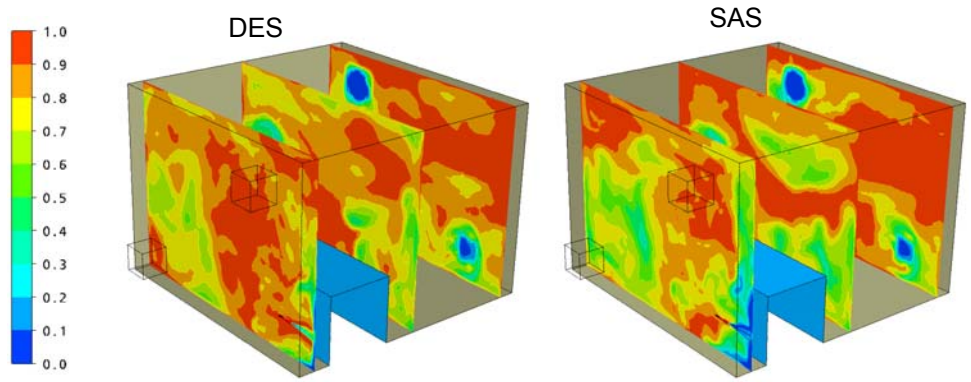

Figure 4.22 Ratio of resolved to total turbulent kinetic energy for the DES and SAS models calculated from Equation (3.27)

4.4.3 Spectra

As mentioned in Section 3.3.6, one of the means of assessing the degree of grid resolution is to plot the power spectra of the turbulence. The spectra should exhibit a -5/3 slope if the grid has sufficiently resolved part of the inertial subrange. The power spectrum based on the concentration fluctuations at Position 11 for the DES model with the coarse, medium and fine grids is shown in Figure 4.23. The graph shows that the power spectra decays less rapidly with the fine grid than the coarse grid, as expected. However, there is no clearly discernible inertial subrange with a slope of -5/3.

To explore why a distinct -5/3 slope is absent, Figure 4.24 shows the ratio of the integral to the Kolmogorov length scales $\left(k^{3/2}/\varepsilon\right)/\left(\nu^3/\varepsilon\right)^{1/4}$, i.e. the ratio of the largest to the smallest turbulent length scales. At Position 11 where the power spectra was plotted, the length-scale ratio was approximately 350. This suggests that the separation of scales could be too small for there to be a well-defined inertial subrange.

Another possible reason for the lack of a -5/3 slope is the influence of buoyancy forces. A number of previous experimental studies [133-135] have identified that the concentration spectra decays with a slope of -3 rather than -5/3 in buoyant plumes. This behaviour was observed in the LES of buoyant plumes by Zhou *et al*. [128, 129] and Abdalla *et al*. [198]. At very high frequencies in the dissipation range, Elicer-Cortés *et al*. [136] also found that the slope was -7 in their buoyant plume experiments.

The results for the DES model in Figure 4.23 show some evidence of a -3 power-law decay which seems to agree with the anticipated effect of the buoyancy forces. At higher frequencies there is a reasonably well-defined region with a slope of -7. Whilst this might at first be considered to shows signs that the DES resolving the dissipation range, it is more likely to be coincidental that the slope agrees with that in the experiments of Elicer-Cortés *et al*. [136]. The energy at the high frequencies is expected to decay relatively rapidly due to the effects of numerical and model dissipation. Based on the previous grid-resolution indicators, it seems

highly unlikely that the grid is sufficiently fine to resolve the very small turbulence length scales in the dissipation range.

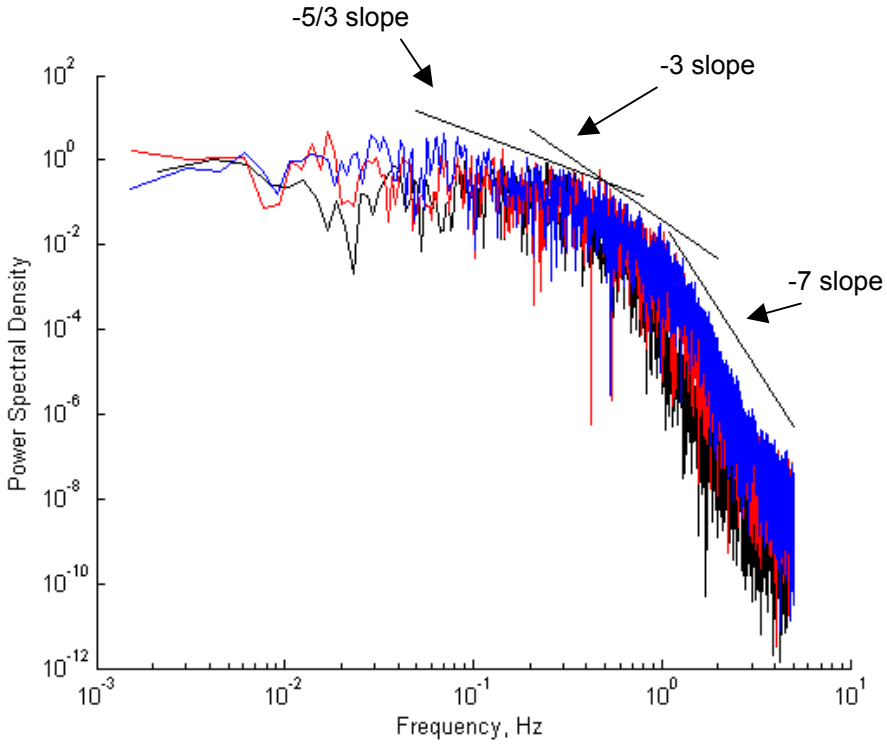

Figure 4.23 Power spectral density based on the concentration fluctuations of the DES model at Position 11 using coarse (–), medium (–) and fine (–) grids.

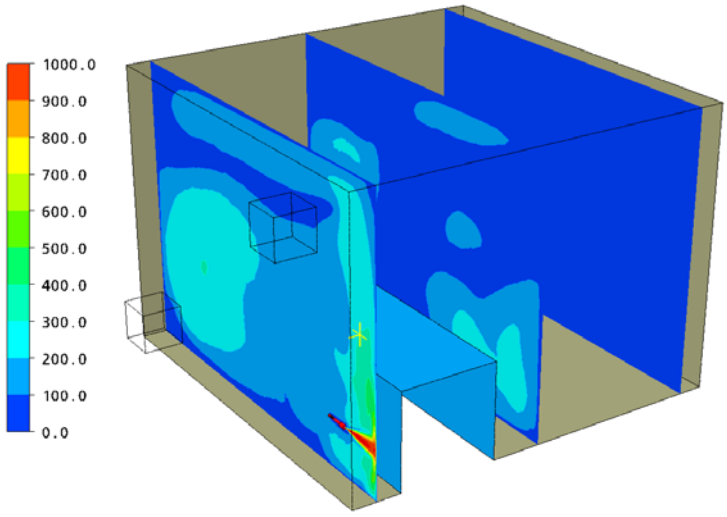

Figure 4.24 Ratio of the integral to the Kolmogorov length scales, calculated from the fine-grid RANS model. The yellow cross shows the location of Position 11.

4.4.4 LES Index of Quality

The "Index of Quality", *LES-IQ*$_k$, based on Richardson extrapolation of the turbulent kinetic energy between the medium and fine grids is shown for the DES model in Figure 4.25. Since in some regions of the flow the resolved turbulent kinetic energy, k_{res}, is higher with the medium than the fine grid (Figure 4.26), the modified *LES-IQ*$_k$ has been calculated using Equation (3.44). The speckled pattern of colour is due to the non-smooth distribution of the ratio of cell sizes on the medium and fine grids (see Figure 4.27).

Generally, in the region above the jet the *LES-IQ*$_k$ value is above 60% although the rapid changes in value between one cell and its neighbour makes it difficult to draw conclusive trends. This is especially the case in regions where the value of *LES-IQ*$_k$ reaches 100%, where it alternately flips to a value of 0% in close proximity.

At various points within the flow the *LES-IQ*$_k$ value either exceeded a value of 100% or became negative. The former problem was linked to the total turbulent kinetic energy, k_{tot}, becoming negative in certain regions. The value of k_{tot} was calculated from:

$$k_{tot} = k_{res} + a_k h^p \qquad (4.2)$$

where h is the cell size calculated from the cube-root of the cell volume, p is a constant taken as 2 since a second-order accurate numerical scheme was employed and a_k was determined from the ratio of k_{res} to the cell-size-squared:

$$a_k = \frac{(k_{res})_1 - (k_{res})_2}{h_2^2 - h_1^2} \qquad (4.3)$$

where subscripts 1 and 2 refer to medium and fine grid values respectively. In some locations the k_{res} on the medium grid was much larger than on the fine grid so that the value of a_k was negative and of sufficient magnitude that the product $a_k h^p$ was larger than k_{res}, which made the total turbulent kinetic energy, k_{tot}, negative. In other locations, the ratio $|k_{tot} - k_{res}| / k_{tot}$ was larger than unity which led to negative values of *LES-IQ*$_k$.

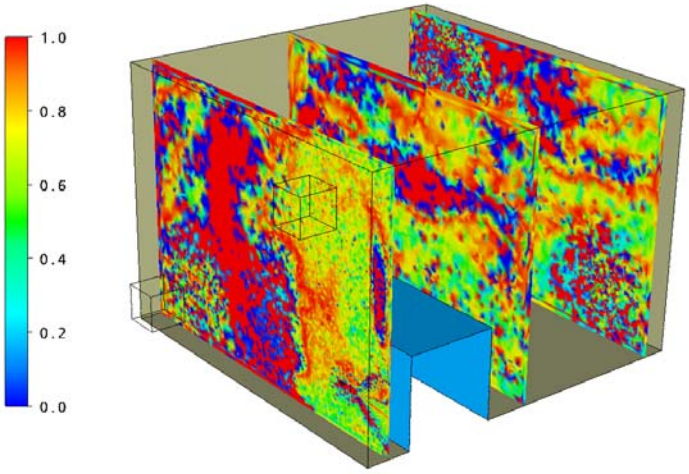

Figure 4.25 "Index of Quality", *LES-IQ*$_k$ calculated using Equation (3.44) based on the medium and fine DES results.

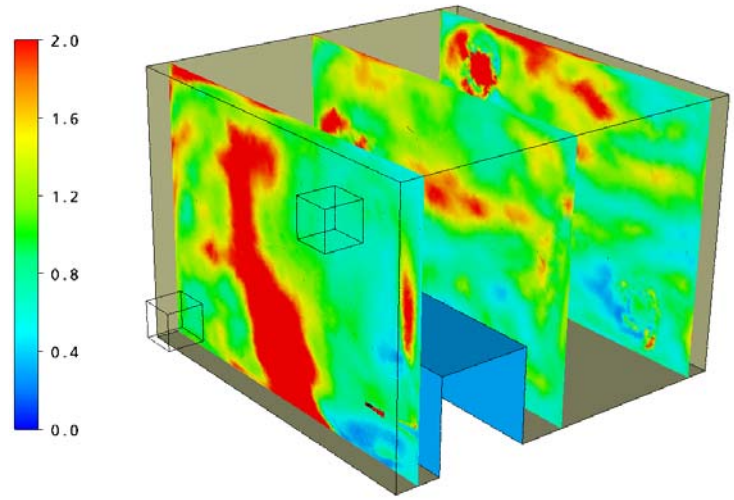

Figure 4.26 Ratio of the resolved turbulent kinetic energy produced using the medium grid DES to that produced on the fine grid DES, k_1/k_2

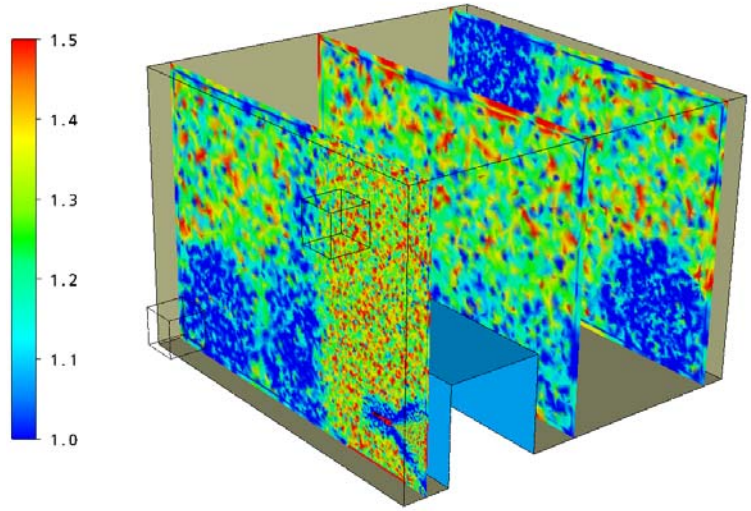

Figure 4.27 Ratio of the cell size on the medium grid to that on the fine grid, h_1/h_2.

4.5 RESULTS

4.5.1 Gas Concentrations

Comparisons of the CFD results on the fine grid versus the experimental measurements are presented as coloured contours of gas concentration in Figures 4.28 – 4.31. In each of these plots, the black dots mark the location of the experimental measurements. Around each black dot is a circular fringe, the colour of which denotes the gas concentration measured experimentally. The coloured contours in the background are the mean gas concentrations from the CFD models. Adjacent to each black dot are given the gas concentrations in terms of percentage gas by volume for both the mean experimental and CFD values. The mean concentrations are calculated for the DES, SAS and URANS results by averaging over a long period (typically 7 minutes) once the simulations have reached a fully-developed state. The steady RANS values were generated without any averaging.

The DES and SAS results are broadly similar to each other but show some notable differences compared to the URANS and RANS results, which are almost identical. Whilst the URANS and RANS results show quite marked concentration gradients near to the gas jet, the concentration decays more smoothly in the DES and SAS results. The gas concentration behind the nozzle within the cavity between the box and the adjacent walls is slightly overpredicted by the DES and SAS models but reasonably well predicted by the URANS and RANS models. Above the jet in the plume region, however, the DES and SAS models predict lower gas concentrations which are in better agreement with the experiments than the URANS and RANS results.

Figure 4.32 provides a summary of the differences between CFD and measured gas concentrations averaged across all the measurement points in the room. The average error using either the URANS or RANS models on the fine grid (approx. 0.33% vol/vol) is less than half that of the fine-grid DES model (just over 1.0% vol/vol). In comparison, the lower explosive limit of methane is 4.4% vol/vol. Whilst for the RANS model the error diminishes as the grid is refined from coarse to medium to fine, with the DES and SAS models the reverse trend is produced with the greatest error on the finest grid.

The average differences between the experimental and CFD mean gas concentrations expressed as a percentage of the local measured gas concentrations are summarised in Figure 4.33. The error in regions where the gas concentrations are low are given greater weighting in these results than in the previous case (Figure 4.32). The variation between the 12 different simulations is less significant using this error measure. The mean error is lowest at 35% for the RANS predictions on the fine grid and largest with DES model on the medium grid at 51%. Since the actual value of the gas concentration is quite low at a number of points, a difference of less than one percent in gas concentration accounts for a significant percentage in relative terms.

The breakdown of the measured versus experimental mean gas concentrations for each of the measurement locations is given in Figure 4.34 and a similar breakdown for the relative errors in Figure 4.35. The former of these figures illustrates quite clearly that the gas concentration is low at most of the measurement locations and in actual terms the differences between model and experimental values are reasonably small at most of the measurement locations. A significant fraction of the total error in the gas concentrations with the DES and SAS models is produced by the two measurement positions within the gas jet, near the nozzle (Positions 1 and 2). The DES and SAS models predict too much re-entrainment of gas or too little mixing of fresh air into the jet and overpredict the gas concentrations by up to 7.8% vol/vol and 5.1% vol/vol respectively. There is a consistent trend across all the model results to overpredict significantly the measured values at Positions 12 and 13, by up to a factor of three in some cases. These measuring points, shown in Figure 4.6, are at roughly the mid-height of the room and towards

the outer edge of the plume (see plan views in Figures 4.28 – 4.31). Gas concentrations in the upper part of the room, at Positions 9 and 10, are also generally overpredicted.

The second-highest errors in relative terms occur at Position 8, which is located directly behind the nozzle within the cavity formed by the box and the adjacent walls. In this region of the flow, the gas concentrations fluctuate significantly. To explore whether statistical uncertainties in the predictions could be partly responsible for the poor agreement here, the fractional error in the 95% confidence intervals of the mean concentrations are presented for the fine-grid DES results in Figure 4.36. The confidence intervals are calculated based on the bootstrapping approach described in Section 3.2.2. These show that the largest fractional errors, of the order 10%, are at Position 8. The underlying cause for the significant uncertainty in the mean value at this position is the large temporal oscillations in the predicted concentration. To illustrate this, Figure 4.37 shows the predicted concentrations at Positions 4, 8 and 11. The magnitude of the oscillations is noticeably larger at Positions 4 and 8, that both featured large fractional errors in the confidence intervals, than at Position 11. Figures 4.36 and 4.37 appear to show therefore that the poor agreement between the mean gas concentrations in the experiments and the DES results at Position 8 could be partly attributable to the statistical uncertainty in the mean values. In principle, this uncertainty could be reduced by running the DES calculations for a longer period of time in order to generate more reliable mean statistics. However, the simulations were already quite protracted with the fine-grid DES calculation taking around one and a half months.

Position 11 was one of only two locations in the room where the gas concentrations were monitored continuously during the experiments. Figure 4.38 compares the gas concentrations predicted by the DES model on the fine grid against the experimental measurements at this position, which was situated roughly in the middle of the plume (see Figure 4.4). The corresponding mean and 95% confidence intervals in the mean are shown in Figure 4.39. There are significant temporal fluctuations in the gas concentrations at this position in both the experimental and model values. Although the mean gas concentration is underpredicted by the DES model by 23%, there is a significant variation in the instantaneous values, with predicted concentrations well above and below the measured mean value.

The power spectra of the concentration fluctuations from the measurements at Position 11 are compared to the DES, SAS and URANS predictions in Figure 4.40. To create the power spectra, the three CFD model predictions have been sampled at the same frequency (1 Hz) as used in the experiments. The DES and SAS results both show reasonable agreement with the experiments, whereas the URANS results show much lower values, due to the URANS model damping most of the turbulent fluctuations. In the experiments the gas was pumped from Position 11 along 5 metres of flexible piping before reaching the measuring device outside the room and this could have led to some localized mixing which would tend to damp high-frequency fluctuations in the gas concentrations.

A full discussion on the experimental errors is provided in the earlier HSL report [192]. It was estimated that errors of the order of 5% in the mean gas concentration may have occurred due to leakage of gas at the joints between the flexible plastic pipes used to connect the measurement probes to the sampling bags. Although every effort was made to seal the room by taping around the door and other openings, the room was operated at a negative pressure and there could have been some leakage in the fabric of the enclosure which would tend to give rise to locally higher dilution and lower gas concentrations than accounted for in the CFD model. The effects of possible thermal stratification were monitored in the experiments using a rake of five thermistors between the ceiling and floor. The temperature differences were generally between 0.1 and 0.3 $^{\circ}$C and logs showed that the temperature inside the enclosure remained constant during a test. A reproducibility test was undertaken in the experiments where the ventilation, gas nozzle and measurement system was dismantled and then reconstructed and the test

repeated. This produced differences in the mean gas concentrations on average of approximately 6.5% – this can be compared to the modelling error shown in Figure 4.33.

Other possible reasons for the differences between the CFD model and experimental gas concentrations include the boundary conditions adopted for the fresh air inlets and the gas jet. In both cases, the turbulence levels have been assumed at these inlets since no measurement data was available. Some limited tests with the steady RANS model were undertaken to investigate the effect of increasing the turbulence intensity in the gas jet from 5 to 10% and the eddy-viscosity ratio from 10 to 100. This led to minor changes in the predicted gas concentration of on average less than 1%. Further simulations were undertaken where the turbulence levels in the fresh air inlets were increased a similar amount. This produced slightly larger differences in the gas concentration and increased the average error between the modelled and experimental gas concentrations from 34 to 36%.

Ideally, more comprehensive sensitivity tests would have been undertaken to examine the effect changing the inlet turbulence levels or of introducing resolved unsteady turbulent fluctuations with the DES and SAS models. However, due to the high cost of repeating the calculations these tests have not been undertaken. In any case, it is likely that the strong shear layers produced at the edges of the jet and in the high-speed impingement region, and buoyancy-related instabilities in the plume were the main driving forces for the turbulence rather than fluctuations in the inlet velocity.

The pseudo-source simplification adopted in modelling the choked gas release could also have introduced some error in the simulations, although previous work has shown this approach to be reasonably reliable [3]. The geometry of the CFD model neglected some of the smaller scale structures such as the measurement probes and stands shown in Figure 4.4, which were impractical to resolve by the mesh. These small obstacles could have had some limited localised effects in redirecting the flow, generating turbulence and modifying the gas concentrations.

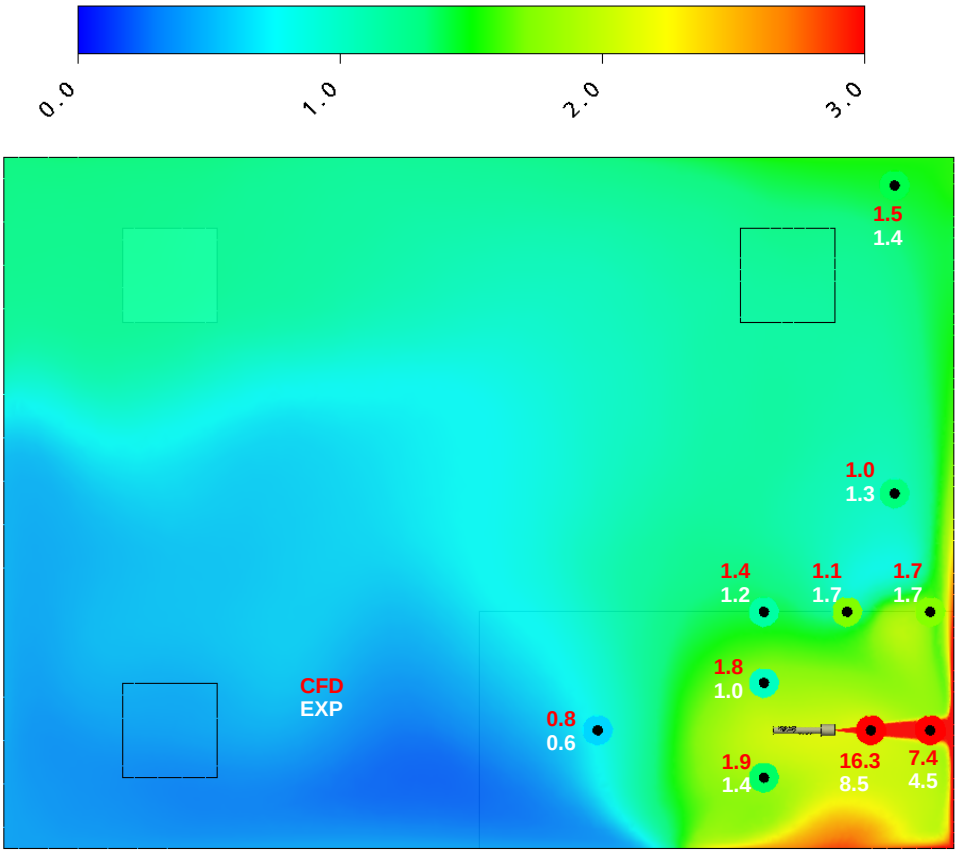

Side View

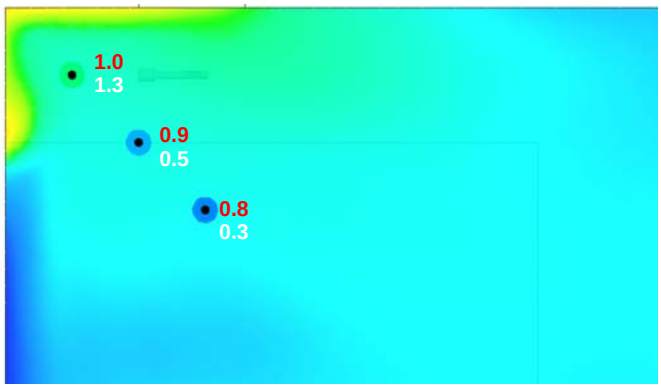

Plan View

Figure 4.28 Mean gas concentrations predicted by the DES model on side and plan sections through the room

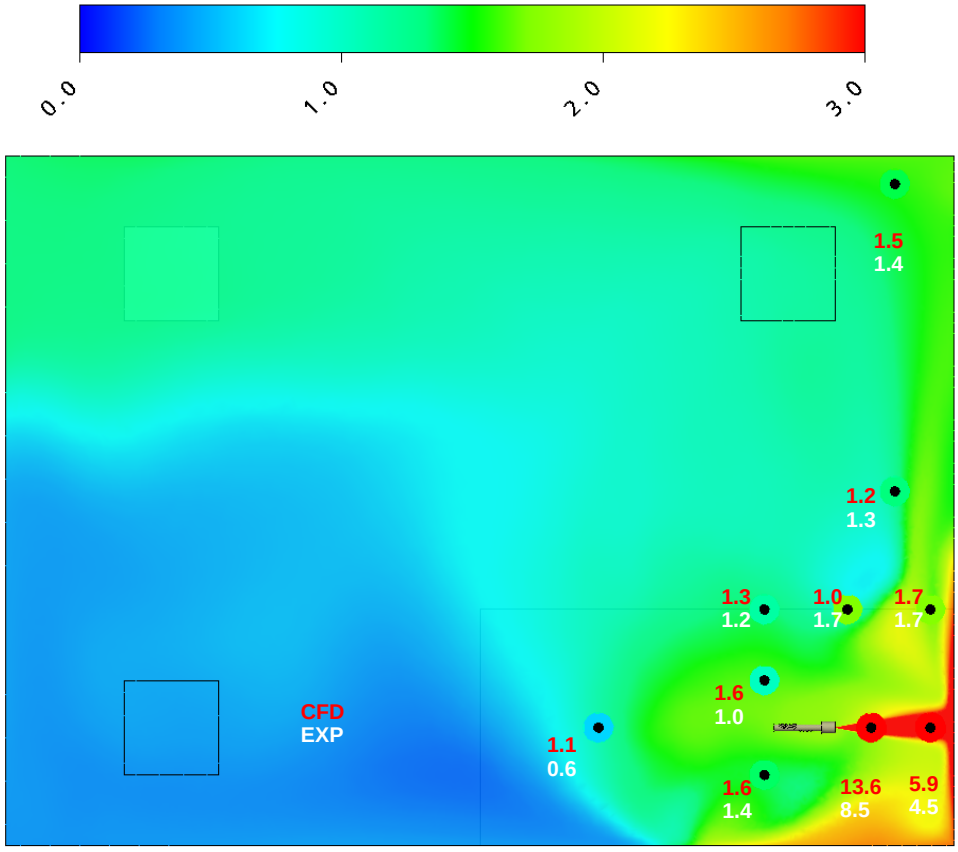

Side View

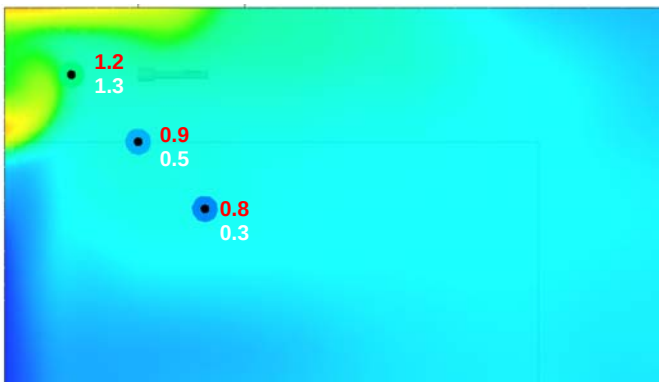

Plan View

Figure 4.29 Mean gas concentrations predicted by the SAS model on side and plan sections through the room

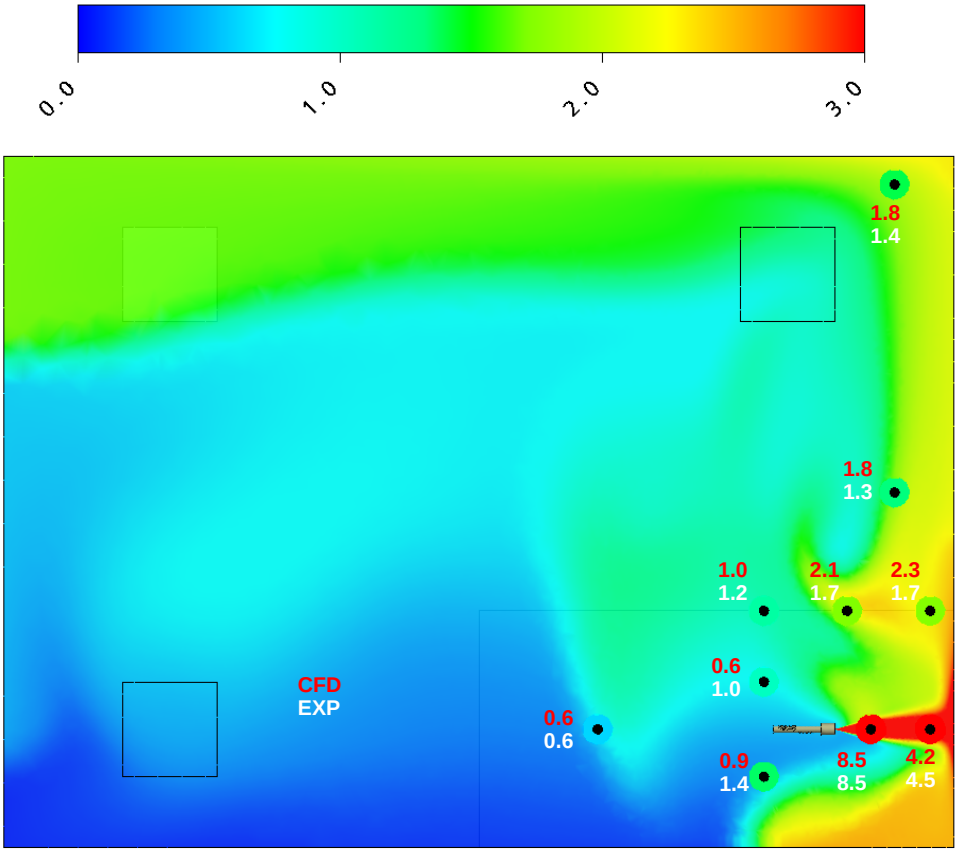

Side View

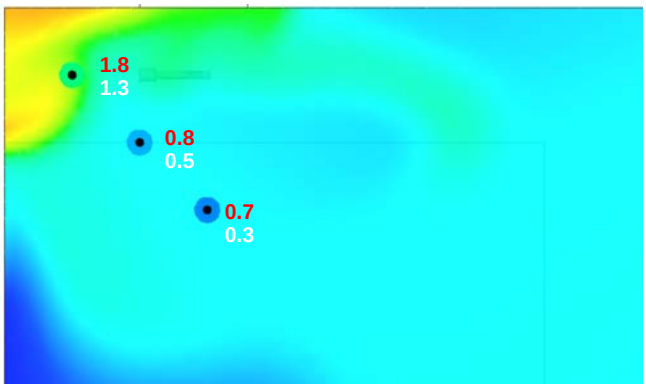

Plan View

Figure 4.30 Mean gas concentrations predicted by the URANS model on side and plan sections through the room

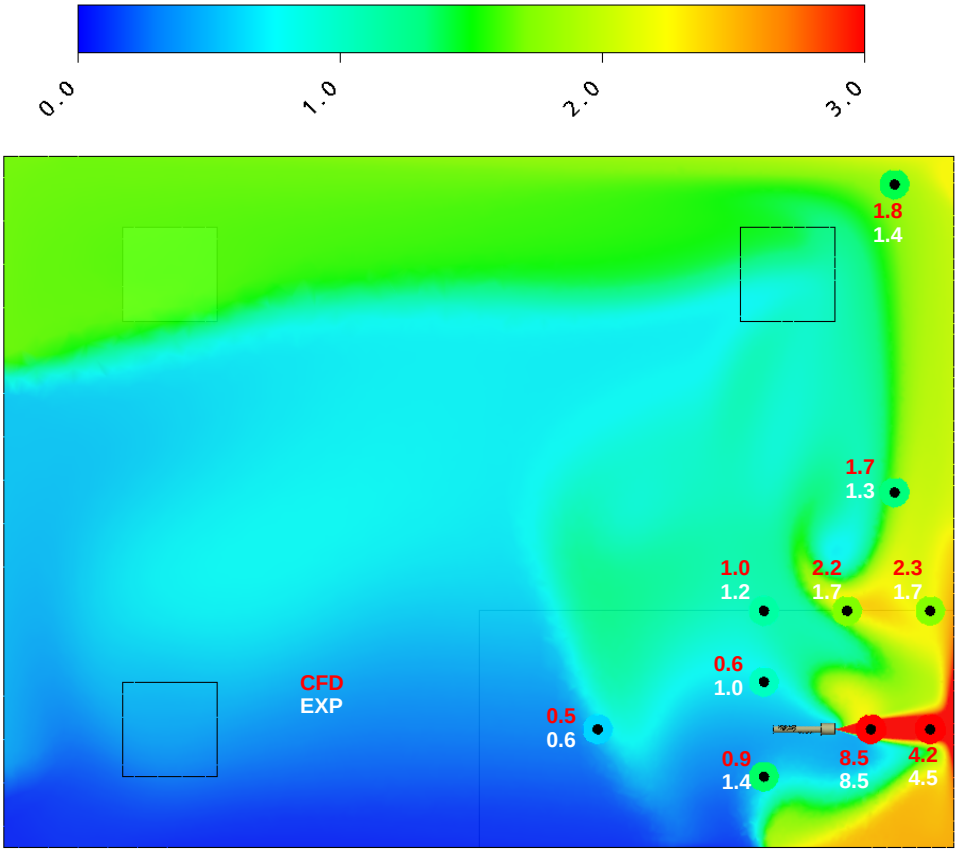

Side View

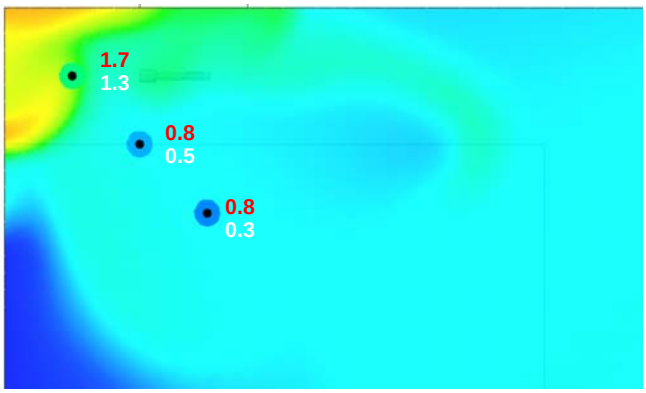

Plan View

Figure 4.31 Mean gas concentrations predicted by the RANS model on side and plan sections through the room

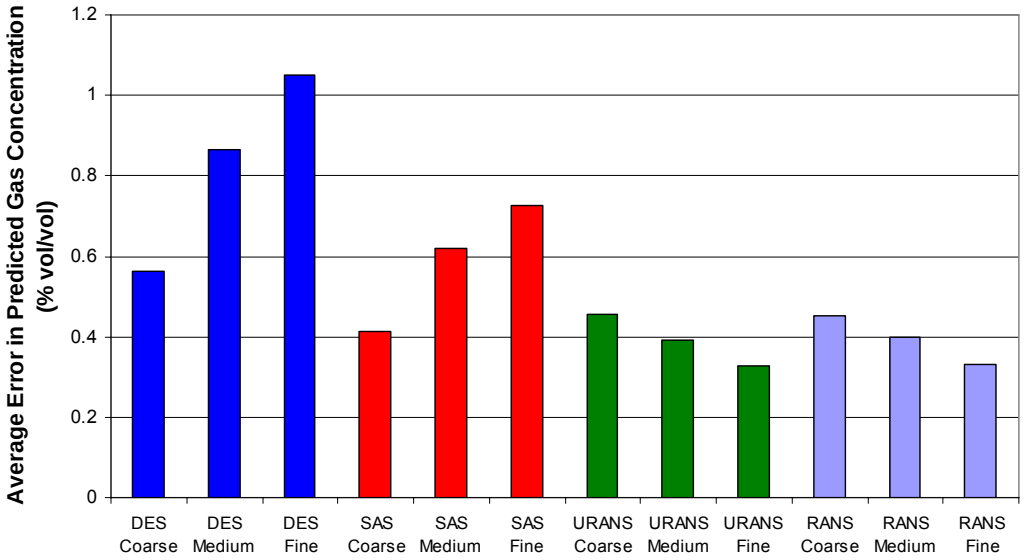

Figure 4.32 Error between the CFD and experimental mean gas concentrations averaged over all the measurement locations.

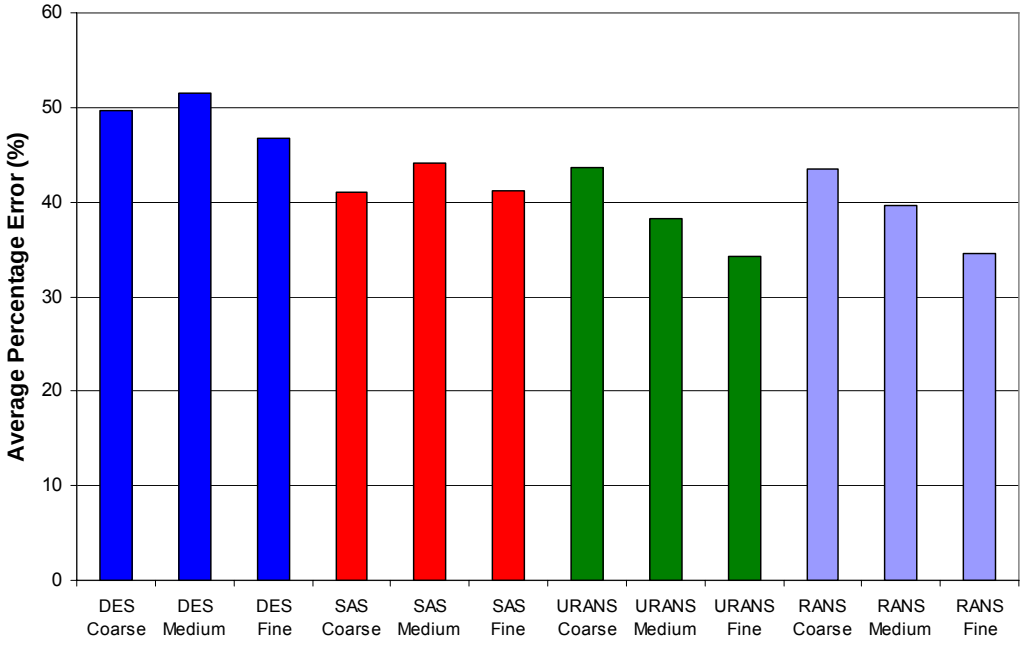

Figure 4.33 Error between the CFD and experimental mean gas concentrations expressed as a percentage of the experimental gas concentration and averaged over all the measurement locations.

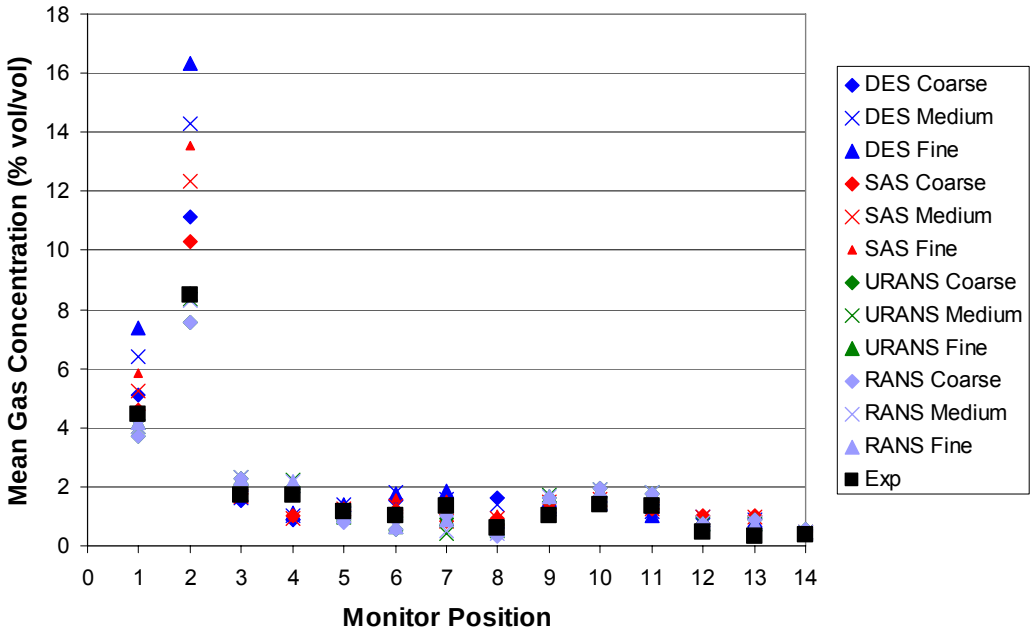

Figure 4.34 Predicted and measured mean gas concentrations at each of the 14 measurement locations

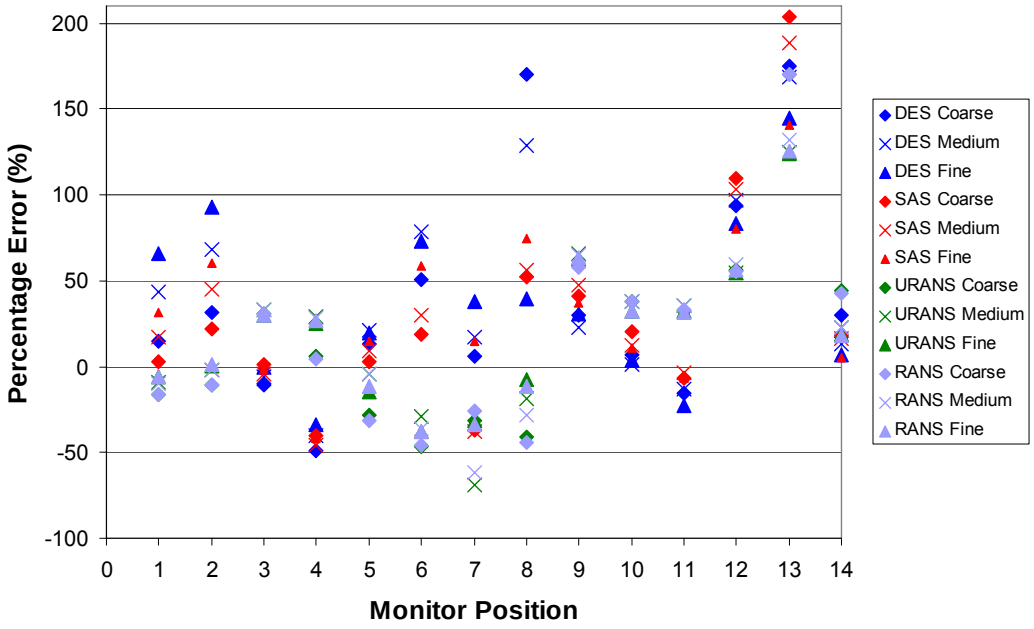

Figure 4.35 Error between the CFD and experimental mean gas concentrations expressed as a percentage of the experimental gas concentration at each of the measurement locations.

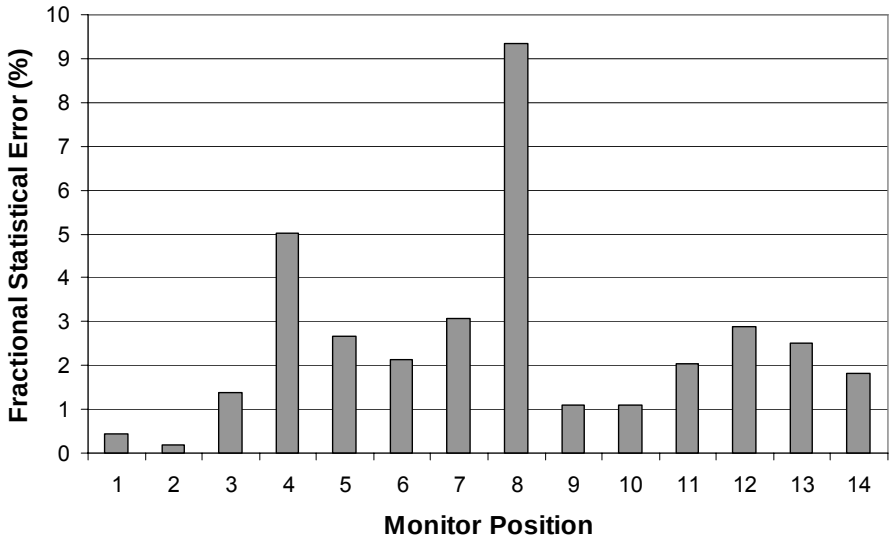

Figure 4.36 Fractional statistical error from the 95% confidence intervals in the predicted gas concentrations at the 14 measurement locations with the fine grid DES results.

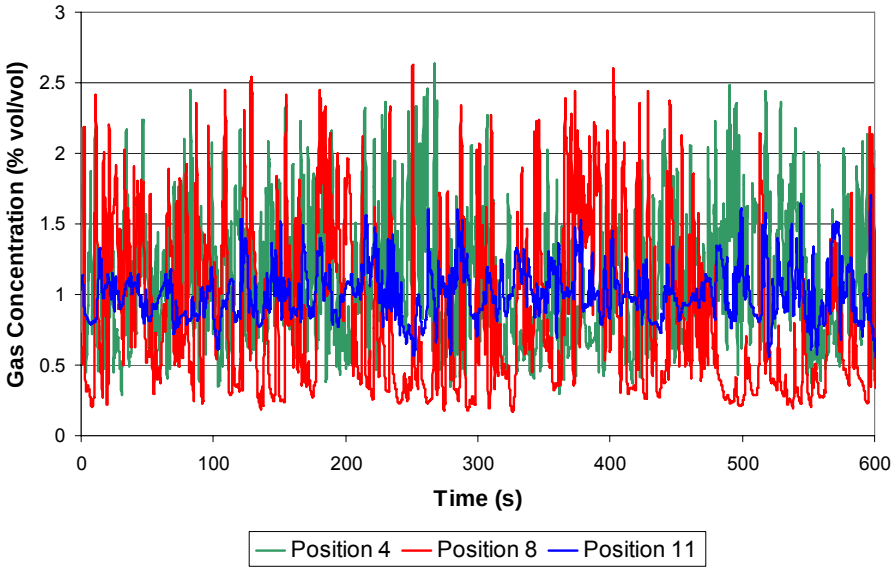

Figure 4.37 Gas concentrations at three monitoring positions in the fine-grid DES simulations

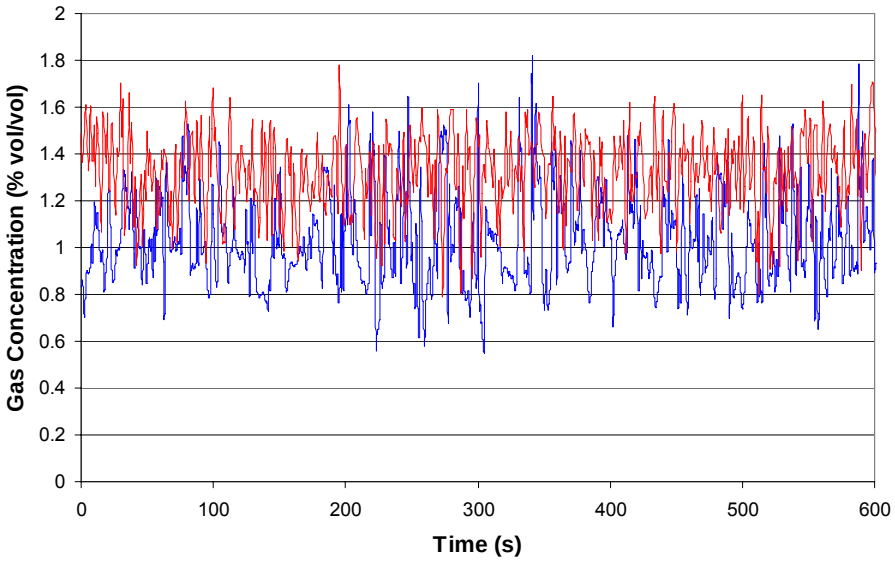

Figure 4.38 Gas concentrations at Position 11 measured in the experiments (–) and predicted by the DES model on the fine grid (–).

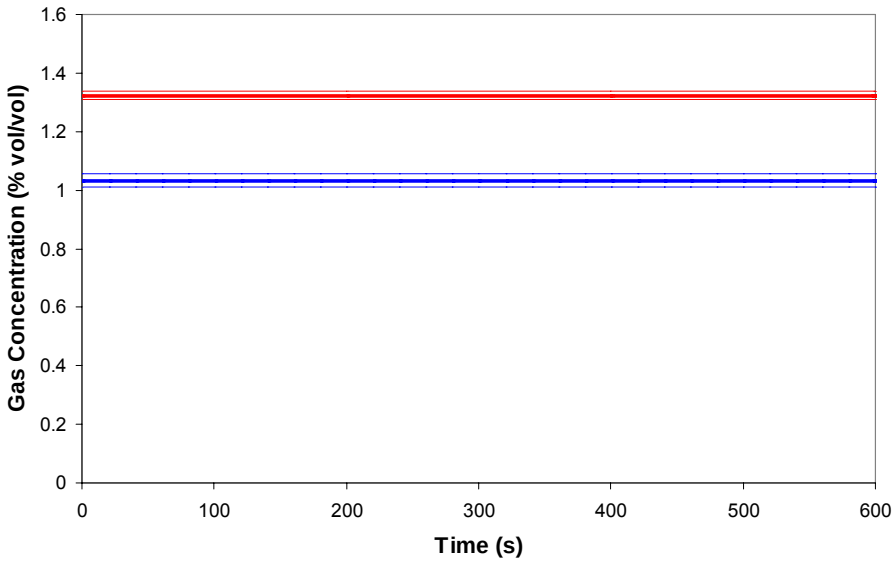

Figure 4.39 Mean gas concentrations and their 95% confidence intervals at Position 11 measured in the experiments (–) and predicted by the DES model on the fine grid (–). Mean values are shown as bold lines and the upper and lower confidence intervals by faint lines.

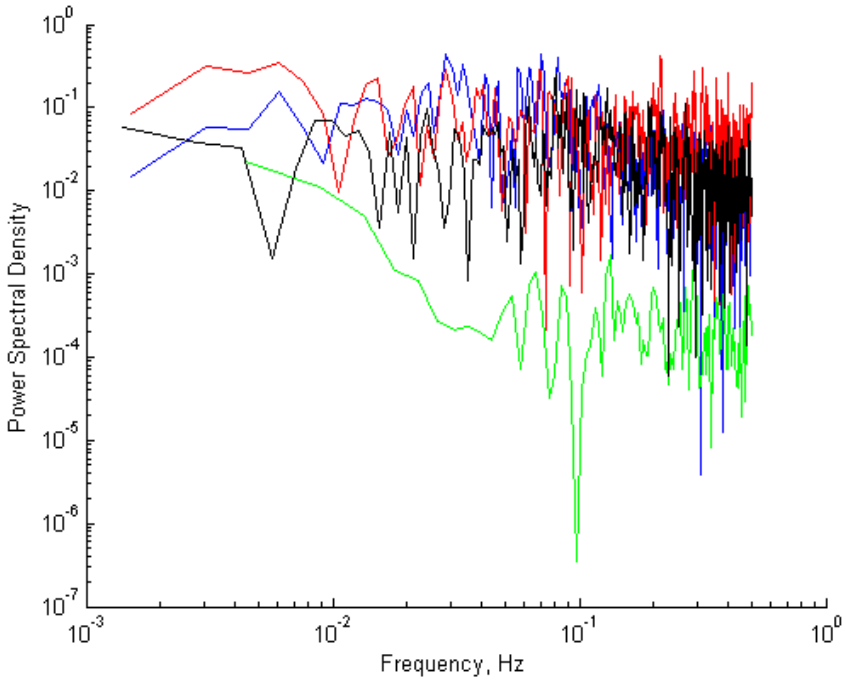

Figure 4.40 Power Spectra based on gas concentration at measurement position 11: –: experiments; –:DES; –:SAS; –: URANS. The three CFD calculations used the fine grid and their data are sampled at intervals of 1 second to match the experimental sampling rate.

4.5.2 Gas Cloud Size

The size of the gas clouds predicted by the DES, SAS, URANS and RANS models are presented in Figures 4.41 and 4.42. The gas cloud is defined as the volume enclosed by an iso-surface at the 50% LEL gas concentration (Figure 4.41) and by the Vz criterion (Figure 4.42). Since the RANS calculation is not time-dependent, instead of plotting the variation over time it is shown per solver iteration with the time interval between iterations taken as the physical timescale used by the solver[41]. The graphs show a period of 10 minutes which, based on the ventilation rate, corresponds to the time for two air-changes in the room. The DES and SAS models both exhibit large fluctuations in the gas cloud volumes. The 50% LEL volume varies between roughly 0.1 and 0.5 m^3 and Vz between 0.3 and 1.1 m^3. In contrast, the URANS and RANS cloud volumes stays relatively steady at around 0.3 and 0.7 m^3 for the 50% LEL and Vz volumes respectively. Since the URANS results were practically steady, the simulations were only run for a period of around seven minutes.

To examine the sensitivity of the gas cloud volume to the grid resolution, Figure 4.43 plots the Vz volume for the DES model using the coarse, medium and fine grids. This shows that the

[41] *In the present case, the physical timescale was 0.1 s, the same as that adopted for the time-step in the unsteady calculations. The physical timescale in the coupled ANSYS-CFX solver performs a similar role to the under-relaxation factors used in segregated solvers. With the steady RANS model, once the flow has reached a fully-developed state, and even though the residuals are very low (around 10^{-6}), the cloud volumes changed slightly from one iteration to the next.*

predictions are somewhat sensitive to the grid resolution, although from the graph it is difficult to draw precise conclusions because of the large spread in the fluctuating values.

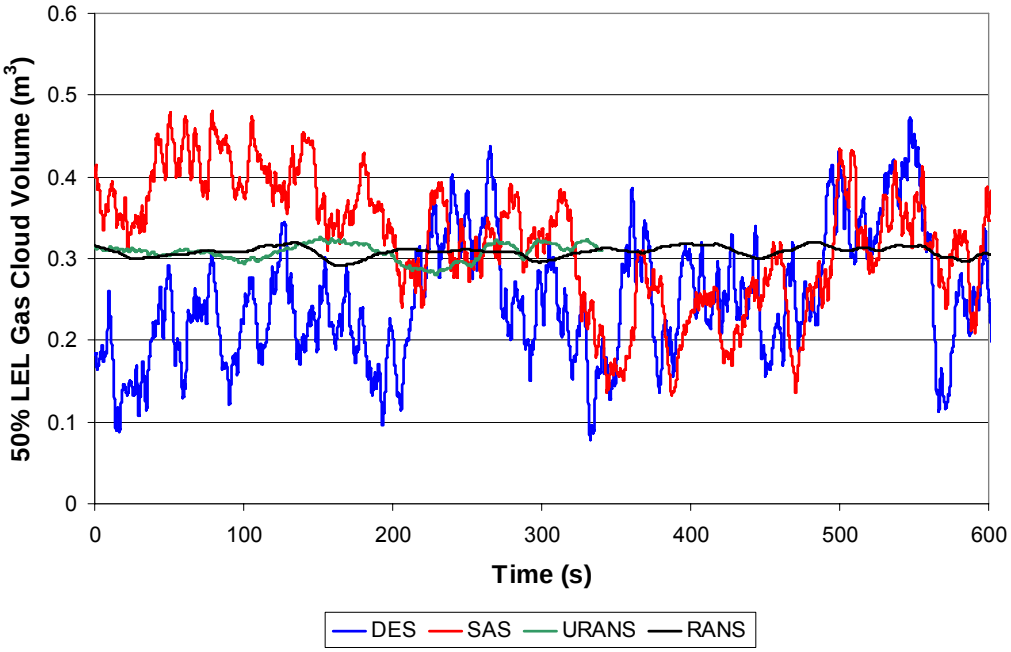

Figure 4.41 Variation of 50% LEL gas cloud volume over time for the four different CFD models using the fine grid.

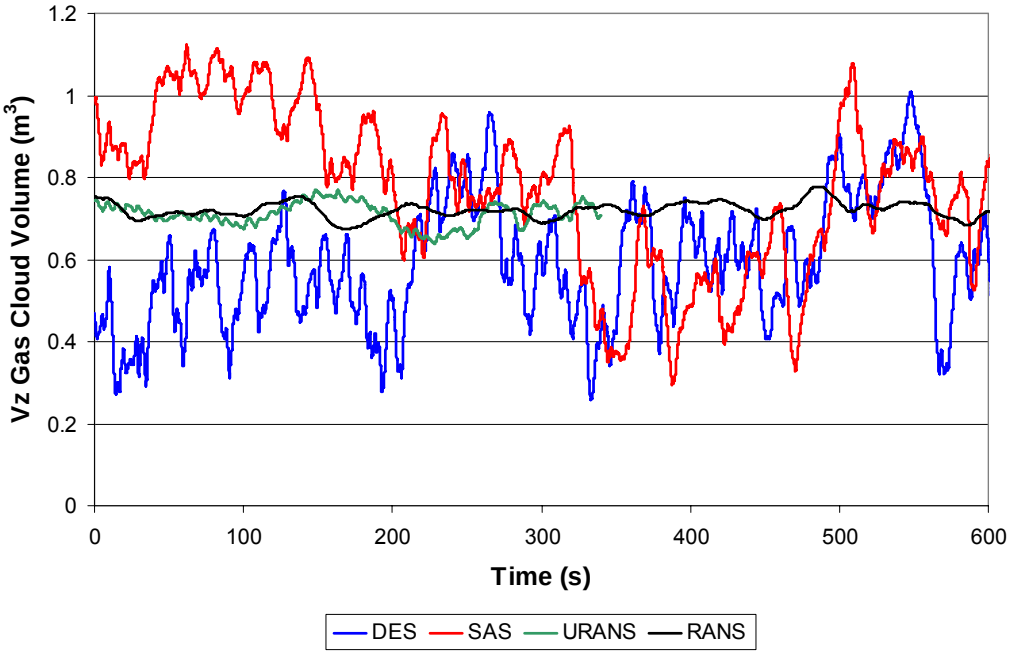

Figure 4.42 Variation of Vz gas cloud volume over time for the four different CFD models using the fine grid.

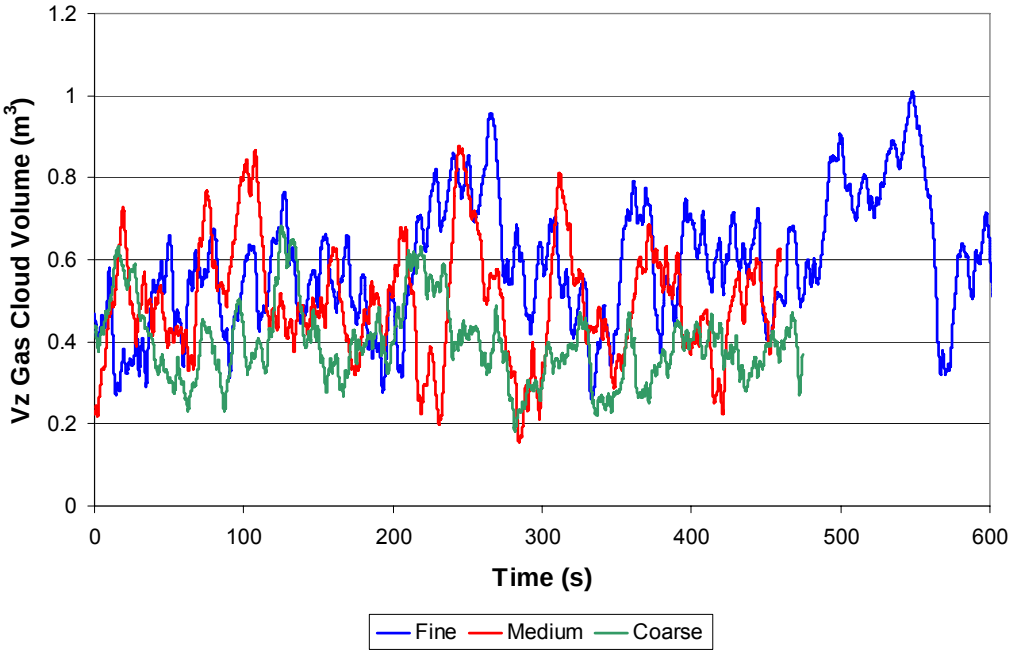

Figure 4.43 Variation of Vz gas cloud volume over time for the DES model with the coarse, medium and fine grids.

A summary of the mean predicted gas cloud volumes and their 95% confidence intervals are presented in Table 4.2 and Figure 4.44. The confidence intervals are calculated based on the bootstrapping approach described in Section 3.2.2. The large fluctuations in the cloud size with the DES and SAS models produce relatively wide confidence intervals, typically around 8%, compared to less than 1% for the URANS or RANS. The mean gas cloud volumes defined based on the 50% LEL and Vz criteria are compared in Figure 4.45. The Vz volume varies from around 0.3 m^3 for the SAS model on the coarse grid to a maximum of approximately 0.8 m^3 for the URANS model on the medium grid. For the fine grid results, the difference is less marked with minimum and maximum Vz's from 0.6 to just over 0.7 m^3. The URANS and RANS results on the fine grid, which showed best agreement with the experiments in terms of the mean gas concentrations, predicted mean Vz volumes of approximately 0.72 m^3.

One of the claimed advantages of the SAS model is that it shows less grid dependence than LES models, since the SAS equations do not rely explicitly on the size of the grid cell. However, in the results shown in Figure 4.45 the SAS model shows the greatest grid sensitivity of the four models tested.

One of the significant advantages in using an unsteady approach such as DES or SAS to model gas dispersion is that in addition to calculating the mean gas cloud volume, the simulations provide predictions of the peak values. The DES and SAS results indicate that for the case considered here the peak gas cloud volume is around 30 – 40% larger than the mean, based on the Vz volume, and around 50 – 60 % larger based on the 50% LEL volume.

Table 4.2 Mean Vz and 50% LEL gas cloud volumes and their 95% confidence intervals

Model	Grid	Mean Vz (m^3)	50% LEL (m^3)
DES	Coarse	0.41 ± 6.0%	0.17 ± 6.9%
	Medium	0.50 ± 8.1%	0.20 ± 9.1%
	Fine	0.60 ± 5.7%	0.25 ± 6.7%
SAS	Coarse	0.32 ± 6.9%	0.14 ± 8.0%
	Medium	0.43 ± 8.8%	0.19 ± 9.3%
	Fine	0.73 ± 7.9%	0.31 ± 7.0%
URANS	Coarse	0.62 ± 0.2%	0.30 ± 0.2%
	Medium	0.80 ± 0.9%	0.33 ± 0.7%
	Fine	0.71 ± 1.5%	0.31 ± 1.3%
RANS	Coarse	0.63 ± 0.8%	0.30 ± 0.8%
	Medium	0.79 ± 0.9%	0.33 ± 0.7%
	Fine	0.72 ± 0.9%	0.31 ± 0.7%

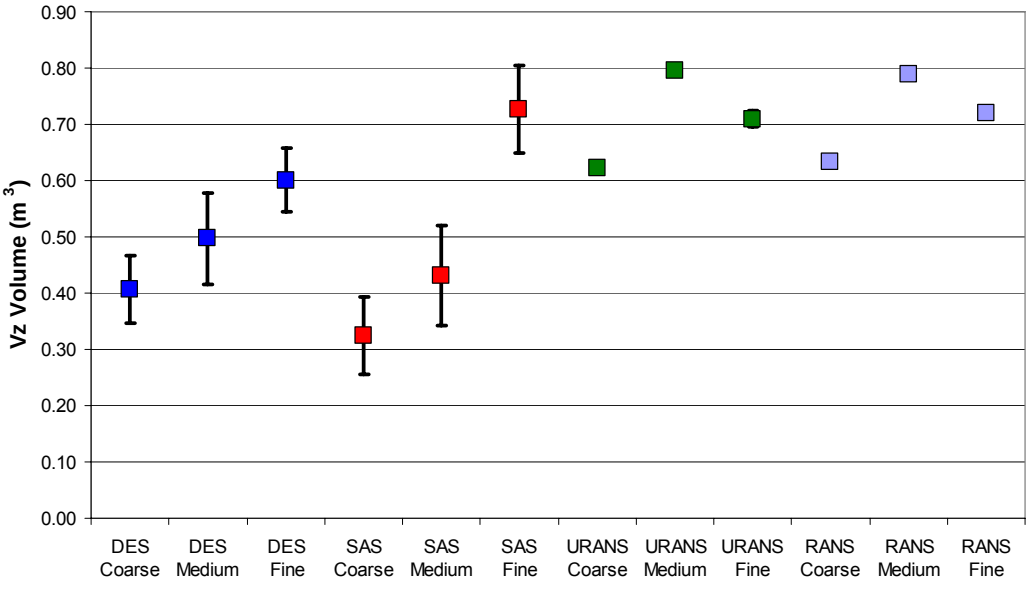

Figure 4.44 Mean Vz gas cloud volumes and their 95% confidence intervals

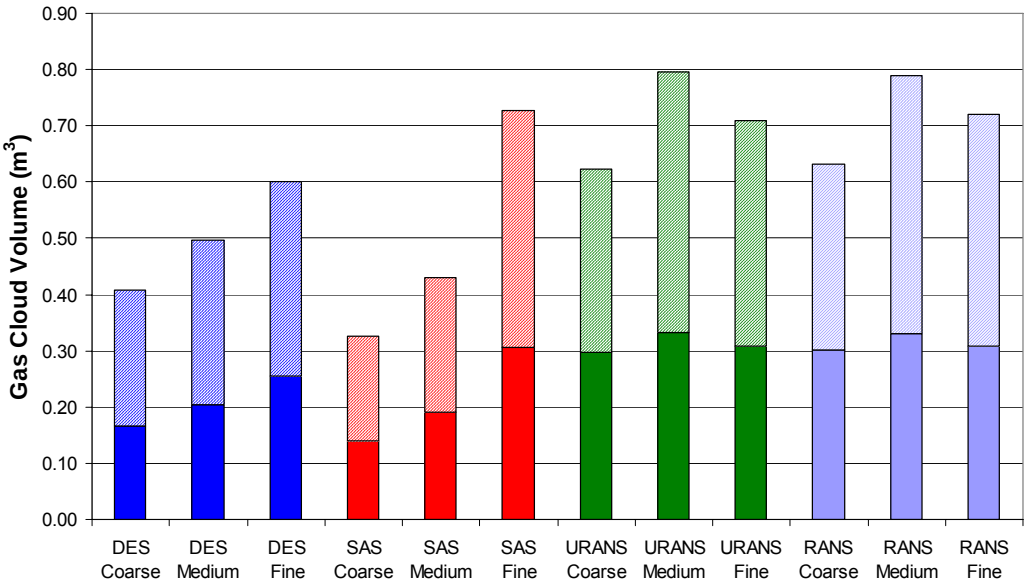

Figure 4.45 Predicted gas cloud volumes for the 12 simulations defined by a 50% LEL iso-surface (solid) and the Vz criterion (hatched).

4.5.3 Computing Times

The computing times for the 12 CFD calculations are presented in Figure 4.46. All of the calculations were started from a previously converged steady RANS solution and were performed on fast desktop PC's (with two-processor dual-core 3Ghz Intel Xeon CPU's). The fine grid DES and SAS calculations took roughly three times as long as the fine-grid URANS calculation and 16 times longer than the fine-grid RANS calculation.

The CPU time per iteration is almost identical between all four models used since they all involved solving seven transport equations (three for momentum, two for turbulence, and one each for energy and species mass fraction). The large differences shown in Figure 4.46 reflect the number of iterations required to obtain a converged solution at each time-step and the number of time-steps required in order to produce reasonably converged averaged statistics. Since the DES and SAS models produced far greater temporal variations in the gas concentration than the URANS model it was necessary to run these calculations for a greater period of time. The effect of solving fewer time-steps can be seen in the confidence intervals shown in Table 4.2. The fine-grid URANS has a larger error of around 1.5% compared to the medium grid value of around 1% since statistics have been averaged over a shorter interval.

A more precise and objective approach to the comparison would have been to run the simulations for a sufficient duration in order to achieve a prescribed confidence level, as suggested by Moene & Michels [199]. If this approach had been taken the differences between the DES or SAS and the URANS or RANS models would be even more marked, since the DES and SAS models simulations would have had to be continued for a significantly longer period of time to bring the error in confidence intervals down to the level of the URANS and RANS results.

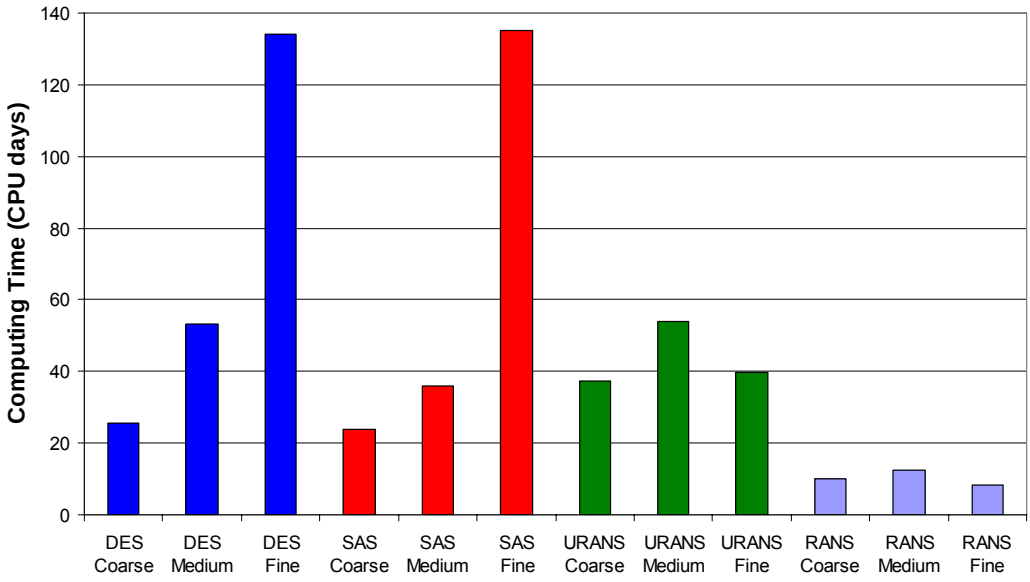

Figure 4.46 Computing times for the 12 CFD simulations

5 DISCUSSION

In Section 3 a number of techniques that can be used to assess the grid resolution in large-eddy simulations were identified from a literature survey. A selection of these were then used in Section 4 to investigate a flow involving a gas release in a ventilated room, a case typical of an industrial CFD problem. The grid resolution measures tested here included the ratio of the cell size to the integral and Kolmogorov length scales, the eddy-viscosity ratio, the relative effective viscosity index, the subgrid activity parameter, the ratio of resolved to modelled turbulent kinetic energy, the LES index of quality and analysis of the concentration power spectra.

A number of the measures tested were unable to provide useful information in some regions of the room due to the low turbulence levels present, where far from the gas jet and the ventilation inlets the flow was practically laminar. In particular, this was a problem for the approaches based on prior RANS simulations, where the modelled turbulent kinetic energy and dissipation rate fell to zero in laminar regions, and hence the length-scale ratios became meaningless. Also in the spectral analysis the absence of a well-defined inertial subrange and the influence of buoyancy effects introduced difficulties when comparing the spectrum from the CFD simulations against the theoretical -5/3 slope.

In the plume region, where the flow was more turbulent and the DES model operated in LES mode, the calculated ratio of the integral turbulence length scale to the cell size was of the order 8 for the fine grid, which was towards the coarse end of the range of values recommended for LES in the literature. The ratio of the cell size to the Kolmogorov length scale was also around 40, which is nearly double the value used in other LES studies in the literature, indicating again that the fine grid used here was still too coarse for well-resolved LES.

The subgrid activity parameter proposed by Geurts & Fröhlich [89] was found to take a value close to unity across most of the room and showed little sensitivity to the grid resolution. Similar results were obtained using the more recent modified version of this parameter, devised by Celik *et al*. [58]. This behaviour was related to the relatively large turbulent viscosity in all but the laminar regions of the flow.

The ratio of the resolved to the total turbulent kinetic energy indicated that both the DES and SAS models on the fine grid resolved between 70 and 90 % of the turbulence energy in the plume region, which suggested that the grid resolution in that region was actually quite reasonable for LES. As noted in the review of this approach in Section 3.3.7, however, the measure does not account for the effects of numerical dissipation and since the resolved turbulent kinetic energy can actually be higher on coarse grids than on finer grids, this conclusion should be interpreted with care.

The LES "index of quality", *LES-IQ*$_k$, which was based on Richardson extrapolation using the medium and fine-grid LES solutions, produced values in excess of 100% and less than 0%. This was found to be related to significantly larger values of the resolved turbulent kinetic energy on the coarser of the two grids. In addition, the ratio of cell sizes of the two tetrahedral grids did not vary smoothly which caused *LES-IQ*$_k$ to vary discontinuously and made interpreting the results more challenging. It has been pointed out in the literature that the measure can produce incorrect values when the resolution is marginal and grid convergence is not within the asymptotic range. This is almost certain to be a factor in the present simulations.

Comparisons of the various model predictions on the three different grids against the experimental data produced some unexpected results. Predictions of the mean gas concentrations were on average worst with DES and best with the URANS and RANS models.

Moreover, the error in the DES model predictions actually increased rather than decreased as the grid was refined. This makes it difficult to draw useful conclusions from the various LES grid quality measures, since these would naturally indicate that a finer grid would be of higher quality, whereas the model predictions show the reverse trend. It should be noted however, that the experimental data was relatively sparse for the case studied, consisting entirely of gas concentration measurements at only 14 locations.

For the application considered, the main parameter of interest is the size of the gas cloud. The range of predicted gas cloud volumes using the different modelling approaches was presented in Section 4.5.2, together with confidence intervals which were calculated using the novel bootstrapping statistical method described in Section 3.2.2. It was shown that the mean Vz volume varied between 0.5 and 0.8 m^3 depending upon which turbulence model and grid was used. The fine grid RANS model results, which showed best agreement with the measured gas concentrations, predicted a mean Vz volume of approximately 0.72 m^3.

Finally, it should be noted that the results showed that even the RANS model predictions were not totally grid-independent. In refining the mesh from the medium to the fine grid, the Vz volume decreased from 0.79 to 0.72 m^3 and the 50% LEL volume from 0.33 to 0.31 m^3. In the context of hazardous area classification, however, this degree of sensitivity may be considered acceptable. The SAS model, which should in theory have shown less sensitivity to the grid resolution than the DES model since it does not explicitly involve the cell size in its constitutive equations, in fact showed the largest degree of grid sensitivity with the predicted Vz volume varying from 0.32 to 0.73 m^3.

6 CONCLUSIONS

The present work has surveyed a number of techniques that have been suggested in the literature for assessing the quality of large-eddy simulations. Issues related to the unsteady, time-varying nature of the simulations and the computational grid resolution have been examined in some detail, and other topics such as LES model choice, wall treatments, numerical methods and turbulent inflow conditions briefly discussed.

To assess the statistical uncertainty in time-averaged values, a relatively novel technique for calculating confidence intervals from correlated time-varying data has been presented. The approach, based on bootstrapping, has a number of advantages over previous methods used to assess confidence intervals in LES.

A total of ten separate measures to assess the quality of the spatial resolution used in LES have been identified. These included approaches based on rules-of-thumb or prior RANS simulations, single-grid estimators involving just one LES calculation, and other approaches involving multiple LES calculations. The advantages and disadvantages of each approach were documented and references provided for examples of their use in the literature.

Simulations of a low-pressure choked gas release in a ventilated room using Detached-Eddy Simulation (DES) were presented. The particular flow studied was typical of a practical scenario investigated as part of an industrial safety study. The DES results were compared to those obtained using steady and unsteady RANS models and Scale-Adaptive Simulation (SAS). A number of quality indices were used to assess the grid resolution. Overall, these measures indicated that even the finest grid used in the present study was relatively coarse for LES. The practical limitations of various indices were also documented.

The results from the simulations were compared to experimental measurements where it was found that the DES model performed relatively poorly in comparison to the RANS-based models. Contrary to the anticipated behaviour, the DES and SAS predictions also deteriorated as the grid was refined. The mean size of the gas clouds predicted using the various models were calculated together with their confidence intervals, using the bootstrapping technique. Of the four models tested, the SAS model was found to exhibit greatest sensitivity to the grid resolution. Computing times for the different modelling approaches were also compared.

Overall, the literature review and case study showed that there is no single criterion that provides wholly reliable estimates of the quality of the grid used in LES of complex industrial flows. Data from RANS was shown to be useful in designing the grid for LES but as the case study showed, there were problems when the flow is partly transitional or laminar. Other quality measures encountered difficulties with being sensitive to the Reynolds number, in accounting for numerical dissipation or in dealing with situations where the resolved turbulent kinetic energy was higher on coarse grids than on fine grids.

Although the various quality measures can provide some limited useful information, at present it appears that the spatial resolution needs to be assessed by performing multiple simulations on different grids with a range of cell sizes, similar to the approach usually taken with RANS simulations. As well as undertaking these tests, to provide confidence in the LES results additional simulations may need to be undertaken to assess the sensitivity of the predictions to the turbulence model, the numerical treatment and the boundary conditions. Such sensitivity tests are often avoided in industrial studies as they are usually costly in terms of computing time. The present work highlights that for indoor-air gas dispersion studies, the computing power of fast multi-processor desktop PC's is barely sufficient to consider using LES-based

techniques. If the main interest in undertaking the study is to predict *peak* values or understand the statistical spread in values about the mean, then LES is clearly the appropriate model for the task instead of unsteady RANS. However, the computing times involved in LES should not be underestimated.

The issue of quality and trust in LES encompasses a huge volume of research and the field is currently developing rapidly. Whilst every effort has been made to provide a reasonably comprehensive and accessible review, by the nature of the subject this report cannot fully cover all of the research carried out in this area and it is likely to become outdated relatively rapidly. In view of the foreseeable use of LES for modelling safety critical applications in the near future, it is recommended that further work be carried out to help understand LES quality issues.

7 APPENDIX A: SMAGORINSKY TURBULENCE MODEL

The filtered momentum equation in Cartesian tensor notation is given by:

$$\frac{\partial}{\partial t}\left(\rho U_i\right)+\frac{\partial}{\partial x_j}\left(\rho U_i U_j\right)=-\frac{\partial P}{\partial x_i}+\frac{\partial}{\partial x_j}\left(2\mu S_{ij}-\tau_{ij}\right) \qquad (7.1)$$

where U_i is the filtered velocity, ρ the density, P the pressure, μ the molecular viscosity, S_{ij} the strain-rate tensor, given by:

$$S_{ij}=\frac{1}{2}\left(\frac{\partial U_i}{\partial x_j}+\frac{\partial U_j}{\partial x_i}\right) \qquad (7.2)$$

and τ_{ij} the subgrid-scale (SGS) stress, calculated from

$$\tau_{ij}-\frac{1}{3}\tau_{kk}\delta_{ij}=-2\mu_t S_{ij} \qquad (7.3)$$

where the term involving the Kronecker delta, δ_{ij}, is included to make the expression on the left-hand-side deviatoric. The subgrid-scale dynamic viscosity, μ_t, is:

$$\mu_t=\rho\left(C_s\Delta\right)^2 S \qquad (7.4)$$

The other terms in the above equations include: C_s the Smagorinsky constant, Δ the filter width, x_j the Cartesian coordinates and S the strain-rate invariant, which is calculated from:

$$S=\sqrt{2S_{ij}S_{ij}} \qquad (7.5)$$

Laurence [95] noted that in many industrial LES papers, the factor of 2 in Equation (7.3) is neglected, which can lead to misleading comparisons based on values of C_s.

In the text of this report, the kinematic instead of the dynamic viscosity is often used, which is given by: $\nu_t=\mu_t/\rho$.

8 APPENDIX B: SPECTRAL ANALYSIS

Turbulent flows are characterised as having eddy structures which feature a range of time and spatial scales. Figure 8.1 presents a typical trace of velocity recorded at a point in a turbulent flow over time showing the seemingly random fluctuations characteristic of turbulence. Spectral analysis as applied to turbulent flows consists of decomposing these fluctuations according to their frequency, either in space or time.

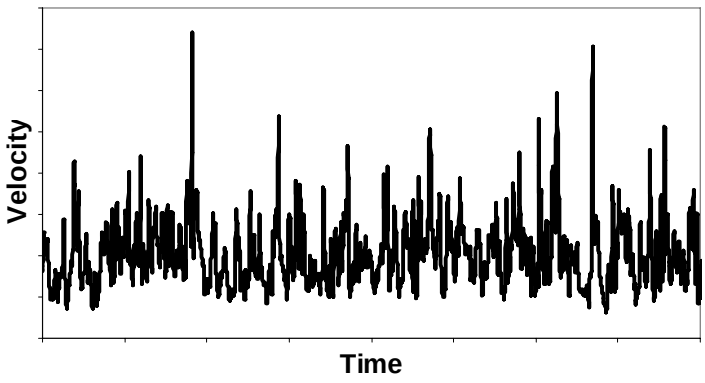

Figure 8.1 Turbulent velocity signal taken from DNS of a channel flow

The following sections briefly describe some of the basic functions that are commonly used in spectral analysis, including the Fourier transform, autocovariance, autocorrelation, convolution and power spectral density. More detailed descriptions can be found in the text books on digital signal processing by Lynn & Fuerst [200] and Ifeachor & Jervis [201].

8.1 FOURIER TRANSFORMS

As was mentioned above, spectral analysis is based on the principle of representing a complex turbulent signal such as that shown in Figure 8.1 in terms of the summation of many sine or cosine waves. The Fourier transform provides a method of calculating the amplitudes of each of these component waves.

The continuous Fourier transform is defined as:

$$\hat{u}(\omega) = \frac{1}{2\pi} \int_{-\infty}^{\infty} u(t) e^{-i\omega t} dt \qquad (8.1)$$

and the inverse transform as:

$$u(t) = \int_{-\infty}^{\infty} \hat{u}(\omega) e^{i\omega t} d\omega \qquad (8.2)$$

where $u(t)$ is the fluctuating signal which varies as a function of time, ω is the frequency, $\hat{u}(\omega)$ is the Fourier coefficient which represent the amplitude of the component waves. There is no accepted standard format for the position of the factor $(1/2\pi)$ in Equations (8.1) and (8.2). Here, the $(1/2\pi)$ appears in the forward transform, following the convention of Pope [15], Batchelor [202] and Tennekes & Lumley [203]. In some texts the factor is split evenly between the forward and inverse transforms. Similarly, the exponents ($-i\omega t$) and ($i\omega t$) must be of opposite sign in the forward and inverse transform but are shown differently in various texts (e.g. [204, 205]).

In most practical cases, the signal $u(t)$ is not a continuous function but a set of discrete measurements. This is the true both for numerical simulations, where values are given at intervals dictated by the chosen time-step, Δt, or in measurements where there is a given sampling frequency. In these cases, where the signal is $u(t)$ and the time is $t = k\Delta t$ and $k = 0, 1, 2, \ldots, (n-1)$, the discrete Fourier transform is given by:

$$\hat{u}(\omega) = \sum_{k=0}^{n-1} u(t) e^{-i\omega t} \qquad (8.3)$$

and the inverse discrete transform by:

$$u(t) = \frac{1}{N} \sum_{k=0}^{n-1} \hat{u}(\omega) e^{i\omega t} \qquad (8.4)$$

There are a number of software tools that can be used to calculate the discrete forward and inverse Fourier transforms, notably the commercial software Matlab[42] and the freeware programs SciLab[43] and Octave[44].

8.2 AUTOCOVARIANCE AND AUTOCORRELATION

The autocovariance, R, is defined as follows:

$$R(s) = \overline{u(t)u(t+s)} \qquad (8.5)$$

where $u(t)$ is the signal which is varying over time, s is an interval in time and the overbar represents a long time-average. The process of calculating the autocovariance involves multiplying the velocity fluctuation signal by a copy of itself which has been offset in time by an interval s, and then taking the time-average of the result. As mentioned above, most turbulence signals are not recorded as a continuous function but a set of discrete measurements. The autocovariance for a discrete signal is calculated from:

$$R_k = \frac{1}{N} \sum_{n=1}^{N} u_n u_{n+k} \qquad (8.6)$$

where u_n is the velocity fluctuation at time $t = n\Delta t$, the offset in time is $s = k\Delta t$ and N is the total number of data points, which should be sufficiently large to obtain a statistically steady average.

[42] http://www.mathworks.com, *accessed June 2008.*
[43] http://www.scilab.org, *accessed June 2008.*
[44] http://www.octave.org, *accessed June 2008*

The autocovariance is a measure of how similar the signal is to itself when it is offset by a certain time interval. The maximum value of $R(s)$ is therefore obtained when the offset is zero $\left[R(0) = \overline{u(t)u(t)}\right]$, when the signal is multiplied by an exact copy of itself. The autocovariance with zero offset, $R(0)$, of a velocity fluctuation signal with zero mean is the same as the Reynolds stress.

A function that is identical when the sign of the independent variable is changed [$f(t) = f(-t)$] is known as an "even" function. The cosine function is even, since it is symmetric about zero, whereas the sine function is odd. The autocovariance is an even function, since multiplying a signal by a copy of itself with a time offset of s or of -s produces the same result.

The autocorrelation, $\rho(s)$, is the autocovariance normalized by its maximum value:

$$\rho(s) = \frac{\overline{u(t)u(t+s)}}{\overline{u(t)^2}} \qquad (8.7)$$

Consequently, the autocorrelation for a zero time offset is unity, i.e. $\rho(0) = 1$ and the autocorrelation is always less than or equal to unity, $\rho(s) \leq 1$. In turbulent flows, the autocorrelation usually decreases rapidly with increasing s. The autocorrelation for the velocity signal shown in Figure 8.1 is shown in Figure 8.2.

The integral timescale, τ, in a turbulent flow can be calculated by integrating $\rho(s)$ over all values of s until the autocorrelation decreases to zero, as shown by the shaded area in Figure 8.2.

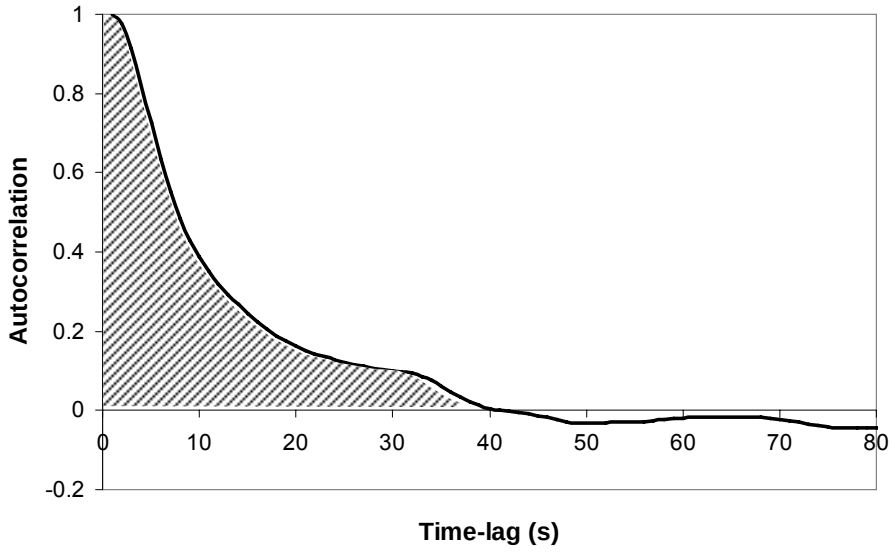

Figure 8.2 Autocorrelation calculated from the velocity signal shown in Figure 8.1

8.3 CONVOLUTION

For two functions, $f(t)$ and $g(t)$ which are both functions of time, their convolution, $h(t)$ is defined as

$$h(t) = \int_{-\infty}^{\infty} f(\tau) g(\tau + t) d\tau \qquad (8.8)$$

taking the Fourier transform of both sides of this equation, it can be shown[45] that:

$$F\{h(t)\} = 2\pi F\{f(t)\} F\{g(t)\} \qquad (8.9)$$

where F represents the Fourier transform. The above equation shows that the Fourier transform of the convolution is equal to 2π times the product of the Fourier transforms of the two functions $f(t)$ and $g(t)$.

The convolution operation is useful in simplifying the calculation Fourier transform of the autocovariance. Rather than first having to calculate the discrete autocovariance in physical space from:

$$h_k = \sum_{n=1}^{N} u_n u_{n+k} = NR_k \qquad (8.10)$$

and then take its Fourier transform, instead it can be determined by simply taking the Fourier transform of the velocity to obtain the Fourier coefficients, $\hat{u}$, and then by taking the square of the coefficients and multiplying by 2π obtain the same result:

$$F\{h\} = 2\pi\hat{u}^2 \qquad (8.11)$$

8.4 POWER SPECTRAL DENSITY (PSD)

The energy spectrum or power spectral density, $E(\omega)$, provides a useful indicator of the amount of energy contained in turbulent fluctuations of different frequency. It is calculated from twice the Fourier transform of the velocity autocovariance, $R(s)$, or in other words:

$$E(\omega) = 2F\{R\} = 2F\left\{\frac{h}{N}\right\} = \frac{2}{N} 2\pi\hat{u}^2 \qquad (8.12)$$

There are three common approaches taken to create a plot of the PSD:

1.) Using one of the in-built routines in MatLab, such as ‘psd’ or ‘pwelch’

2.) Taking the Fast Fourier Transform (FFT) of the velocity fluctuation and plotting the square of the Fourier components

3.) Determining the autocovariance in physical space and plotting its Fourier transform

Sample MatLab code for calculating the PSD using these three approaches is given below. Please note that the code has not been optimised and cannot be guaranteed to be error free. A plot of the PSD generated from running the code is shown in Figure 8.3. Further details of the calculation procedures involved in determining the PSD, such as “data windowing”, can be

[45] *See for example p681 in Pope [14].*

found in Numerical Recipes [204]. The methods described here are based on those described in course on "Unsteady Simulations for Industrial Flows"[46] by Davidson [206].

```
% A MatLab program for calculating the Power Spectral
% Density using three alternative approaches
% ================================================

% Open and read data
% ==================
load u_v_time_4nodes.dat
u1=u_v_time_4nodes(:,1);

% number of points and time-step
% ==============================
nmax=5000;
dt=0.0033;

% find mean and fluctuations
% ==========================
umean1=mean(u1);
u1=u1-umean1;

% Method 1: Use the Matlab PSD function
% =====================================
[psd0,f0]=psd(u1,nmax,1/dt);
plot(f0,psd0,'b-o');
h=gca;
set(h,'yscale','log','xscale','log')
hold

% Method 2: The square of the Fourier components
% ==============================================
H=hann(nmax); % data windowing
u1win=H.*(u1);
u1fft=fft(u1win);
psd1=u1fft(1:nmax/2).*conj(u1fft(1:nmax/2));
psd1=0.85*pi*psd1/nmax;
f1(1:nmax/2)=0;
for m=1:nmax/2
   f1(m)=(m-1)/(nmax*dt);
end;
plot(f1,psd1,'r-');

% Method 3: Find autocovariance and then take FFT
% ===============================================
autocov(1:nmax)=0;
for k=1:nmax
  for n=1:nmax
    noffset=n+k-1;
    if (noffset > nmax)
      noffset=noffset-nmax; %<-- even periodic signal
    end;
    autocov(k)=autocov(k)+u1(n)*u1(noffset);
```

[46] http://www.tfd.chalmers.se/~lada, *accessed June 2008.*

```
  end;
end;
autocov=autocov'/nmax;
acwin=H.*autocov;
E=fft(acwin);
psd2=abs(E(1:nmax/2));
plot(f1,psd2,'g-');

% add line with -5/3 slope
% ========================
pk(1)=100;
fk(1)=1;
a=pk(1)/fk(1)^(-5/3);
fk(2)=10;
pk(2)=a*fk(2)^(-5/3);
plot(fk,pk,'k-');

% scale and label axes
% ====================
%axis([0.5 1000 1e-7 10000])
title('spectrum of u','fontsize',20)
xlabel('f','fontsize',20)
ylabel('E(u)','fontsize',20)
h=gca;
set(h,'yscale','log','xscale','log')
set(h,'fontsi',[10])

legend('psd','square of fft coeffs','fft of
autocovariance','5/3','location','SouthWest');
```

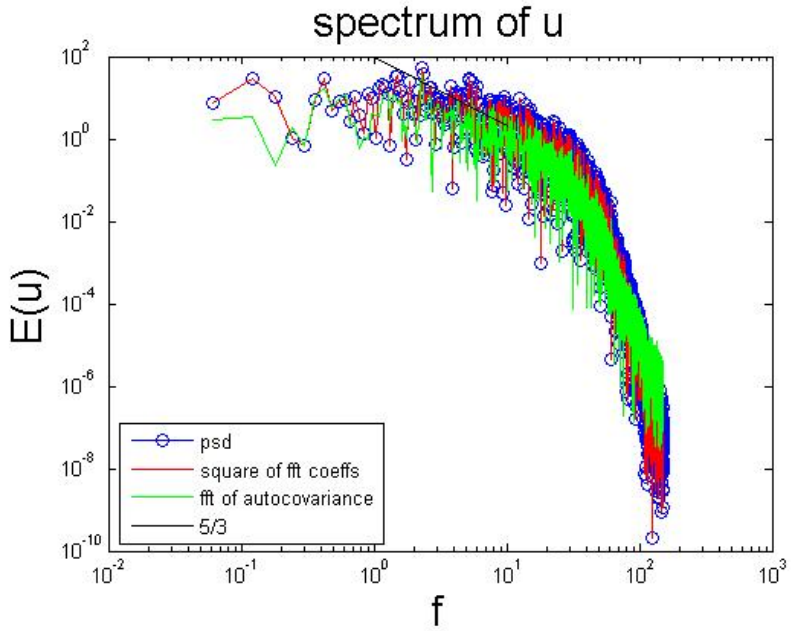

Figure 8.3 Power spectral density of the data shown in Figure 8.1 calculated using three alternative approaches.

9 APPENDIX C: BOOTSTRAPPING

In Section 3.2.2 a statistical technique known as "circular dependent bootstrapping" is described for calculating confidence intervals from data obtained from LES. The approach has previously been widely used in the field of economics but has only recently been applied to fluid dynamics and turbulence [106, 107].

A good introduction to bootstrapping is given in the book by Wilks [108]. The general approach used in the present work is similar to that described in Theunissen *et al*. [106]. The block length was calculated using the approach devised by Politis, White and Patton [207, 208], using the MatLab code available on Dr. Andrew Patton's website[47]. The MatLab code for the bootstrapping procedure used in the present work is presented below. No effort has been made to optimise the code and it cannot be guaranteed to be error free.

```
% A MatLab program for calculating Confidence Intervals using
% the circular dependent bootstrapping method
============================================================

% Read in data
% ============
load RANS_fine_CI_data.dat;
series=RANS_fine_CI_data(:,2);

% Calculate block length
% ======================
Bstar = opt_block_length_REV_dec07(series); %← calls Patton's code
BstarCB = Bstar(2);
blockLengthCB = ceil(BstarCB);

% Set the number of bootstraps
% ============================
numberBootStraps = [100 200 500 1000 2000 5000 10000 20000 50000
100000];

% Determine positions of 68% and 95% confidence intervals
% =======================================================
lower_68position = int32(0.16 * numberBootStraps);
upper_68position = int32((1.0 - 0.16) * numberBootStraps);
lower_95position = int32(0.025 * numberBootStraps);
upper_95position = int32((1.0 - 0.025) * numberBootStraps);

% Run bootstrapping algorithm
% ===========================
for i=1:length(numberBootStraps)
    means = zeros(numberBootStraps(i),1);
    for j=1:numberBootStraps(i)
        circularBootStrap = createCircularBootStrap(blockLengthCB,
series);
        means(j) = mean(circularBootStrap);
    end
```

[47] http://www.economics.ox.ac.uk/members/andrew.patton, *accessed June 2008.*

```
% Calculate the means of each series of n-thousand bootstraps
% ============================================================
    circMeans(i)=mean(means(:));

% Order the series
% ================
    circsort=sort(means(:));

% Find the upper and lower CI's
% =============================
    lower68_CI1(i)=circsort(lower_68position(i))
    upper68_CI1(i)=circsort(upper_68position(i))
    lower95_CI1(i)=circsort(lower_95position(i))
    upper95_CI1(i)=circsort(upper_95position(i))

% Percentage of CI's above or below mean
% ======================================
    percent68_CI1(i)=(circMeans(i)-lower68_CI1(i))/circMeans(i)*100.0
    percent95_CI1(i)=(circMeans(i)-lower95_CI1(i))/circMeans(i)*100.0

% Save 10,000 bootstrap data for post-processing
% ==============================================
    if(numberBootStraps(i) == 10000)
       bs10k = means(:);
       bs10k_mean = circMeans(i);
    end
end

% Plot histogram of means
% =======================
figure(1)
hold on
nbars=40;
[count_of_means,mean_value] = hist(bs10k,nbars);
bar(mean_value,count_of_means);

% Calculate standard deviation of means
% =====================================
bs10k_fluct= bs10k - bs10k_mean;
bs10k_variance=dot(bs10k_fluct,bs10k_fluct)/10000;
bs10k_std_dev = sqrt(bs10k_variance);

% Draw Gaussian curve too
% =======================
gauss_min = bs10k_mean - 5.0 * bs10k_std_dev;
gauss_max = bs10k_mean + 5.0 * bs10k_std_dev;
gauss_step = bs10k_std_dev / 5.0
gauss_x = [gauss_min:gauss_step:gauss_max];
gauss_scaling = max(count_of_means);
nbmax=size(gauss_x);
for nb=1:nbmax(2)
   gauss_y(nb)=(exp(-1/2*((gauss_x(nb)-
bs10k_mean)/bs10k_std_dev)^2))*gauss_scaling;
end
plot(gauss_x,gauss_y,'-r')
xlabel('Mean Velocity (m/s)')
ylabel('Occurence')
```

```
% Plot the means and first Confidence Intervals
% ============================================
figure(2)
hold on
semilogx(numberBootStraps,circMeans,'-k')
semilogx(numberBootStraps,lower68_CI1,'--r')
semilogx(numberBootStraps,upper68_CI1,'--b')
xlabel('Number of Bootstraps');
ylabel('Mean Velocity (m/s)')

% Write data to CSV file for Excel
% ================================
disp('Writing data to bootstrap_results.csv ...');
fid=fopen('bootstrap_results.csv','w');
fprintf(fid,'No. of bootstraps,Mean Vel., Lower68 CI1, Upper68 CI1,
Percent68 Error, Lower95 CI1,Upper95 CI1, Percent95 Error\n');
for i=1:length(numberBootStraps)
   fprintf(fid,'%d,%f,%f,%f,%f,%f,%f,%f\n',
numberBootStraps(i),circMeans(i),lower68_CI1(i),upper68_CI1(i),
percent68_CI1(i),lower95_CI1(i),upper95_CI1(i),percent95_CI1(i));
end
fclose(fid);
disp('                                  ... OK');
```

```
% Circular Bootstrap Function
% ===========================
function bootStrap = createCircularBootStrap(blockLength, series)
    noBlocks = ceil(length(series)/blockLength);
    circularSeries = cat(1,series,series(1:blockLength-1));
    starts = ceil(length(series).*rand(noBlocks,1));
    bootStrap = [];
    for i=1:noBlocks
        bootStrap =
cat(1,bootStrap,circularSeries(starts(i):starts(i)+blockLength-1));
    end
```

10 REFERENCES

1. Spalart, P.R., *Strategies for turbulence modeling and simulations*, Int. J. Heat Fluid Flow, **21**, p.252-263, 2000.

2. Ledin, H.S., Ivings, M.J., Allen, J.T., and Bettis, R.J., *Evaluation of CFD modelling of smoke movement in complex enclosed spaces - production of small-scale experimental data and assessments of CFD*, Health & Safety Laboratory Report CM/04/07, 2004.

3. Ivings, M.J., Azhar, M., Carey, C., Lea, C.J., Ledin, S., Sinai, Y., Skinner, C., and Stephenson, P., *Outstanding Safety Questions Concerning the Use of Gas Turbines for Power Generation: Final Report on the CFD Modelling Programme of Work*, Health & Safety Laboratory Report CM/03/08, 2003.

4. Peng, S.-H., Holmberg, S., and Davidson, L., *On the assessment of ventilation performance with the aid of numerical simulations*, Building & Environment, **32**(6), p.497-508, 1997.

5. Davidson, L., Nielsen, P.V., and Topp, C., *Low-Reynolds number effects in ventilated rooms: a numerical study*, Proc. 7th Int. Conference on Air Distribution in Rooms (Roomvent 2000), p.307-312, 2000.

6. Emmerich, S.J. and McGrattan, K.B., *Application of a large eddy simulation model to study room airflow*, ASHRAE Transactions, SF-98-10-2, **104**, 1998.

7. Wang, H., Colvile, R.N., Pain, C.C., De Oliveira, C.R.E., and Aristodemou, E., *Airflows in the vicinity of an intersection,* in 9th Int. Conf. on Harmonisation with Atmospheric Dispersion Modelling for Regulatory Purposes, Garmisch-Partenkirchen, 2004

8. Davidson, L. and Nielsen, P.V., *Large eddy simulations of the flow in a three-dimensional ventilated room,* in Proc. 5th Int. Conference on Air Distribution in Rooms (Roomvent '96), Yokohama, Japan, 1996

9. Cai, X.-M., Barlow, J.F., and Belcher, S.E., *Dispersion and transfer of passive scalars in and above street canyons - Large-eddy simulations*, Atmospheric Environment, **42**, p.5885-5895, 2008.

10. Casey, M. and Wintergerste, T., eds. *ERCOFTAC Special Interest Group on "Quality and Trust in Industrial CFD" Best Practice Guidelines*. version 1.0 ed., 2000.

11. McGrattan, K.B. and Hamins, *Numerical simulation of the Howard Street Tunnel Fire, Baltimore, Maryland, July 2001*, in NISTIR 6902; NUREG/CR-6793, NRC Job Code J5414, January, 2003.

12. Hamins, A., Maranghides, A., McGrattan, K.B., Ohlemiller, T., and Anleitner, R., *Experiments and modeling of multiple workstations burning in a compartment*, in Federal Building and Fire Safety Investigation of the World Trade Center Disaster, NIST NCSTAR 1-5E, National Institute for Standards and Technology, Gaithersburg, Maryland, Sept, 2005.

13. Mahaffy, J., Chung, B., Dubois, F., Dubois, F., Graffard, E., Heitsch, M., Henriksson, M., Komen, E., Moretti, F., Morii, T., Mühlbauer, P., Rohde, U., Scheuerer, M., Smith, B.L., Song, C., Watanabe, T., and Zigh, G., *Best practice guidelines for the use of CFD*

in nuclear reactor safety applications, in NEA/CSNI/R(2007)5 (http://www.nea.fr/html/nsd/docs/2007/csni-r2007-5.pdf, accessed March 2008), Organisation for Economic Co-operation and Development, 2007.

14. Ferziger, J.H. and Perić, M., *Computational Methods for Fluid Dynamics*, Springer-Verlag, Berlin, 1999.

15. Pope, S.B., *Turbulent Flows*, Cambridge University Press, 2000.

16. Deevy, M.T., Ledin, H.S., and Zhou, X.X., *Initial evaluation of the applicability of large-eddy simulation techniques to health and safety related flows*, Health & Safety Laboratory Report CM/05/01, 2005.

17. Gant, S.E., *Large-Eddy Simulation of Gas Dispersion in a Room*, Health & Safety Laboratory Report CM/05/15, 2006.

18. Kline, S.J., Cantwell, B.J., and Lilley, G.M., *Objectives, evaluation of data, specification of test cases, discussion and position papers*, in The 1980-81 AFOSR/HTTM-Stanford Conference on Complex Turbulent Flows, Vol. 1, ThermoSciences Division, Mechanical Engineering Dept., Stanford University, USA, 1981.

19. Roache, P.J., *Verification and validation in computational science and engineering*, Hermosa Publishers, 1998.

20. AGARD, *Experimental data base for computer program assessment*, in Report of the fluid dynamics panel working group 04, AGARD-AR-138, May, 1979.

21. AGARD, *Validation of Computation Fluid Dynamics Conference*, in Advisory Group for Aeronautical Research and Development, AGARD CP 437: Lisbon, Portugal, May 2-5, 1988.

22. Menter, F.R., Hemstrom, B., Henrikkson, M., Karlsson, R., Latrobe, A., Martin, A., Muhlbauer, P., Smith, B.L., Takacs, T., and Willemsen, S., *CFD best practice guidelines for CFD code validation for reactor-safety applications*, in Report EVOL-ECORA-D01, Contract No. FIKS-CT-2001-00154, 2002.

23. Scheurerer, M., Heitsch, M., Menter, F.R., Egorov, Y., Toth, I., Bestion, D., Pigny, S., Paillere, H., Martin, A., Boucker, M., Willemsen, S., Muhlbauer, P., Andreani, M., Smith, B.L., Karlsson, R., Henriksson, M., Hemstrom, B., Karppinen, I., and Kimber, G., *Evaluation of computational fluid dynamic methods for reactor safety analysis (ECORA)*, Nuclear Eng. Design, **235**, p.359-368, 2005.

24. IAEA, *Validation of fast reactor thermomechanical and thermohydraulic codes*, in Final report of a co-ordinated research project 1996-1999, IAEA-TECDOC-1318, International Atomic Energy Agency, November, 2002.

25. Roache, P.J., Ghia, K., and White, F., *Editorial policy statement on the control of numerical accuracy*, J. Fluids Eng., **108**(1), p.2, 1986.

26. ASME, *Guide for verification and validation in computational solid mechanics*, American Society of Mechanical Engineers, ASME V&V 1-2006: New York, USA, 2006.

27. ASME, *Journal of heat transfer editorial policy statement on numerical accuracy*, J. Heat Transfer, **116**, p.797-798, 1994.

28. Mehta, U.B., *Credible computational fluid dynamics simulations*, AIAA J., **36**(5), p.665-667, 1998.

29. Jameson, A. and Martinelli, L., *Mesh refinement and modeling errors in flow simulations* AIAA J., **36**(5), p.676-686, 1998.

30. Habashi, W.G., Dompierre, J., Bourgault, Y., Fortin, M., and Vallet, M.-G., *Certifiable Computational Fluid Dynamics Through Mesh Optimization*, AIAA J., **36**(5), p.703-711, 1998.

31. Obercampf, W.L. and Blottner, F.G., *Issues in computational fluids dynamics code calibration/validation*, AIAA J., **36**(5), p.687-695, 1998.

32. Barber, T.J., *Role of code validation and certification in the design environment*, AIAA J., **36**(5), p.752-758, 1998.

33. Aeschliman, D.P. and Obercampf, W.L., *Experimental methodology for computational fluid dynamics code validation*, AIAA J., **36**(5), p.733-741, 1998.

34. Roache, P.J., *Verification of codes and calculations*, AIAA J., **36**(5), p.696-702, 1998.

35. Rizzi, A. and Vos, J., *Towards establishing credibility in compuational fluid dynamic simulations*, AIAA J., **36**(5), p.1998, 1998.

36. Yee, H.C. and Sweby, P.K., *Aspects of numerical uncertainties in time marching to steady state numerical simulations*, AIAA J., **36**(5), p.712-724, 1998.

37. Reed, H.L., Haynes, T.S., and Saric, W.S., *Computational fluid dynamics validation issues in transition modeling*, AIAA J., **36**(5), p.742-751, 1998.

38. Celik, I.B. and Freitas, C.J., *Benchmark test cases for computational fluid dynamics*, in ASME FED Vol. 93 Book No. H00598-1990, 1990.

39. Freitas, C.J., *Perspective: selected benchmarks from commercial CFD codes*, J. Fluids Eng., **117**, p.210-218, 1995.

40. Johnson, R.W. and Hughes, E.D., *Quantification of uncertainty in computational fluid dynamics,* in ASME/JSME Fluids Engineering and Laser Anemometry Conference, Hilton Head, South Carolina, 1995

41. Hills, R.G., Pilch, M., Dowding, K.J., Red-Horse, J., Paez, T.L., Babuška, I., and Tempone, R., *Validation challenge workshop*, Compu. Meth. Appl. Mech. Eng., **197**, p.2375-2380, 2008.

42. AIAA, *Editorial policy statement on numerical accuracy and experimental uncertainty*, AIAA J., **32**(1), 1994.

43. AIAA, *Guide for the verification and validation in computational fluid dynamics simulations*, in AIAA Report G-077-1998: Reston, VA, 1998.

44. Lea, C.J. and Gobeau, N.C.H., *How to undertake a smoke movement analysis in complex enclosed spaces using CFD*, NAFEMS (http://www.nafems.org, accessed June 2008), 2007.

45. Ledin, H.S., McBride, M.A., O'Sullivan, S., and Roberts, T.A., *Review of hydrocarbon fire models for offshore applications*, in Health & Safety Laboratory Report MSU/2008/07, 2008.

46. Ledin, H.S., *Review of gas explosion models*, in Health & Safety Laboratory Report MSU/2008/01, 2008.

47. Ivings, M.J., Jagger, S.F., Lea, C.J., and Webber, D.M., *Evaluating vapor dispersion models for safety analysis of LNG facilities*, in Technical Report, Fire Protection Research Foundation (http://www.nfpa.org/assets/files//PDF/Research/LNGVaporDispersionModel.pdf, accessed June 2008), 2008.

48. Ivings, M.J., Lea, C.J., and Ledin, H.S., *Outstanding safety questions concerning the analysis of ventilation and gas dispersion in gas turbine enclosures: best practice guidelines for CFD*, in Health & Safety Laboratory Report CM/03/12, 2003.

49. Stern, F., Wilson, R.V., Coleman, H.W., and Paterson, E.G., *Verification and validation of CFD simulations*, in IIHR Report No. 407, Iowa Institute of Hydraulic Research, University of Iowa, USA, 1999.

50. Stern, F., Wilson, R.V., Coleman, H.W., and Paterson, E.G., *Comprehensive approach to verification and validation of CFD simulations - Part 1: methodology and procedures*, J. Fluids Eng., **123**, p.793-810, 2001.

51. Stern, F., Wilson, R.V., and Shao, J., *Quantitative V&V of CFD simulations and certification of CFD codes*, Int. J. Num. Meth. Fluids, **50**, p.1335-1355, 2006.

52. Obercampf, W.L., Trucano, T.G., and Hirch, C., *Verification, validation, and predictive capability in computational engineering and physics*, Appl. Mech. Rev., **57**(5), p.345-384, 2004.

53. Obercampf, W.L. and Barone, M.F., *Measures of agreement between computational and experiment: validation metrics*, J. Comput. Phys., **217**(1), p.5-36, 2006.

54. Schwer, L.E. and Obercampf, W.L., *Editorial: Special issue on verification and validation*, Engineering with Computers, **23**, p.243-244, 2007.

55. Celik, I.B., Chen, C.P., Roache, P.J., and Scheurer, G., *Quantification of uncertainty in computational fluid dynamics,* in ASME Fluids Engineering Division Summer Meeting, Washington, D. C., USA, 1993

56. Celik, I.B., Li, J., Hu, G., and Shaffer, C., *Limitation of Richardson extrapolation and some possible remedies*, J. Fluids Eng., **127**, p.795-805, 2005.

57. Celik, I.B. and Li, J., *Assessment of numerical uncertainty for the calculations of turbulent flow over a backward facing step*, Int. J. Num. Meth. Fluids, **49**, p.1015-1010, 2005.

58. Celik, I.B., Cehreli, Z.N., and Yavuz, I., *Index of resolution quality for large eddy simulations*, J. Fluids Eng., **127**, p.949-958, 2005.

59. Celik, I.B., Klein, M., Freitag, M., and Janicka, J., *Assessment measures for URANS/DES/LES: an overview with applications*, J. Turbulence, **7**(48), p.1-27, 2006.

60. Iaccarino, G., *Prediction of the turbulent flow in a diffuser with commercial CFD codes*, in CTR Annual Research Briefs, Stanford University, USA, 2000.

61. Franke, J., Hellsten, A., Schlünzen, H., and Carissimo, B., *Best practice guidelines for the CFD simulation of flows in the urban environment*, in COST Action 732: Quality assurance and improvement of microscale meteorological models, COST Office, Brussels, Belgium, 2007.

62. Franke, J., Hirsch, C., Jensen, A.G., Krüs, H.W., Schatzmann, M., Westbury, P.S., Miles, S.D., Wisse, J.A., and Wright, N.G., *Recommendations on the use of CFD in predicting pedestrian wind environment*, in COST Action C14 "Impact of Wind and Storms on City Life and Built Environment", Working Group 2 - CFD Techniques, Version 1.0 (http://www.costc14.bham.ac.uk/, accessed November 2008), 2004.

63. Sørensen, D.N. and Nielsen, P.V., *Quality control of computational fluid dynamics in indoor environments*, Indoor Air, **13**, p.2-17, 2003.

64. Knupp, P. and Salari, K., *Verification of Computer Codes in Computational Science and Engineering*, Boca Raton, Florida, USA, Chapman & Hall/CRC, 2002.

65. Meyers, J., Geurts, B.J., and Sagaut, P., eds. *Quality and reliability of large-eddy simulations*. ERCOFTAC Series, Springer, 2008.

66. Sagaut, P., *Large-eddy simulation for incompressible flows*, Heidelberg: Springer, 2001.

67. Geurts, B.J., *Elements of direct and large-eddy simulation*, R. T. Edwards Inc., Philadelphia, PA, 2004.

68. Voke, P.R., Kleiser, L., and Chollet, J.P., *Direct and large-eddy simulation I*, Kluwer Academic Publishers, 1994.

69. Chollet, J.P., Voke, P.R., and Kleiser, L., *Direct and large-eddy simulation II*, Kluwer Academic Publishers, 1997.

70. Voke, P.R. and Sandham, N.D., *Direct and large-eddy simulation III*, Kluwer Academic Publishers, 1999.

71. Geurts, B.J., Friedrich, R., and Métais, O., *Direct and large-eddy simulation IV*, Kluwer Academic Publishers, 2001.

72. Friedrich, R. and Geurts, B.J., *Direct and large-eddy simulation V*, Kluwer Academic Publishers, 2004.

73. Lamballais, E., Friedrich, R., Geurts, B.J., and Métais, O., *Direct and large-eddy simulation VI*, Kluwer Academic Publishers, 2006.

74. Obercampf, W.L., *Discussion: "Comprehensive approach to verification and validation of CFD simulations - Part 1: methodology and procedures" by Stern, F., Wilson, R. V.,*

Coleman, H. W. and Paterson, E. G., 2001, J. Fluids Eng., 123, pp 793-802 J. Fluids Eng., **124**, p.809, 2002.

75. Coleman, H.W., *Closure to "Discussion of 'Comprehensive approach to verification and validation of CFD simulations - Part 1: methodology and procedures' " (2002, ASME J. Fluids Eng., 124, p.809)*, J. Fluids Eng., **124**, p.810, 2002.

76. Stern, F. and Wilson, R.V., *Closure to "Discussion of 'Comprehensive approach to verification and validation of CFD simulations - Part 1: methodology and procedures' " (2002, ASME J. Fluids Eng., 124, p.809)*, J. Fluids Eng., **124**, p.810-811, 2002.

77. Roache, P.J., *Criticisms of the "Correction Factor" verification method*, J. Fluids Eng., **125**, p.732-733, 2002.

78. Coleman, H.W., *Some observations on uncertainties and the verification and validation of a simulation*, J. Fluids Eng., **125**, p.733-735, 2003.

79. Obercampf, W.L., Trucano, T.G., and Hirsch, C., *Verification, validation and predictive capability in computational engineering and physics,* in Workshop on Foundations for Verification and Validation in the 21st Century, John Hopkins University/Applied Physics Laboratory, Laurel, Maryland, 2002

80. Vreman, A.W., Geurts, B.J., and Kuerten, J.G.M., *Comparison of numerical schemes in large-eddy simulation of the temporal mixing layer*, Int. J. Num. Meth. Fluids, **22**, p.297-311, 1996.

81. Versteeg, H.K. and Malalasekera, W., *An introduction to computational fluid dynamics: the finite volume method*, Longman Scientific & Technical, 1995.

82. Ghosal, S., *An analysis of numerical errors in large-eddy simulations of turbulence*, J. Comp. Phys., **125**, p.187-206, 1996.

83. Brandt, T., *Study on numerical and modelling errors in LES using a priori and a posteriori testing*, PhD Thesis, Department of Mechanical Engineering, Helsinki University of Technology, Espoo, Finland, 2007

84. Kravchenko, A.G. and Moin, P., *On the effect of numerical errors in large eddy simulations of turbulent flows*, J. Comp. Phys., **131**, p.310-322, 1997.

85. Park, N., Yoo, J.Y., and Choi, H., *Discretization errors in large eddy simulation: on the suitability of centered and upwind-biased compact difference schemes*, J. Comp. Phys., **198**, p.580-616, 2004.

86. Morinishi, Y. and Vasilyev, O.V., *Subgrid scale modeling taking the numerical error into consideration*, in Annual Research Briefs, Center for Turbulence Research, Stanford University, USA p. 237-253, 1998.

87. Gullbrand, J. and Chow, F.K., *The effect of numerical errors and turbulence models in large-eddy simulations of channel flow, with and without explicit filtering*, J. Fluid Mech., **495**, p.323-341, 2003.

88. Lund, T.S., *The use of explicit filters in large eddy simulation*, Computers & Mathematics with Applications, **46**, p.603-616, 2003.

89. Geurts, B.J. and Fröhlich, J., *A framework for predicting accuracy limitations in large eddy simulation*, Phys. Fluids, **14**, p.41-44, 2002.

90. Kornhaas, M., Sternel, D.C., and Schäfer, M., *Influence of time step size and convergence criteria on large eddy simulations with implicit time discretization*, in *Quality and Reliability of Large-Eddy Simulations*, Meyers, J., Geurts, B.J., and Sagaut, P., Editors, Springer Science and Business Media B. V. p. 119-130, 2008.

91. Canuto, C., Hussaini, M.Y., Quarteroni, A., and Zhang, T.A., *Spectral methods in fluid dynamics*, Springer-Verlag, 1988.

92. Anderson, J.D., *Computational Fluid Dynamics: the basics with applications*, McGraw-Hill International Editions, Mechanical Engineering Series, ed., New York, 1995.

93. McGrattan, K.B., *Fire Dynamics Simulator (Version 4) Technical Reference Guide*, in NIST Special Publication 1018, (http://www.fire.nist.gov/fds, accessed June 2007), 2006.

94. Benhamadouche, S. and Laurence, D., *Global kinetic energy conservation with unstructured meshes*, Int. J. Num. Meth. Fluids, **40**, p.561-572, 2002.

95. Laurence, D., *Industrial LES with unstructured finite volumes,* in Direct and Large-Eddy Simulation VI, Proc. 6th Int. ERCOFTAC Workshop on Direct and Large-Eddy Simulation, Laboratoire d'Etudes Aerodynamiques, Poitiers, France, ERCOFTAC Series, 2005

96. Moulinec, C., Benhamadouche, S., Laurence, D., and Perić, M., *LES in a U-bend pipe meshed by polyhedral cells,* in ERCOFTAC ETMM-6 Conference, Sardinia, Elsevier, 2005

97. Grinstein, F.F., Margolin, L.G., and Rider, W.J., eds. *Implicit Large Eddy Simulation*. Cambridge University Press, 2007.

98. Cetegen, B.M. and Kasper, K.D., *Experiments on the oscillatory behavior of buoyant plumes of helium and helium-air mixtures*, Phys. Fluids, **8**(11), p.2974-2984, 1996.

99. List, E.J., *Mechanics of turbulent buoyant jets and plumes*, in *Turbulent buoyant jets and plumes*, Rodi, W., Editor, Pergamon Press p. 1-68, 1982.

100. Crawley, M.J., *Statistical Computing: an introduction to data analysis using S-Plus*, John Wiley & Sons, 2002.

101. Klein, M., *An attempt to assess the quality of large eddy simulations in the context of implicit filtering*, Flow, Turbulence and Combustion, **75**, p.131-147, 2005.

102. Tritton, D.J., *Physical fluid dynamics*, Oxford Science Publications, ed., Oxford, 1988.

103. Anfossi, D., Rizza, U., Mangia, C., Degrazia, G.A., and Pereira Marques Filho, E., *Estimation of the ratio between the Lagrangian and Eulerian time scales in an atmospheric boundary layer generated by large eddy simulation*, Atmospheric Environment, **40**, p.326-337, 2006.

104. O'Neill, P.L., Nicolaides, D., Honnery, D., and Soria, J., *Autocorrelation functions and the determination of integral length with reference to experimental and numerical data,* in 15th Australian Fluid Mechanics Conference, Sydney, Australia, 2004

105. de Waele, S., van Dijk, A., Broersen, P., and Duynkerke, P., *Estimation of the integral time scale with time series models,* in 15th Conference on Boundary Layer and Turbulence, 2002

106. Theunissen, R., Di Sante, A., Riethmuller, M.L., and Van den Braembussche, R.A., *Confidence estimation using dependent circular block bootstrapping: application to the statistical analysis of PIV measurements*, Exp. Fluids, **44**, p.591-596, 2008.

107. Garcia, C.M., Hackson, P.R., and Garcia, M.H., *Confidence intervals in the determination of turbulence parameters*, Exp. Fluids, **40**, p.514-522, 2006.

108. Wilks, D.S., *Statistical methods in the atmospheric sciences*, 2nd ed, Academic Press, Elsevier, 2006.

109. Brandt, T., *A posteriori study on modelling and numerical error in LES applying the Smagorinsky model*, in *Complex Effects in Large Eddy Simulations*, Kassinos, S., Langer, C., Iaccarino, G., and Moin, P., Editors p. 185-202, 2007.

110. Geurts, B.J., *Interacting errors in large-eddy simulation: a review of recent developments*, J. Turbulence, **7**(9), p.1-16, 2006.

111. Geurts, B.J. and Fröhlich, J., *Numerical effects contaminating LES: a mixed story*, in *Modern simulation strategies for turbulent flow*, Geurts, B.J., Editor, R. T. Edwards Inc., Philadelphia, 2001.

112. Meyers, J., Geurts, B.J., and Baelmans, M., *Database analysis of errors in large eddy simulation*, Phys. Fluids, **15**(9), p.2740-2755, 2003.

113. Meyers, J., Geurts, B.J., and Baelmans, M., *Identification of global error behaviour in LES using a database approach,* in Direct & Large Eddy Simulation V, Munich University of Technology, Germany, Kluwer Academic Publishers, 2003

114. Klein, M., Meyers, J., and Geurts, B.J., *Assessment of LES quality measures using the error landscape approach*, in *Quality and Reliability of Large-Eddy Simulations*, Meyers, J., Geurts, B.J., and Sagaut, P., Editors, Springer Science and Business Media B. V. p. 131-142, 2008.

115. Ma, T.G. and Quintiere, J.G., *Numerical simulation of axi-symmetric fire plumes: accuracy and limitations*, Fire Safety Journal, **38**, p.467-492, 2003.

116. Bounagui, A., Benichou, N., McCartney, C., and Kashef, A., *Grid optimization for the full-scale test facility to evaluate the fire performance of houses - Part 1 - Basement fires*, in Research Report 149, Institute for Research in Construction, National Research Council Canada, Feb., 2004.

117. Smardz, P., *Validation of Fire Dynamics Simulator (FDS) for forced and natural convection flows*, Master of Science Thesis, Fire Safety Engineering, University of Ulster, 2006

118. Petterson, N.M., *Assessing the feasibility of reducing the grid resolution in FDS field modelling*, in Fire Engineering Research Report, School of Engineering, University of Canterbury, Christchurch, NZ, 2002.

119. Tieszen, S., Pitsch, H., Blanquart, G., and Abarzhi, S., *Toward the development of a LES-SGS closure model for buoyant plumes,* in Proc. Summer Program, Center for Turbulence Research, Stanford, California, 2004

120. Tieszen, S.R., Domino, S.P., and Black, A.R., *Validation of a simple turbulence model suitable for closure of temporally-filtered Navier-Stokes equations using a helium plume*, in Sandia Report SAND2005-3210, 2005.

121. Addad, Y., Benhamadouche, S., and Laurence, D., *The negatively buoyant wall-jet: LES results*, Int. J. Heat Fluid Flow, **25**, p.795-808, 2004.

122. Baggett, J.S., Jiménez, J., and Kravchenko, A.G., *Resolution requirements in large-eddy simulations of shear flows*, in Annual Research Briefs, Stanford Centre for Turbulence Research, 1997.

123. Van Maele, K. and Merci, B., *Application of RANS and LES field simulations to predict the critical ventilation velocity in longitudinally ventilated horizontal tunnnels*, Fire Safety Journal, **43**(8), p.598-609, 2008.

124. Jiménez, J. and Moser, R.D., *LES: where are we and what can we expect?*, in AIAA Paper 98-2891, 1998.

125. Hadžiabdić, M. and Hanjalić, K., *Vortical structures and heat transfer in a round impinging jet*, J. Fluid Mech., **596**, p.221-260, 2008.

126. Saddoughi, S.G. and Veeravalli, S.V., *Local isotropy in turbulent boundary layers at high Reynolds number*, J. Fluid Mech., **268**, p.333-372, 1994.

127. Saddoughi, S.G., *Local isotropy in complex turbulent boundary layers at high Reynolds number*, J. Fluid Mech., **348**, p.201-245, 1997.

128. Zhou, X., Luo, K.H., and Williams, J.J.R., *Large-eddy simulation of a turbulent forced plume*, Eur. J. Mech. B - Fluids, **20**, p.233-254, 2001.

129. Zhou, X.H., Luo, K.H., and Williams, J.J.R., *Study of density effects in turbulent buoyant jets using large-eddy simulation*, Theoret. Comput. Fluid Dynamics, **15**, p.95-120, 2001.

130. Ilyushin, B.B. and Krasinsky, D.V., *Large eddy simulation of the turbulent round jet dynamics*, Thermophysics & Aeromechanics, **13**(1), p.43-54, 2006.

131. Tutar, M., Celik, I.B., and Yavuz, I., *Modelling of effect of inflow turbulence on large eddy simulation of bluff body flows*, Math. Comput. Appl., **11**(3), p.225-234, 2006.

132. Mydlarski, L. and Warhaft, Z., *Passive scalar statistics in high Peclet number grid turbulence*, J. Fluid Mech., **358**, p.135-175, 1998.

133. Lumley, J.L., *The spectrum of nearly inertial turbulence in a stably stratified fluid*, J. Atmos. Sci., **21**(1), p.99-102, 1965.

134. Dai, Z., Tseng, L.-K., and Faeth, G.M., *Structure of round, fully developed, buoyant turbulent plumes*, J. Heat Transfer, **116**, p.409-417, 1994.

135. Papanicolaou, P.N. and List, E.J., *Investigations of round vertical turbulent buoyant jets*, J. Fluid Mech., **195**, p.341-391, 1988.

136. Elicer-Cortés, J.C., Contreras, R., Boyer, D., Pavageau, M., and Hernández, R.H., *Temperature spectra from a turbulent thermal plume by ultrasound scattering*, Exp. Thermal Fluid Sci., **28**(8), p.803-813.

137. Pope, S.B., *Ten questions concerning the large-eddy simulation of turbulent flows*, New J. Phys., **6**(35), 2004.

138. Mason, P.J. and Callen, N.S., *On the magnitude of the subgrid-scale eddy coefficient in large-eddy simulations of turbulent channel flow*, J. Fluid Mech., **162**, p.439-462, 1986.

139. Lilly, D., *The representation of small scale turbulence in numerical simulation experiments*, in *Proc. IBM Scientific Computing Symposium on Environmental Sciences* p. 195-210, 1967.

140. Kempf, A., Lindstedt, R.P., and Janicka, J., *Large-eddy simulation of a bluff-body stabilized nonpremixed flame*, Combustion and Flame, **144**, p.170-189, 2006.

141. Krajnović, S. and Davidson, L., *A mixed one-equation subgird model for large-eddy simulation*, Int. J. Heat Fluid Flow, **23**(4), p.413-425, 2002.

142. Celik, I.B. and Karatekin, O., *Numerical experiments on application of Richardson extrapolation with nonuniform grids*, J. Fluids Eng., **119**, p.584-590, 1997.

143. Brandt, T., *Use of Richardson extrapolation in error estimation of LES,* in Proc. 19th Nordic Seminar on Computational Mechanics, Lund, Sweden, 2006

144. Kuczaj, A.K. and Komen, E.M.J., *Large-eddy simulation study of turbulent mixing in a T-junction,* in Experiments and CFD Code Applications to Nuclear Reactor Safety (XCFD4NRS), Commissariat à l'Energie Atomique (CEA), Grenoble, France, 2008

145. Meneveau, C. and Katz, J., *Scale invariance and turbulence models for large-eddy simulation*, Annu. Rev. Fluid Mech., **32**, p.1-32, 2000.

146. Jones, W.P. and Launder, B.E., *The prediction of laminarization with a two-equation model of turbulence*, Int. J. Heat Mass Transfer, **15**, p.301-314, 1972.

147. Launder, B.E. and Sharma, B.I., *Application of the energy-dissipation model of turbulence to the calculation of flow near a spinning disc*, Lett. in Heat Mass Transfer, **1**, p.131-138, 1974.

148. Kato, M. and Launder, B.E., *The modelling of turbulent flow around stationary and vibrating square cylinders,* in Proc. 9th Symposium on Turbulent Shear Flows, Kyoto, Japan, 1993

149. Durbin, P.A., *On the k-ε stagnation point anomaly*, Int. J. Heat Fluid Flow, **17**, p.89-90, 1995.

150. Launder, B.E. and Sandham, N.D., *Closure strategies for turbulent and transitional flows*, Cambridge University Press, 2002.

151. Durbin, P.A. and Pettersson Reif, B.A., *Statistical theory and modeling for turbulent flows*, John Wiley & Sons, 2001.

152. Rodi, W., Ferziger, J.H., Breuer, M., and Pourquié, M., *Status of large-eddy simulation: results of workshop*, J. Fluids Eng., **119**, p.248-262, 1997.

153. Park, N. and Mahesh, K., *A velocity-estimation subgrid model constrained by subgrid scale dissipation*, J. Comp. Phys., **227**, p.4190-4206, 2008.

154. Smagorinsky, J., *General circulation experiments with the primitive equations*, Monthly Weather Review, **91**(3), p.99-164, 1963.

155. McMillan, O.J. and Ferziger, J.H., *Direct testing of subgrid-scale models*, AIAA J., **17**, p.1340-1346, 1979.

156. Deardorff, J.W., *On the magnitude of the subgrid scale eddy viscosity coefficient*, J. Comp. Phys., **7**, p.120, 1971.

157. Moin, P. and Kim, J., *Numerical investigation of turbulent channel flow*, J. Fluid Mech., **118**, p.341-377, 1982.

158. Addad, Y., *Large-eddy simulations of bluff-body, mixed and natural convection turbulent flow with unstructured FV codes*, Thesis, PhD Thesis, School of Mechanical, Aerospace and Civil Engineering, Manchester University, UK, 2004

159. Jiang, Y. and Chen, Q., *Study of natural ventilation in buildings by large eddy simulation*, J. Wind Engineering & Industrial Aerodynamics, **89**(13), p.1155-1178, 2001.

160. Germano, M., Piomelli, U., Moin, P., and Cabot, W.H., *A dynamic subgrid scale eddy viscosity model,* in Proc. Summer Workshop, Center for Turbulence Research, Stanford, CA, 1990

161. Germano, M., Piomelli, U., Moin, P., and Cabot, W.H., *A dynamic subgrid-scale eddy viscosity model*, Phys. Fluids A, **3**, p.1760-1765, 1991.

162. Lilly, D.K., *A proposed modification of the standard Germano subgrid-scale closure method*, Phys. Fluids A, **4**(633-635), 1992.

163. Clark, R.A., Ferziger, J.H., and Reynolds, W.C., *Evaluation of subgrid-scale models using an accurately simulated turbulent flow*, J. Fluid Mech., **91**, p.1-16, 1979.

164. Jiménez, J., *On why dynamic subgrid-scale models work*, in CTR Annual Research Briefs, Stanford University, USA, 1995.

165. DesJardin, P.E., O'Hern, T.J., and Tieszen, S.R., *Large eddy simulation and experimental measurements of the near-field of a large turbulent helium plume*, Phys. Fluids, **16**(6), p.1866-1883, 2004.

166. Piomelli, U., Cabot, W.H., Moin, P., and Lee, S., *Subgrid-scale backscatter in turbulent and transitional flows*, Phys. Fluids A, **3**, p.1766-1771, 1991.

167. da Silva, C.B. and Métais, O., *On the influence of coherent structures upon interscale interaction in turbulent plane jets*, J. Fluid Mech., **473**, p.103-145, 2002.

168. Meneveau, C., Lund, T.S., and Cabot, W.H., *A Lagrangian dynamic subgrid-scale model of turbulence*, J. Fluid Mech., **319**, p.353-385, 1996.

169. Vreman, A.W., *An eddy-viscosity model for turbulent shear-flow: algebraic theory and applications*, Phys. Fluids, **16**(10), p.3670-3681, 2004.

170. Nicoud, F. and Ducros, F., *Subgrid scale stress modelling based on the square of the velocity gradient tensor*, Flow, Turbulence and Combustion, **62**(3), p.183-200, 1999.

171. Klein, S.J., Reynolds, W.C., Schraub, F.A., and Runstadler, P.W., *The structure of turbulent boundary layers*, J. Fluid Mech., **30**, p.741-773, 1967.

172. Blackwelder, R.F. and Eckelmann, H., *Streamwise vortices associated with the bursting phenomenon*, J. Fluid Mech., **94**, p.577-594, 1979.

173. Shi, J.-M., Thomas, T.G., and Williams, J.J.R., *Coarse resolution large-eddy simulation of turbulent channel flows*, Int. J. Num. Meth. Heat & Fluid Flow, **11**(1), p.20-35, 2001.

174. Piomelli, U. and Chasnov, J.R., *Large-eddy simulations: theory and applications*, in *Transition and Turbulence Modelling*, Henningson, A., Hallback, K., Alfredsson, L., and Johansson, M., Editors, Kluwer Academic Publishers, Dordrecht p. 269-336, 1996.

175. Temmerman, L., Leschziner, M.A., Mellen, C.P., and Fröhlich, J., *Investigation of wall-function approximations and subgrid-scale models in large eddy simulation of separated flow in a channel with streamwise periodic constrictions*, Int. J. Heat Fluid Flow, **24**(2), p.157-180, 2003.

176. Spalart, P.R., Jou, W.-H., Strelets, M., and Allmaras, S.R., *Comments on the feasibility on LES for wings, and on a hybrid RANS/LES approach,* in 1st ASFOSR conference on DNS/LES, Ruston, Louisiana, 1997

177. Strelets, M., *Detached eddy simulation of massively separated flows,* in AIAA Paper 2001-0879, 39th Aerospace Sciences Meeting and Exhibit, Reno, Nevada, USA, 2001

178. Spalart, P.R., Deck, S., Shur, M.L., Squires, K.D., Strelets, M., and Travin, A., *A new version of detached-eddy simulation, resistant to ambiguous grid densities*, Theoret. Comput. Fluid Dynamics, **20**(3), p.181-195, 2006.

179. Peng, S.-H. and Haase, W., eds. *Advances in Hybrid RANS-LES Modelling*. Papers contributed to the 2007 Symposium on Hybrid RANS-LES Methods, Corfu, Greece, 17-18 June 2007, Springer-Verlag, Berlin, 2008.

180. Spalart, P.R., *Young-person's guide to detatched-eddy simulation grids*, in National Aeronautics and Space Administration, Report NASA/CR-2001-211032, 2001.

181. Menter, F.R., Kuntz, M., and Bender, R., *A scale-adaptive simulation model for turbulent flow predictions,* in Paper AIAA 2003-0767, 41st Aerospace Science Meeting & Exhibit, Reno, Nevada, USA, 2003

182. Patankar, S.V., *Numerical heat transfer and fluid flow*, McGraw-Hill, New York, 1980.

183. Mittal, R. and Moin, P., *Suitability of upwind-biased finite difference schemes for LES of turbulent flow*, AIAA Journal, **35**(8), p.1415-1417, 1997.

184. Ham, F. and Iaccarino, G., *Energy conservation in collocated discretization schemes on unstructured meshes*, in CTR Annual Research Briefs, Stanford University, USA, 2004.

185. Rhie, C.M. and Chow, W.L., *A numerical study of the turbulent flow past an isolated airfoil with trailing edge separation*, in AIAA Paper 82-0998, 1982.

186. Kempf, A., Klein, M., and Janicka, J., *Efficient generation of initial- and inflow-conditions for transient turbulent flows in arbitrary geometries* Flow, Turbulence and Combustion, **74**, p.67-84, 2005.

187. Shi, S. and Celik, I.B., *Random flow generation technique in large eddy simulations and particle dynamics modeling*, J. Fluids Eng., **123**, p.359-371, 2000.

188. Jarrin, N., Uribe, J.C., Prosser, R., and Laurence, D., *Synthetic inflow boundary conditions for wall bounded flows*, in *Notes on Numerical fluid mechanics and multidisciplinary design, Advances in Hybrid RANS-LES models*, Peng, S.-H. and Haase, W., Editors, 2008.

189. Schluter, J.U., Pitsch, H., and Moin, P., *Large eddy simulation inflow conditions for coupling with Reynolds-averaged flow solvers*, AIAA J., **42**(3), p.478-484, 2004.

190. Davidson, L., *Hybrid LES-RANS: Inlet boundary conditions,* in 3rd National Conference on Computational Mechanics - MekIT'05, Trondheim, Norway, 2005

191. Jarrin, N., *Synthetic inflow boundary conditions for the numerical simulation of turbulence*, Thesis, University of Manchester, 2008

192. Ivings, M.J., Clarke, S.P., Gant, S.E., Fletcher, B., Heather, A., Pocock, D.J., Pritchard, D., Santon, R., and Saunders, C.J., *Area classification for secondary releases from low pressure natural gas systems*, in Health & Safety Executive Report RR630, 2008.

193. *Electrical Apparatus for Explosive Gas Atmospheres, Part 10: Classification of hazardous areas*, in BS EN 60079-10:2003,

194. Menter, F.R., *Two-equation eddy-viscosity turbulence models for engineering applications*, AIAA Journal, **32**, p.1598-1605., 1994.

195. Menter, F.R. and Egorov, Y., *Re-visiting the turbulent scale equation,* in Proc. IUTAM Symposium: One hundred years of boundary layer research, Göttingen, Germany, 2004

196. Menter, F.R. and Egorov, Y., *A scale-adaptive simulation model using two-equation models,* in Paper AIAA 2005-1095, 43rd Aerospace Science Meeting & Exhibit, Reno, Nevada, USA, 2005

197. ANSYS-CFX, *CFX-11 User Guide*, 2006.

198. Abdalla, I.E., Cook, M.J., Rees, S.J., and Yang, Z., *Large-eddy simulation of buoyancy-driven natural ventilation in an enclosure with a point heat source*, Int. J. Computational Fluid Dynamics, **21**(5-6), p.231-245, 2007.

199. Moene, A.F. and Michels, B.I., *Estimation of the statistical error in large eddy simulation results,* in 15th Conference on Boundary Layer and Turbulence, Wageningen, The Netherlands, 2002

200. Lynn, P.A. and Fuerst, W., *Introductory digital signal processing with computer applications*, John Wiley & Sons, 1994.

201. Ifeachor, E.C. and Jervis, B.W., *Digital signal processing: a practical approach*, Prentice Hall, 2002.

202. Batchelor, G.K., *The theory of homogeneous turbulence*, Cambridge University Press, 1953.

203. Tennekes, H. and Lumley, J.L., *A First Course in Turbulence*, MIT Press, 1974.

204. Press, W.H., Flannery, B.P., Teukolsky, S.A., and Vetterling, W.T., *Numerical Recipes in Fortran: The Art of Scientific Computing*, Cambridge University Press (http://www.nr.com, accessed June 2007), 1992.

205. Kreyszig, E., *Advanced Engineering Mathematics*, John Wiley & Sons, 1999.

206. Davidson, L., *How to make energy spectra with Matlab*, in Publication 2006/05, Chalmers University of Technology, Sweden, 2006.

207. Politis, D.N. and White, H., *Automatic block-length selection for the dependent bootstrap*, Econometric Reviews, **23**(1), p.53-70, 2004.

208. Patton, A., Politis, D.N., and White, H., *Correction to "Automatic block-length selection for the dependent bootstrap" by D. Politis and H. White*, Submitted for publication (http://www.economics.ox.ac.uk/members/andrew.patton, accessed June 2008).